DEVELOPMENT OF A METHODOLOGY FOR CALCULATING STRESSES IN TRACK COMPONENTS

FRANCOIS PAULUS NAUDÉ

Submitted in fulfilment of part of the requirements, for the degree of

MASTER OF ENGINEERING (MECHANICAL)

in the

FACULTY OF ENGINEERING

UNIVERSITY OF PRETORIA

October 2004

DEVELOPMENT OF A METHODOLOGY FOR CALCULATING STRESSES IN TRACK COMPONENTS

FRANCOIS PAULUS NAUDÉ

SUMMARY

Supervisor: Professor NJ Theron
Co-Supervisor: Doctor RD Fröhling
Department: Mechanical and Aeronautical Engineering
University: University of Pretoria
Degree: Master of Engineering (Mech)

An existing analytical model, in use by Spoornet for the past two decades for calculating rail stresses on railway track, was revisited and improved. The model provided engineers with an easy-to-use program for evaluating track capacity and authorizing heavier loads on track. The model was modified to calculate rail and track component stresses more accurately. These modifications include the incorporation of current best practices and presentation of guidelines for the engineer on how to determine some input parameters which are normally difficult to obtain.

Firstly it was determined which input parameters the model was the most sensitive to. Thereafter it was determined whether or not the correct information would generally be readily available for those sensitive parameters. The most sensitive parameters were further investigated and test results, as well as best practice analytical methods, were used to establish nominal input values and guidelines for determining such values.

This research was necessary to establish whether or not the currently used analytical model still provided railway engineers with a useful tool and whether or not more modern and popular tools could validate or replace it.

After some modifications to the analytical model, it was proved that it provides engineers with a suitably accurate tool for calculating rail and track component stresses, without the need to build time-consuming models of the track under investigation. It showed that the model, after some modifications, is current with calculational methods in recent publications and provides an immediate answer to "what-if" questions without the need to run lengthy analyses.

ACKNOWLEDGEMENTS

I would like to thank and acknowledge contributions by the following persons:

- All my former Spoornet colleagues for their invaluable assistance and support during this research.
- Mr Hannes Maree for supporting this project and for providing valuable information and guidelines.
- Mr Mike Tomas for sharing his expertise and unlimited supply of test data.
- Professor Nico Theron for his support, enthusiasm and guidance.
- Dr Robert Fröhling for his consistent vision, technical contributions and for his driving force without which this project may not have been completed!
- Spoornet and Land Mobility Technologies (Pty) Ltd for making this research possible.
- I wish to thank my wife for all the hours I spent in seclusion and for her everlasting understanding, support and love, and my daughter, Andrea, whose birthdate marked a D-date for the delivery of this dissertation and forced many a late night's work!

Lastly, I want to echo my wife and thank my Lord and Saviour, in heaven, here and everywhere, for the opportunity to have an occupation that keeps me busy (Ecclesiastes 3:10).

TABLE OF CONTENTS

LIST OF FIGURES

LIST OF TABLES

NOMENCLATURE

A	Section area
A_e	Effective area
A_{rs}	Baseplate area
a	Sleeper spacing
a_0	Coefficient of locomotive maintenance
a_1	Railhead depth
a_2	Top of rail to top of flange
α	Coefficient of thermal expansion
b_1	Width of railhead
b_2	Width of rail flange
β	Inverse of the characteristic length
b_0	Coefficient of track maintenance
C	Foundation modulus
C_1	Torsion stiffness
c	Actual super elevation
D	Wheel diameter [m]
d	Section height
δ	Running top condition
E	Elasticity modulus
e	Eccentricity of vertical forces
F_0	Pretension force of fastening system
f	Flange thickness
fL	Factor of static load
g	Gravitational acceleration
h	Head NA to flange NA
h	Track cant
h_1	Distance from head NA to section rotation point
h_2	Distance from flange NA to section rotation point
η	Influence factor of adjoining wheels

NOMENCLATURE

I	Second moment of area
I_{yy}	Second moment of area yy
I_{zz}	Second moment of area zz
I_{yy} *Head*	Second moment of area yy head
I_1 *or* I_{zh}	Second moment of area zz head
I_2 *or* I_{zf}	Second moment of area zz flange
ϕ	Dynamic factor
k	Equivalent spring stiffness (*MN/m*)
κ	Characteristic value
λ	Characteristic length
L	Lateral load
NA	Neutral Axis
n	Position of lateral force below rail top
P	Static wheel load
p_c	Vehicle centre of gravity height
Q	Dynamic wheel load
q'	Reaction force per unit area
R	Curve radius
R'	Sleeper reaction force
s	Track width (gauge)
σ	Stress
σ_{rs}	Mean contact pressure between rail and sleeper
T	Torsion
ΔT	Temperature change
t	Web thickness
t'	Statistical confidence level
ΔT	Max temp change
UTS	Ultimate Tensile Strength
U	Track modulus

NOMENCLATURE

υ	Poisson
V	Speed (*km/h*)
v	Type of sleeper
x	Distance from wheel
x_1	Distance from wheel in front
x_2	Distance from wheel behind
x_3	Distance from third wheel
Y	Lateral load
yk	Top to section NA
z	Deflection of beam

1 INTRODUCTION

Railway track deteriorates over time due to the dynamic loading of passing rolling stock. To ensure the safe passing of trains, the track has to be properly designed and maintained. This study will focus on the development of a methodology on how to calculate stresses in track components. Emphasis will be placed on how to determine representative input parameter values, with the focus on identifying the parameters of highest importance. An existing analytical method will be utilised and improved with which track component stresses may be calculated in a fast and reliable manner.

Before continuing with the study on the development of a methodology on how to calculate track component stresses, it is important to understand the railway track structure and how it behaves as a system. Some background will also be given on the methods used in the past to calculate track component stresses.

1.1. Background

As railway track deteriorates over time under dynamic loading (1, p. 399), it is important to know which components are critical to maintain. Sometimes, however, it is not the components that deteriorate but the operating conditions could change. The need could arise to increase the traffic volumes, loads or speed on existing lines. It would then be necessary to determine and evaluate if any components should be replaced.

Since the rail is the single most expensive item on track, it is necessary to be able to calculate the stresses in the rail under operating conditions to evaluate its capability to fulfil its function. Maintenance personnel should thus, throughout the life of the track, evaluate its condition and determine whether it is still capable of performing to its design standards. In order to do this, a practical tool is needed to calculate stresses in all the track components, which could also help to identify limits for a number of track parameters.

Under the influence of dynamic track loads, the response and deterioration of the track and the mechanism governing this phenomenon are rather complex. Lombard (2) compiled a method on how to calculate the stresses of a rail under loading conditions using analytical calculations. This method used a number of parameter values describing the track and its condition to calculate the rail and rail seat stresses under a quasi-static load. A computer program was written in GW BASIC, which prompted the user for input and calculated the relevant stresses. The program was named “MOMENT” and is commonly known as “Lombard’s model”.

The Lombard model will be referred to as the 'analytical method' throughout this study since it is a compilation of generic analytical methods to calculate track component stresses and deflections. It is also called the 'analytical model', since it represents the track structure and loads as a system of different components.

The model originally only made provision for standard rail types and was used by SPOORNET Engineering for many years to evaluate rail and rail seat stresses under dynamic conditions. The dynamic loads are taken into account by factoring the static load with a dynamic factor; therefore it can be regarded as a quasi-static analysis.

Recent requests, however, were made to be able to evaluate *worn* rails under various support and track conditions and it became necessary to revise the program. In order to revise the program to have the options of defining worn rails, it was necessary to re-investigate the theory and assumptions made in the model. In this process, it was found that a MS EXCEL spreadsheet could be written to replace the BASIC program, which made the model fast and easy to use, especially when investigating the effect of changing input values.

The derivation of the analytical formulas with which the rail and component stresses (and deflections) are calculated, are presented in detail in report BBB2540ver1 (3). When all the original sources of information on the theory as presented by Lombard (2) were consolidated into a useable format to create the spreadsheet, it became apparent that the model had some shortcomings. The model did not include some important parameters and was sensitive to some parameters for which many users would have difficulty in obtaining representative values. Assumptions in the theory regarding the calculation of rail stresses were also scrutinised.

This dissertation will investigate shortcomings of the analytical model, identify sensitive parameters and propose a methodology on choosing the best values for these critical parameters. The analytical model is not the only or most accurate way to determine rail stresses under dynamic conditions but it will become apparent through this dissertation why this method is favoured and focused on in this study.

1.2. Problem statement

To calculate track component stresses under dynamic loading a practical tool is needed to determine the actual load-carrying capacity of the track and its components. The model currently in use by Spoornet excludes important parameters, such as curve radius, and is sensitive towards certain parameters, such as the dynamic factor. The user may be unaware of these sensitive parameters and

neglect to obtain proper values for them. This could lead to incorrect results regarding the capacity of the track to fulfil its function. Since it is important to use appropriate values for the most sensitive parameters of the model, a methodology on how to calculate stresses in track components is required with specific reference to the method of determining reasonable values for the most sensitive input parameters.

1.3. Objectives and scope of research

The primary objective of the study is:

- to present a methodology to calculate track component stresses accurately and reliably under different operating conditions.

The secondary objectives are:

- to identify parameters not included in the current analytical method that may have a significant effect on track component stresses
- to identify the parameters to which the analytical method is the most sensitive
- to provide nominal values to be used for the sensitive parameters where uncertainty exists regarding appropriate values to use when calculating track component stresses
- to validate the analytical method with other proven methods and empirical results.

In order to achieve the objectives, a brief reference will be made to different methods that can be utilised when determining the load-carrying capacity of the track structure. The focus will, however, remain on the analytical method currently used by Spoornet. Different methods will be used to test the analytical method's sensitivity towards each of the input parameters and, furthermore, the results from empirically developed formulas will be compared with field measurements to determine nominal values for each of the most sensitive parameters. As part of the scope of this project, results from the instrumented wheelset tests and wayside measurement tests, executed by Spoornet Engineering, will be analysed to determine actual input loads to the track structure. The results of these tests will primarily be used to validate or enhance certain theoretical and popular empirical formulas used in the analytical method and to determine values for the most sensitive model parameters.

It should be emphasised that in this study structural dynamics will not be considered since the operating conditions on Spoornet track only allow for low speed and high axle loads in which case the track dynamics do not play a significant part. The "dynamic effect" of moving loads will, however, be taken into account by means of a factored value (dynamic factor) in a quasi-static analysis.

1.4. Conclusion

This study will focus on the development of a methodology on how to calculate stresses in track components. Emphasis will be placed on how to obtain representative input parameter values with the focus on identifying the parameters of highest importance. An existing analytical method will be utilised and improved with which track component stresses may be calculated in a fast and reliable manner.

2 LITERATURE STUDY

To understand modern railways and current engineering practices, it is important to look into the history of the railways and how they were developed from earliest concepts to modern-day track.

2.1. History of the railways

Like so much in present day society, the railroad, as we know it, was a product of the industrial revolution although the idea of a special 'track' for hauling goods dates back about 2,000 years (4). The ancient Greeks built roads paved with stone blocks that had grooves cut in them. Wagons that had wheels the widths of the grooves were pulled over the roads by horses. These grooves kept the wagons on the road, and the stone paving was much smoother than dirt roads, so heavier loads could be transported much faster.

Roads of rails, called ‘wagon ways’, were being used as early as 1550 in Germany. These primitive railed roads consisted of wooden rails over which horse-drawn wagons or carts moved with greater ease than over dirt roads (5). By 1776, iron had replaced the wooden wheels and rails. Wagon ways evolved into tramways and spread throughout Europe. Horses still provided all the pulling power and, in 1789, William Jessup designed the first wagons with flanged wheels (5). The invention of the steam engine was then critical to the invention of the modern railroad and trains. In 1803, a man named Samuel Homfray decided to fund the development of a steam-powered vehicle to replace the horse-drawn carts on the tramways (5) and a new era dawned.

Railways had a much greater influence on modern day life than we normally realise. Railways in a sense have 'created' time as is evidenced from this extract from 'This day in American History' by E. Gross (6): *"On November 18, 1883, four standard time zones for the continental U.S.A. were introduced at the instigation of the railroads. At noon on this day, the U.S. Naval Observatory changed its telegraphic signals to correspond to the change. Until the invention of the railway, it took such a long time to get from one place to another that local 'sun time' could be used. When travelling to the east or to the west, a person would have to change his or her watch by one minute every twelve miles. When people began travelling by train, sometimes hundreds of miles in a day, the calculation of time became a serious problem. Operators of the new railroad lines realised that a new time plan was needed in order to offer a uniform train schedule for departures and arrivals."*.

In this way, the railway industry helped to revolutionise our world by presenting us with a fast and efficient transport method to haul heavy bulk goods in a most efficient way. To continue this

life-enhancing curve, railway engineers should continue to develop ways to reduce maintenance costs and to prolong the life of the track structure, thereby reducing the costs and increasing the benefits.

2.2. Track design philosophy

The railway track structure, or so-called "permanent way", is all *but* permanent and is a maintenance intensive item, which adds to the overall transporting costs. The sole purpose of the track is to transport rail vehicles safely from one point to another but it has a double function, namely, to support and guide the vehicles simultaneously (4). The track is designed according to the expected traffic loads and the load bearing approach (1, p. 14), (7) is utilised to ensure that the concentrated loads of the wheels are transferred to the formation while ensuring that the strength of the components are not exceeded (8), (9). The most important strength parameters are: rail stresses; sleeper stresses and ballast subgrade pressures. The Guidelines to Best Practices for Heavy Haul Railway Operations (10, p. 1-2) state that: *"The materials must be strong enough to resist the vertical forces introduced by very heavy loads and the dynamic response at the wheel-rail interface introduced by vertical accelerations of the car induced by track and wheel irregularities"*. Both the wheel and rail are responsible for transmitting the static and dynamic loads from the car body through to the track structure. At the contact patch between the wheel and rail, the vertical load of the wheel must be supported, and the steering, braking, and traction forces transmitted (10, p. 1-2). The following conditions (1, p. 14) should be met by the design objectives:

- Component dimensions should be sufficient for successful fulfilment of their function under the traffic load.
- Correct geometry of the track must be maintained, whether the track is loaded or not.
- Cost over service life should be as low as possible.

It is important that railway engineers design and evaluate cost effective track components that will not fail under prevailing traffic conditions (11). It is therefore necessary for them to utilise a method that would calculate component stresses under prevailing operating conditions, to enable them to judge whether or not the components will survive.

2.3. Engineering Modelling of track

As demands for improvement in technology have increased, research has developed to the point where the traditional theoretical tools for the classroom have now moved into the construction and maintenance departments of railway companies. These tools assist in the improvement of safety and the reduction of construction and maintenance costs. Advances in computer technology have made it

possible to create elaborate models of the railway track with which its behaviour could be predicted. However, modelling railway track is not an easy task since different models serve different purposes.

Modelling railway track is necessary to optimise[¥] the design of the components and to assist engineers in understanding and maintaining the track. Due to fatigue, wear, settlement and degradation of components of the structure, it is also necessary to quantify the condition of the track and its components in order to determine if corrective action should be taken (1, p. 409). 200 years after the steam engine revolutionised the railway industry, in an age where paying passengers can enter earth's orbit, it is ironic that railway track is still a complex structure for engineers to describe mathematically.

Traditionally, in the railway industry, mechanical engineers were more involved with vehicle dynamics and civil engineers were more involved with the track structure. For a civil engineer, a structure, such as a road, building or bridge, is stationary. Railway track consisting of the formation, ballast, sleepers and rails is also deemed a stationary structure. Due to the impact of the dynamic loads, however, it cannot be analysed or modelled in the same way. This causes technical problems that should be solved in both static and dynamic terms (13, p. 1). When analysing the track structure, its complexity is evident. A major problem the engineer is faced with is the elasticity of the track and defining its boundary conditions. To mathematically describe fixed or freely supported beams is quite straightforward, but defining the continuous beams (the rails) whose ends are neither fixed nor free and which are supported by discrete elastic supports (pads-sleeper-ballast combination), is quite a different matter. Although the track structure consists of easily identifiable components with clear functions, the interaction between them under dynamic loading is not always fully understood. To simplify complex structures, engineers often use symmetry in structures to represent three-dimensional structures in two dimensions. The rails and supporting structure cannot be adequately modelled by a two dimensional system, since the rails do not only bend in-plane but can also bend or move out-of-plane, with the elastic fastening system as a restraint. This phenomenon has a major influence on the rail stresses and thus cannot be ignored.

Modelling is called an engineering art and a general rule is: *"Models should be as simple as possible and as accurate as necessary regarding the task they serve for"* (14). The demand for model simplicity is especially important with respect to computational efficiency. Although computational effort becomes less and less time-consuming as higher computational power becomes available, the need for models that are more detailed will always catch up with the speed of computer processors and more efficient models will always be in demand. The second-mentioned requirement for a sufficient model is accuracy. Every type of model introduces its own limitations and subsequent

[¥] Apologies to Marczyk (12) who strongly disagrees with the optimising philosophy, which is so deeply rooted in the field of engineering. Marczyk promotes 'robust design' as superior to 'optimisation'.

errors. In general, there is not a single adequate model of a system but many different ones, depending on the task they are created for (14). Modelling the track structure is a good example of the diversity of models that can be used to represent a real structure. These models could range from the classical continuous models, like the Bernouli-Euler beam, to disturbance and damage models where the modelling involves more than the mere feeding of information to mathematical equations. Some models are based on static principles and others on dynamic behaviour of structures. Continuous models, like the ones that date back to Timeshenko, represent the track as an infinite continuous model on an elastic Winkler foundation (1, p. 71).

Apart from the continuous models, there are the discrete models, where the sleepers, for instance, are modelled as separate supports as in the real structure. These models, where elements are of finite length, are mostly based on the finite element method. Finite element modelling is yet another art and can be applied in an unlimited number of different ways. As the range of models and their applications become endless, first and foremost, the question to answer is what we want out of a model in order to determine which model would suit the task best. J. Box said, as quoted by Marczyk (12, p. iii):*"All models are wrong. Some are useful"*.

This study will focus on a model (or practical tool) that will be useful to the engineer:

- to ensure the safe functioning of the track structure,
- to assist in the design thereof by calculating stresses in the components,
- to help identify limits for a number of track parameters.

2.4. Available approaches relevant to this project

Several tools are currently available to describe railway track mathematically, each with its own advantages and disadvantages. Since the rail is the single most expensive item on track, the fatigue life of rails is an important issue to consider and the engineer should throughout the rail's life evaluate its capability to fulfil its function. It is therefore necessary to be able to calculate the stresses in the rail and other track components under all significant loading conditions.

The tools currently available to describe the track mathematically are: finite element modelling, dynamic modelling, quasi-static analytical methods and any combination of these.

2.4.1. Finite element modelling

Finite element modelling (FEM) is a method that can be utilised to model discrete track components and determine the interaction between them, as well as stresses, under both static and dynamic conditions. FEM is not limited to static analyses. However, dynamic analyses are computationally expensive. Another disadvantage of finite element analyses (FEA) is that one model can represent only one chosen track layout and cannot easily be adapted to model a track with different geometry. This means that a new model should be created for each new layout.

Finite element analyses can be useful to calculate stresses of components in complicated structures. The challenge when building finite element models is to determine the amount of detail needed to represent the reality accurately. In order to do this the engineer needs to know the behaviour of the structure to some extent to ensure the correct elements, boundary conditions and loads in order to represent the structure adequately.

There is currently no set of rules on how to model railway track structures with finite element methods and different researchers have used different methods to obtain results. According to Popp, Kruse and Kaiser (14), it is the frequency range of interest that dictates which track model is best suited to the investigation of a certain task. For investigating vehicle behaviour in curves, their stability or passenger comfort, only frequencies below 20Hz have to be considered and therefore simple track models are sufficient. Ballast and subsoil properties have a strong effect on track dynamics in the range up to 250Hz and, for higher frequencies up to 700Hz, the geometry of the rails has to be taken into account. It is concluded that, for the mid frequency range of 50Hz to ±500Hz, detailed models are needed for pads, ballast and the subgrade. According to the Guidelines to best practices for heavy haul railway operations (10, p. 2-11), the typical exciting mechanisms are:

- Vehicle body dynamics in the frequency range between 1 and 30 Hz
- Out-of round wheels (10 to 20 Hz)
- Wheel flats (10 to 20 Hz)
- Rail irregularities, such as rail joints and skid marks*

The European Rail Research Institute (ERRI) (15) built a 3D model for wheel-rail contact studies where the principle of the rail, being a simple beam on a continuously supported elastic foundation, was examined. In their study of rail rolling contact fatigue cracks, they classified the stresses in the rails as either “bulk” or “contact” stresses. In order to study the contact stresses, the bulk stresses as a result of wheel loads, thermal forces and residual stresses had to be examined. Of particular interest for their study were the rail and sleeper deflections as well as the sleeper-ballast pressures under static

* No frequency range was published in the source document, supposedly because irregularities could be highly discreet (which result in infinitely high frequencies) or continuous and small (low frequency vibration).

loads. The ERRI used a 3D solid FEA model and included the rail, Polyethylene pad, base plate, rubber pad, timber sleeper and ballast. The model consisted of 3309 solid elements representing a track model symmetric about the longitudinal axis and 9.7*m* in length. The loads were spaced according to an EU 07 Locomotive wheelbase and the stresses calculated for a static load case.

Finite element analyses are therefore useful when studying detailed phenomena and when computational efficiency does not come at a high premium.

2.4.2. Dynamic modelling

Many different dynamic models have been developed to simulate the actual field conditions and to determine the dynamic loads on track (16, p. 2.1). Some models are more complex than others; depending on the specific purpose they fulfil (14). When a vehicle is moving over the track, it experiences vibrations of varying frequencies, which excite the various modes of the vehicle structure, body and the payload (10, p. 2-11). The dynamic modes are generally in bounce, roll, pitch, nosing, and sway. Some of the exciting mechanisms are long wavelength track alignment irregularities in the vertical profile, track twist and rail discontinuities. These irregularities typically result in vehicle input frequencies between 0.5 and 30 Hz. High frequency impacts at rail discontinuities often excite the vehicle body vertical modes to induce the so-called lower frequency reaction forces. A multi-body model representing a typical vehicle and track by means of springs and dampers could be used to simulate the movement of a vehicle over an irregularity (17).

Another method that can be utilised is kinematic modelling such as used by software packages like Medyna, DADS or MSC.ADAMS. The advantage of these packages is in the possibility to accurately model a specific railway vehicle and to have it run on a specific track with pre-defined geometry, even including irregularities. From these analyses the forces acting on the track while the vehicle is travelling over it can be determined. These packages do not, however, calculate stresses in the rail or track components as yet, but the acting forces can be exported into finite element packages with which the stresses can be determined (see paragraph 2.4.4).

As with finite element modelling, these dynamic models cannot be changed quickly to represent different track layouts or different loading conditions and can only present results for the specific vehicle and track under consideration.

2.4.3. Analytical methods

Analytical methods normally assume universal boundary conditions but use all geometrical input in the form of input parameters. Analytical models do not solve derivative equations (such as the equations of motion), which involve iterative calculations, and modelling is done statically. This makes analytical methods more economical to use than finite element methods when the same results are required for different track layouts (provided that the applicable parameters are supported in the model).

Since these models represent static loading, some models incorporate a dynamic factor, which artificially represents the magnified effect of dynamic forces and deflections due to moving loads. These dynamic factors are always a point of discussion since the amplified effect of forces and deflections due to dynamic forces is neither constant nor linear and depend on the characteristics of the whole system.

When designing track in general, or evaluating a railway line under changing operating conditions, analytical model are the most economical to use. Analytical models make it possible to quickly evaluate different layouts and loading conditions without the necessity to build detailed models for each scenario.

2.4.4. Combination of methods

Bezin, Iwnicki and Stow (18) approached the problem of defining input loads for a detailed track model using the following methodology: The wheel-rail forces of a particular vehicle were predicted on a range of curves with MSC.ADAMS/Rail. The results were then validated with test measurements and the predicted forces were then transferred to two different finite element models. The first model was called the “Global model” and represented the track in a simplified manner to predict bending stresses in the rails. The second model was called the “Contact stress model” and represented a short piece of railhead and a portion of a wheel rim to simulate rail/wheel contact. With the MSC.ADAMS/Rail model, the vehicle dynamics and resulting track loads were determined for specific operating conditions and track geometry. The supporting track conditions were then accounted for in the ‘Global model’ and the rail bending stresses were determined.

By using these methods in combination, each method complemented the other by being used for the purpose it was developed for. Through this interaction, global dynamic forces were translated into detailed wheel-rail contact forces and subsequently detailed wheel and rail stresses.

2.5. Conclusion

Following the history of the railways and how they helped to shape the world as we know it today makes us realise that there is an ever-increasing drive to improve on existing technologies. In an era where detailed designs have to precede construction and maintaining infrastructure becomes a financial challenge, modelling railway track - in the various phases of its life - has become a necessity. It is thus imperative to improve on existing methods of modelling railway track to find cost effective ways to improve the life of track components and the track as a whole.

3 THE ANALYTICAL METHOD

Lombard (2) compiled an analytical method with which to calculate the stresses of a rail with a number of input parameters that described the loading conditions. This included the static load, factored by a dynamic factor, the track geometry condition and support conditions. A computer program was written in GWBASIC, which prompted the user for input and subsequently calculated the rail and rail seat stresses. The model of Lombard made provision only for standard rail types and recent requests were made to do the evaluations on worn rails to determine at what stage these rails had to be replaced. In order to revise the software program to have the option of defining worn rails, the theory was re-visited to understand and modify the program. In this process, it was found that a spreadsheet could be written to replace the GWBASIC program, which made the process more understandable and the model easy to use. When all the different sources of information on the theory, as presented by Lombard, were consolidated into a useable format for creating the spreadsheet, it became apparent that the model was sensitive to some parameters. For some of these parameters many users would not have direct access to correct or realistic values and may mistakenly assume that a thumb-suck value would suffice. When using any method to model railway track, it is not only important to know the model's limitations, but also to know which parameters the results are the most sensitive to, to ensure that proper values for those parameters are sought.

3.1. Input parameters

Table 3-1 lists all the input parameters for the analytical method with an indication of whether or not the input value is currently uniquely identifiable. It is important to know which parameter values are not currently uniquely identifiable in order to later identify for which of these parameters research will be needed to determine nominal values or to put proper guidelines in place for obtaining such values. It is most often encountered that engineers tend to use "default" values for those difficult-to-obtain values, unaware of whether or not the results from the method are sensitive to these values.

In order to understand the analytical method under investigation and identify shortcomings and possible areas for improvement, the underlying theory will be described in sufficient detail. For convenience it will be divided into the following sections: "Dynamic factor", "Support condition", "Rail stresses" and "Sleeper reaction force".

Table 3-1: Input parameters of the analytical method

No.	Symbol	Parameter	Uniquely Identifiable?
1	δ	Running top condition	✗
2	t'	Confidence level parameter	✗
3	V	Speed (V)	✓
4	P	Static wheel load	✓
5	C	Foundation modulus	✗
6	a	Sleeper spacing	✓
7	ν	Type of sleeper	✓
8	Ae	Effective area of sleeper	✓
9	E	E modulus rail	✓
10	υ	Poisson's ratio	✓
11	UTS	Ultimate tensile strength	✓
12	e	Eccentricity of vertical force Q	✗
13	n	Position of lateral force below top	✗
14	A	Section area	✓
15	b_1	Width of head	✓
16	b_2	Width of flange	✓
17	t	Web thickness	✓
18	d	Section height	✓
19	a_1	Head depth	✓
20	f	Flange thickness	✓
21	yk	Top to section NA	✓
22	h	Head NA to flange NA	✓
23	a_2	Top to top of flange depth	✓
24	I_{xx}	Second moment of area xx	✓
25	I_{zz}	Second moment of area zz	✓
26	I_{xx} Head	Second moment of area xx head	✓
27	I_1 or I_{zh}	Second moment of area zz head	✓
28	I_2 or I_{zf}	Second moment of area zz flange	✓
29	x_1	Distance from wheel in front	✓
30	x_2	Distance from wheel behind	✓
31	fL	Factor of static load	✗
32	ΔT	Max temperature change	✓

3.1.1. Dynamic factor

The first calculation of the analytical method is that of the dynamic (amplification) factor (1, p. 83). The dynamic factor converts a static wheel load to that of an equivalent dynamic wheel load. The empirical formula of Eisenmann is used in the analytical method and is a function of not only the static wheel load but of the speed of the vehicle, the running top (geometric condition) of the track

and the statistical confidence. This empirical calculation has been accepted by European railway companies (1, p. 83) and is based on the following observations and assumptions:

- Measurements have shown that the stresses in the rail foot, from a statistical point of view, have a normal distribution about the mean value.
- The mean value is independent of running speed and can be determined with sufficient accuracy using Zimmermann's (19) longitudinal beam theory.
- The standard deviation is dependent on the running speed and the state of the track.

The dynamic load (Q) is calculated by (2, p. 65):

$$Q = P \cdot (1 + \delta \cdot t') \qquad \text{if } V \le 60\ km/h \qquad (3.1)$$

$$Q = P \cdot \left(1 + \delta \cdot (1 + \frac{V - 60}{140}) \cdot t'\right) \qquad \text{if } 60 \le V \le 200\ km/h \qquad (3.2)$$

with P the static load[§], δ the running top condition (0.1 = Excellent track, 0.3 = Bad track), V the vehicle speed in km/h and t' being a multiplication factor of standard deviation which depends on the confidence interval. In equations 3.1 and 3.2 the bracketed expressions constitute the dynamic factor φ. For a statistical confidence level of 68.3%, t'=1, for 95.4%, t'=2 and for 99.7% t' = 3. It is recommended by Esveld (1, p. 84) to use $t'=3$ when investigating rail, pad and sleeper stresses, $t'=2$ when only looking at ballast bed stresses and $t'=1$ for the subgrade stresses. With $t'=3$ there is only a 0.15% probability that the maximum calculated rail stresses may be exceeded.

This relationship may prove to be irrelevant or inaccurate for use with Spoornet operating conditions since it was developed in a European high-speed environment while local conditions are more in the low speed and high axle load environment. Figure 3-1 indicates a typical train speed distribution from which it can be derived that approximately 70% of the trains travel at 60km/h or slower on the particular section of track. According to the Eisenmann formula (3.2), the speed of the vehicle affects the dynamic factor only at speeds above 60km/h.

It will thus be investigated in this study whether or not a new relationship between static and dynamic forces should be developed and if other parameters should be used, like, for instance, track design life or rolling stock type. Furthermore, the formula used here to determine the dynamic factor includes two parameters, namely, the running top condition and the statistical confidence level for which values are not uniquely identifiable. Firstly, the value for running top condition is subject to the interpretation and experience of the engineer doing the analysis. It is therefore advisable that a scientific method is developed to quantify the condition of the running top by incorporating one of the

[§] Esveld (1, p. 58) proposes the use of the static wheel load multiplied by an additional factor (paragraph 4.1.1.2, page 63) to account for the increase in wheel loads in curves due to cant deficiency or excess.

existing quality measurement parameters into the dynamic factor's formula. It is intended in this study to identify typical dynamic factors measured in service and to compare these to the results from the Eisenmann formula.

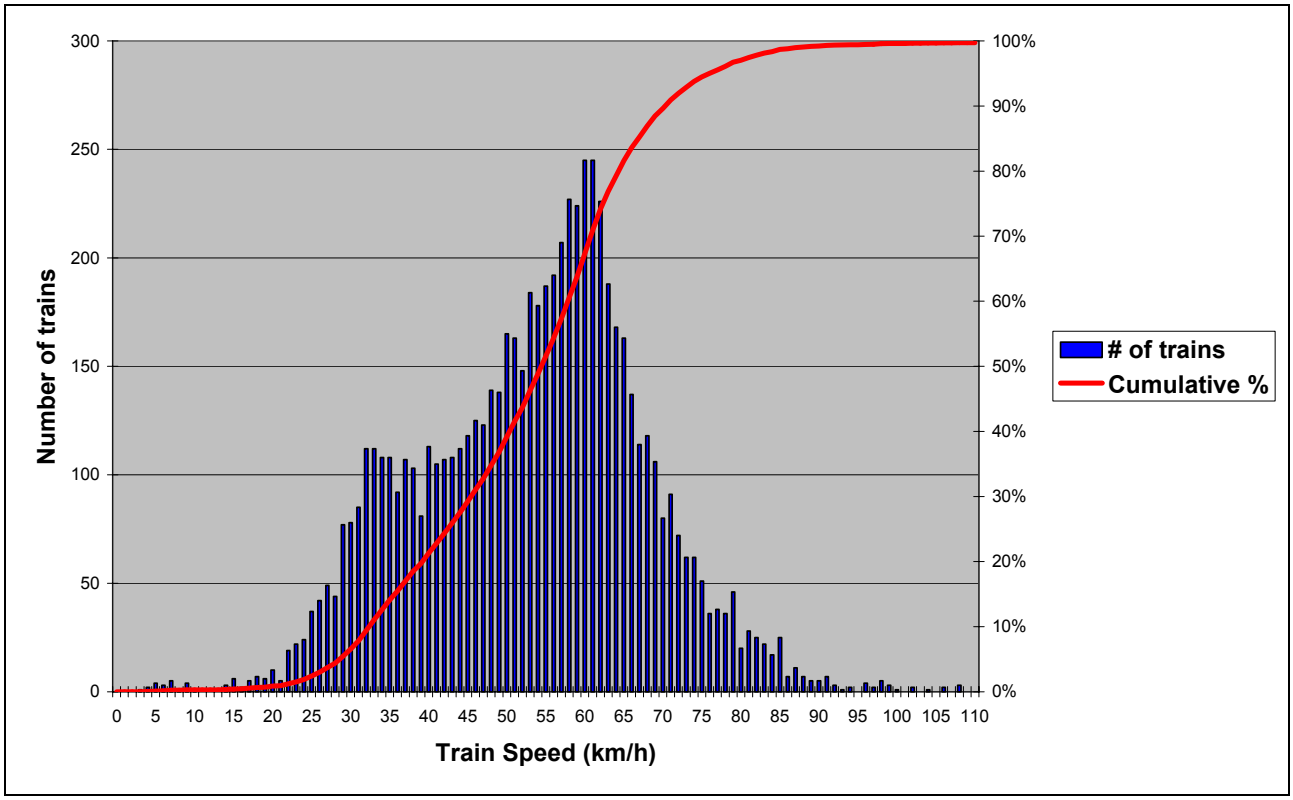

Figure 3-1: Typical train speed distribution

Based on this comparison it is foreseeable that a clearer guideline would be established, regarding specific values that would be appropriate for various circumstances, or that a methodology would be defined with which to determine dynamic factors.

The next section of the analytical method defines the support condition and how it affects the way the input load is transferred to the substructure.

3.1.2. Support condition

The localised input load from the wheel is transferred directly to the rail and then via the pads, sleepers and ballast to the substructure (8). In the analytical model the rail is defined as an infinite beam on an elastic support (20, p. B3.4) without differentiating between the different rail support components. The components which contribute largely to the elasticity of the rail support are the ballast and substructure. Due to the moving loads, which cause ballast break down, and drainage

conditions, which cause ballast fouling, the elasticity of the track (or *support condition*) changes with time.

The support condition is quantified in the analytical method and described by two parameters: the foundation modulus (C) and the track modulus (U) (2, p. 36).

$$U = \frac{\kappa \cdot C}{a} \tag{3.3}$$

$$\kappa = \frac{A_e \cdot \nu}{2} \tag{3.4}$$

with A_e the effective area of the sleeper, ν the type of sleeper (ν=1: Concrete sleeper, ν=0.91: Wood sleepers with $C > 60 MPa/m$), a the sleeper spacing and κ being the characteristic value.

According to Lombard (2, p 36-37), values for C range from 20 *MPa/m*, for a very bad† clay formation and bad ballast condition, to 100+ *MPa/m*, for a very good formation and ballast condition. According to Esveld (1, p. 79), the value for C is also 20*MPa/m* for a poor foundation but 200*MPa/m* for a good foundation.

According to Lombard (2, p. 10), Hetényi stated that if $U \prec 1.522 \cdot \frac{E \cdot I}{a^4}$ then the effect of discrete supports is negligible and the theory of a continuous beam on a continuous elastic foundation is valid (I is the second moment of area of the rail about its horizontal axis). Lombard states that if $U \prec 2.23 \cdot \frac{E \cdot I}{a^4}$ the error of the stresses in the rail will be less than 10% under the assumptions that the sleeper spacing is in the order of 700*mm* and the track modulus (U) is in the order of between 6 and 30*MPa*.

The analytical methods assume that the discrete supports may be represented by continuous supports; therefore results from finite element models with discrete support conditions will be compared to the results from analytical calculations in order to test this assumption's validity.

In the above calculations the value for the foundation modulus is a subjective value, based on testing experience, and may be interpreted differently by different analysts. The effect of using a high or low value can incidentally have opposite effects in the results investigated, based on whether the deflection or rail stresses are investigated. Thus, an operator of the model may think a conservative answer is being obtained whereas the opposite may be true. Many tests have been executed on

† Unfortunately, these terms: "very bad", "very good", etc., are not quantified by the authors and this is identified as one of the shortcomings of this method.

Spoornet track with the BSSM (Track Stiffness Measuring System) and MDD's (Multi-Depth Deflection metres) but all these tests are expensive, time-consuming and only give results for the immediate area under investigation. Other methods are being developed that include the usage of the track geometry measuring car to relate the deflection of the track under the car to the track stiffness. One such possibility is to vary the weight distribution of the vehicle while measuring the displacement of the track. However, this option is undesirable since it would require the vehicle to run multiple passes over a given piece of track while the first objective of the geometry car is to occupy the track for as short a time as possible.

The rails are the most important component of the track structure and the theory regarding the calculation of rail stresses will be presented in the following section.

3.1.3. Rail stresses

The rail stresses are calculated using the classic Zimmerman-theory, based on the principle of a beam on an elastic Winkler foundation (20, p. B3.4).

$$q' = C \cdot z \tag{3.5}$$

with q' = reaction force per unit area that the rail will experience from its support under a deflection of z. C is thus the Foundation modulus and expressed in *MPa/m*, which is the amount of stress under the rail that will result from a unit deflection of the rail. In order to calculate the deflection of a long continuous beam on an elastic foundation, the foundation modulus C is converted to the track modulus U using equation 3.3. U has the units of *MPa*, or rather *MN/m/m*, which is the distributed force reaction of the continuous rail support due to a unit deflection of the rail.

The solution of the deflection of a long continuous beam on an elastic foundation and a single point load (Q) is (21); (2, p. 6):

$$z = \frac{Q \cdot \beta}{2 \cdot U} \cdot e^{-\beta \cdot |x|} \cdot \left(\cos(\beta \cdot |x|) + \sin(\beta \cdot |x|)\right) \tag{3.6}$$

where

$$\beta = \sqrt[4]{\frac{U}{4 \cdot E \cdot I}} \tag{3.7}$$

The so-called characteristic length is defined by

$$\lambda = 1/\beta \tag{3.8}$$

$$\lambda = \sqrt[4]{\frac{4 \cdot E \cdot I}{U}} \tag{3.9}$$

and x is the distance from the point load Q.

Following from the deflection, the bending moment (M)

$$M = -E \cdot I \cdot \frac{d^2 z}{dx^2} = \frac{Q}{4 \cdot \beta} \cdot e^{-\beta \cdot |x|} \cdot \left(\cos(\beta \cdot |x|) - \sin(\beta \cdot |x|)\right) \quad (3.10)$$

In equations 3.6 and 3.10, x was substituted with $|x|$ due to symmetry conditions and since the equations are only mathematically valid for $x \geq 0$.

The stresses in the rail are then calculated from the bending moment M. The load case on the rail is seen as the sum of different load cases as illustrated in Figure 3-2. When the stresses are then calculated for each of these separate load cases, it can be summed up again with careful consideration of the sign at each location along the rail profile.

Under a centre vertical load the stresses σ in the rail, a distance y from the neutral axis will be

$$\sigma = \frac{M}{Z} \quad (3.11)$$

$$Z = \frac{I}{y} \quad (3.12)$$

with Z being the section modulus and I the second moment of area of the whole section about the horizontal axis. Due to the Timosenko effect, the web of the rail is regarded as an elastic foundation to the head of the rail, which influences the stress distribution throughout the rail section as indicated in Figure 3-2. Figure 3-2 indicates how the rail stresses under an off-centre vertical load and simultaneous lateral load, could be calculated by decoupling the off-centre loads into a centred vertical and lateral load and moments about the neutral axis. The stresses at various points on the rail profile are then calculated as follows:

$$\sigma_a = -\sigma_1 - \sigma_3 + \sigma_4 - \sigma_6 + \sigma_8 \quad (3.13)$$

$$\sigma_b = \sigma_c + \sigma_3 \quad (3.14)$$

$$\sigma_c = \sigma_a - \sigma_3 - \frac{\sigma_a - \sigma_3 + \sigma_d}{d} \cdot a_1 \quad (3.15)$$

$$\sigma_d = \sigma_2 + \sigma_5 - \sigma_7 + \sigma_9 \quad (3.16)$$

$$\sigma_e = -\sigma_1 - \sigma_3 - \sigma_4 + \sigma_6 - \sigma_8 \quad (3.17)$$

$$\sigma_f = \sigma_g + \sigma_3 \quad (3.18)$$

$$\sigma_g = \sigma_e - \sigma_3 - \frac{\sigma_e - \sigma_3 + \sigma_h}{d} \cdot a_1 \quad (3.19)$$

$$\sigma_h = \sigma_2 - \sigma_5 + \sigma_7 - \sigma_9 \quad (3.20)$$

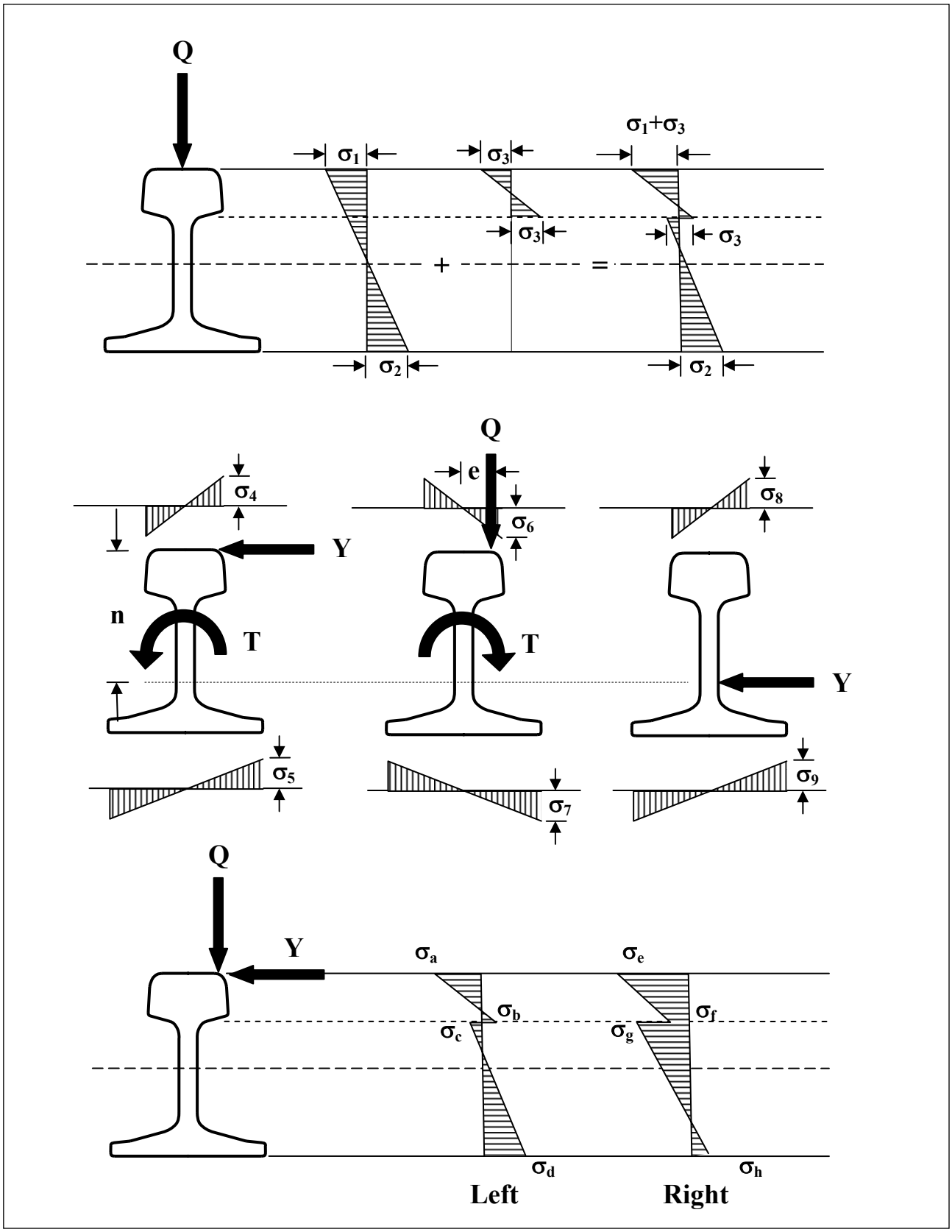

Figure 3-2: Load decomposition for calculation of rail stresses

$$\sigma_1 = \frac{M}{Z_k} \quad (3.21)$$

$$\sigma_2 = \frac{M}{Z_f} \quad (3.22)$$

$$Z_k = \frac{I_{xx}}{y_k} \quad (3.23)$$

$$Z_f = \frac{I_{xx}}{y_f} \quad (3.24)$$

and with y_k and y_f being the distance from the neutral axis to the top of the railhead and bottom of the flange respectively. I_{xx} is the second moment of area of the rail profile about the horizontal axis. Then, due to the Timoshenko effect (2, p. 14),

$$\sigma_3 = \frac{P \cdot \lambda'}{4 \cdot Z_k} \quad (3.25)$$

with

$$\lambda' = \frac{1}{\beta'} = \sqrt[4]{\frac{4 \cdot E \cdot I_k}{U_w}} \quad (3.26)$$

and I_k being the second moment of area of the railhead about its neutral axis and

$$U_w = \frac{t \cdot E}{2.3 \cdot a_1 \cdot \log\left(\frac{a_2}{a_1}\right)} \quad (3.27)$$

where a_1 is the railhead depth and a_2 is the distance from the top of the rail to the top of the rail flange. Due to torsion of the rail, the stresses can be calculated with the definition of the rotational centre as in Figure 3-3: The position of the shear centre or rotational axis is given by:

$$h_1 = \frac{h \cdot I_2}{I_1 + I_2} \quad (3.28)$$

$$h_2 = \frac{h \cdot I_1}{I_1 + I_2} \quad (3.29)$$

with $I_1 = I_{zh}$ = Second moment of area of the head about the vertical axis
and
with $I_2 = I_{zf}$ = Second moment of area of the flange about the vertical axis.

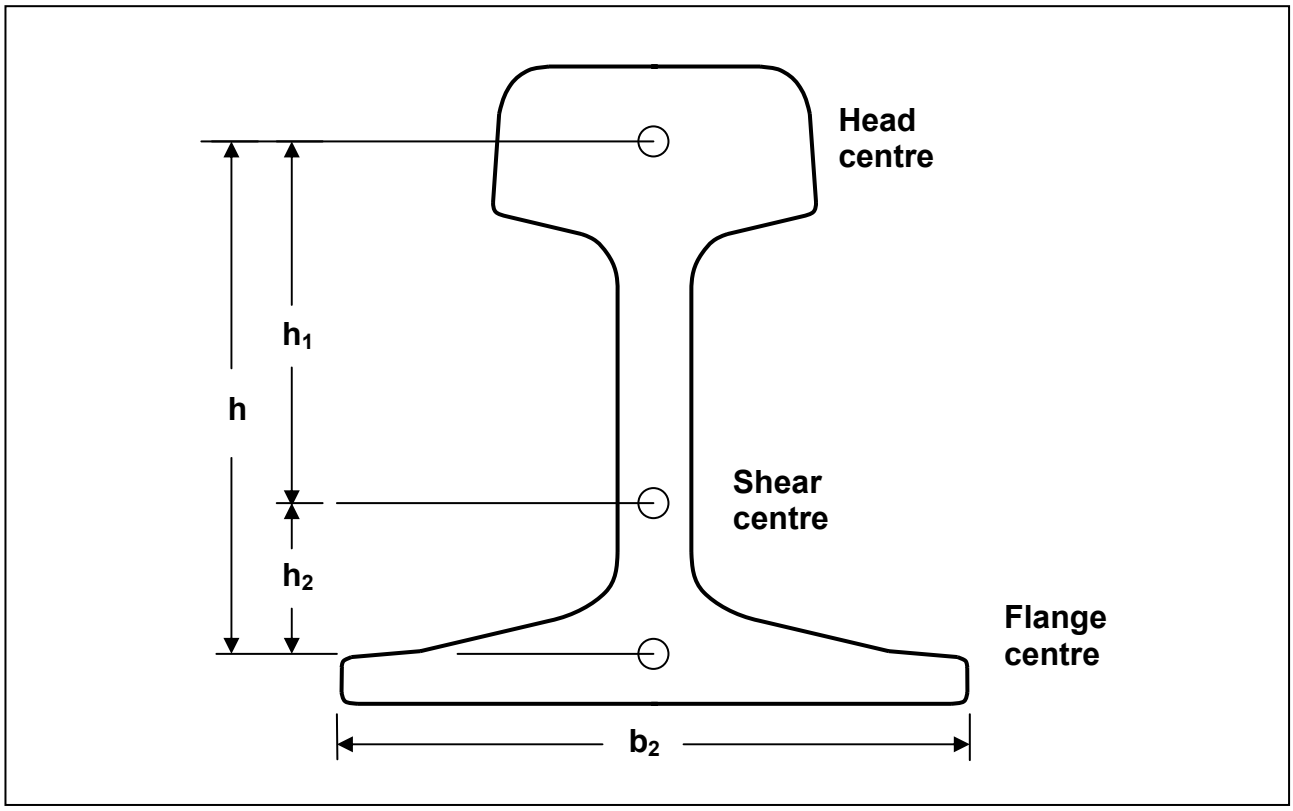

Figure 3-3: Position of shear centre / rotational axis

Then the stresses in the railhead are:

$$\sigma_k = \frac{E \cdot I_1 \cdot h_1}{Z_1} \cdot \frac{T}{C_1} \cdot \gamma \qquad (3.30)$$

and in the flange

$$\sigma_f = -\frac{E \cdot I_2 \cdot h_2}{Z_2} \cdot \frac{T}{C_1} \cdot \gamma \qquad (3.31)$$

with

$$C_1 = \frac{A^4 \cdot G}{4 \cdot \pi^2 \cdot J_x} \qquad (3.32)$$

$$G = \frac{E}{2 \cdot (1 + \upsilon)} \qquad (3.33)$$

$$Z_1 = \frac{I_1}{\left(\frac{b_1}{2}\right)} \qquad (3.34)$$

$$Z_2 = \frac{I_2}{\left(\frac{b_2}{2}\right)} \quad (3.35)$$

$$T = \frac{Y \cdot n - P \cdot e}{2} \quad (3.36)$$

and

$$\gamma = \sqrt{\frac{C_1}{D \cdot h^2}} \quad (3.37)$$

with

$$D = E \cdot \frac{I_1 \cdot I_2}{I_1 + I_2} \quad (3.38)$$

Axial stresses due to torsion (constrained warping) of the lateral force Y alone:

$$T = \frac{Y \cdot n}{2} \quad (3.39)$$

$$\sigma_4 = \frac{E \cdot I_h \cdot h_1}{Z_h} \cdot \frac{Y \cdot n}{2 \cdot C_1} \cdot \gamma \quad (3.40)$$

$$\sigma_5 = \frac{E \cdot I_f \cdot h_f}{Z_f} \cdot \frac{Y \cdot n}{2 \cdot C_1} \cdot \gamma \quad (3.41)$$

Axial stresses due to torsion (constrained warping) of the vertical force Q alone:

$$T = -\frac{Q \cdot e}{2} \quad (3.42)$$

$$\sigma_6 = \frac{E \cdot I_h \cdot h_h}{Z_h} \cdot \frac{Q \cdot e}{2 \cdot C_1} \cdot \gamma \quad (3.43)$$

$$\sigma_7 = \frac{E \cdot I_2 \cdot h_2}{z_2} \cdot \frac{Q \cdot e}{2 \cdot C_1} \cdot \gamma \quad (3.44)$$

Due to sideways bending, the stresses σ_8 and σ_9 are given as:

$$\sigma_8 = \frac{Y \cdot a}{6 \cdot Z_8} \quad (3.45)$$

$$\sigma_9 = \frac{Y \cdot a}{6 \cdot Z_9} \quad (3.46)$$

with

$$Z_8 = \frac{I_{yy}}{\left(\frac{b_1}{2}\right)} \qquad (3.47)$$

and

$$Z_9 = \frac{I_{yy}}{\left(\frac{b_2}{2}\right)} \qquad (3.48)$$

After the stresses in the rail due to the load are calculated, the additional stresses in the rail due to temperature are calculated with

$$\sigma = \alpha \cdot \Delta T \cdot E \qquad (3.49)$$

with α being the coefficient of thermal expansion of the material and ΔT being the change in temperature.

The final stresses in the rail at the various positions are then simply calculated by adding the relevant stresses from σ_1 to σ_9, (while taking the sign of each into account) to additional axial stress (σ) from equation 3.49.

Due to the assumption that the above theory for a continuously supported and infinitely long beam will be valid for a discretely supported beam of finite length (under certain conditions), it was deemed necessary to compare the stress results from the analytical method with those from finite element analyses where a beam of finite length is discretely supported.

The following sections will compare the results from the analytical method to results from finite element methods and to actual rail stress measurements for validation purposes.

3.1.3.1. Comparison of rail stress calculations from the analytical method to those of Finite Element Analysis results

A finite element model as depicted in Figure 3-4 was used to test the assumption that the derived theory for calculating stresses in continuously supported and infinitely long beams will be valid for discretely supported beams of finite length (under certain conditions). According to the Zimmerman theory of a *continuous* beam on an elastic support (24, p. 111), the deflection and bending moment formulas will also be valid for a *finite* beam of length greater than $2\pi\lambda$, with λ as defined in (3.9). For

a 57*kg/m* rail, the characteristic length (λ) ranges from 0.696*m* (*U*=200*MPa*) to 1.238*m* (*U*=20*MPa*) which results in a beam longer than 4.4*m* (*U*=200*MPa*) or 7.8*m* (*U*=20*MPa*).

The choice of length for the finite element model should therefore be longer than the maximum length of these restrictions. For convenience, and to ensure that the constraints on the beam ends do not influence the bending in the middle of the model, an 11.05*m* section (a multiple of 0.650*m* - the chosen sleeper spacing) of a 57*kg/m* rail was modelled. Since the model and load cases were symmetrical with respect to the length of the rail, a symmetry plane was used as indicated in Figure 3-4 to reduce the length of the model to 5.525*m*. The symmetry plane was chosen to be halfway between sleeper supports and a 100*kN* (50*kN* for symmetry) wheel load was applied in this area. This position gave higher stresses than when the wheel load was applied directly on top of a sleeper. The model consisted of a combination of approximately 25000 3D 8-node elements and 60 1D beam elements.

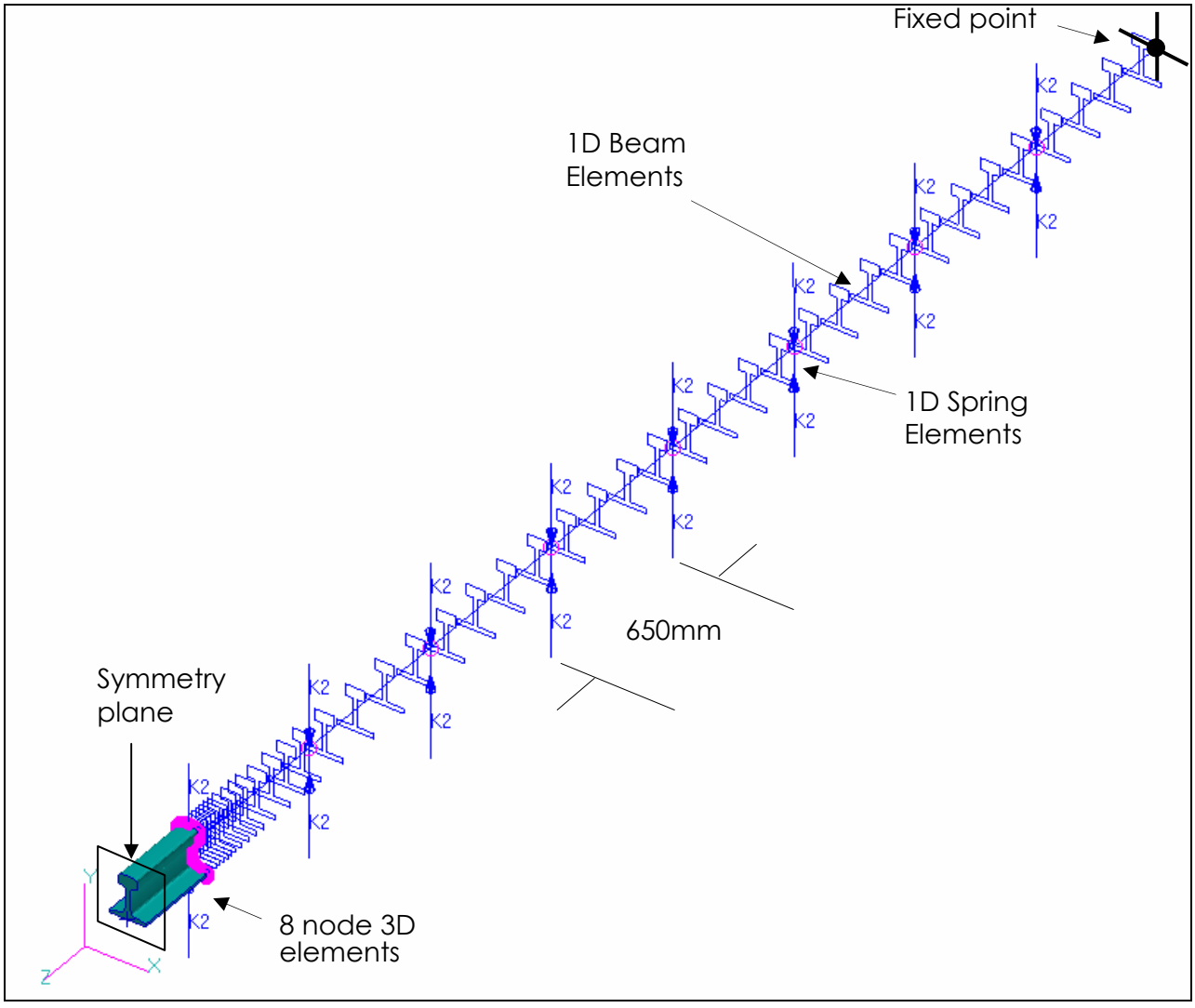

Figure 3-4: Finite element model – combination of 3D 8-node elements and 1D beam elements

At the symmetry plane the complete rail profile was modelled with 3D Hex (8 node) elements to enable reporting on detailed stresses along the varying profile. The 3D elements were used for a half sleeper spacing distance of 325*mm*, from the end where the load was applied, to the first spring element, which represented a sleeper support. Spring elements were used at 650*mm* intervals to represent the discrete support of the rail pads and sleepers. The rest of rail was modelled with simple beam elements, which had the same nominal section properties as the 57*kg/m* rail to reduce computational cost. In order to evaluate the effect of the rigid connection between the solid elements and beam elements, a vertical displacement plot was produced for the nodes on the neutral axis of the rail (see Figure 3-5). From the deflection results of the FEA models, it can be seen that there is a smooth transition in the deflection from the solid elements to the beam elements. These displacements have been compared with analytically determined deflections, which are also indicated in Figure 3-5.

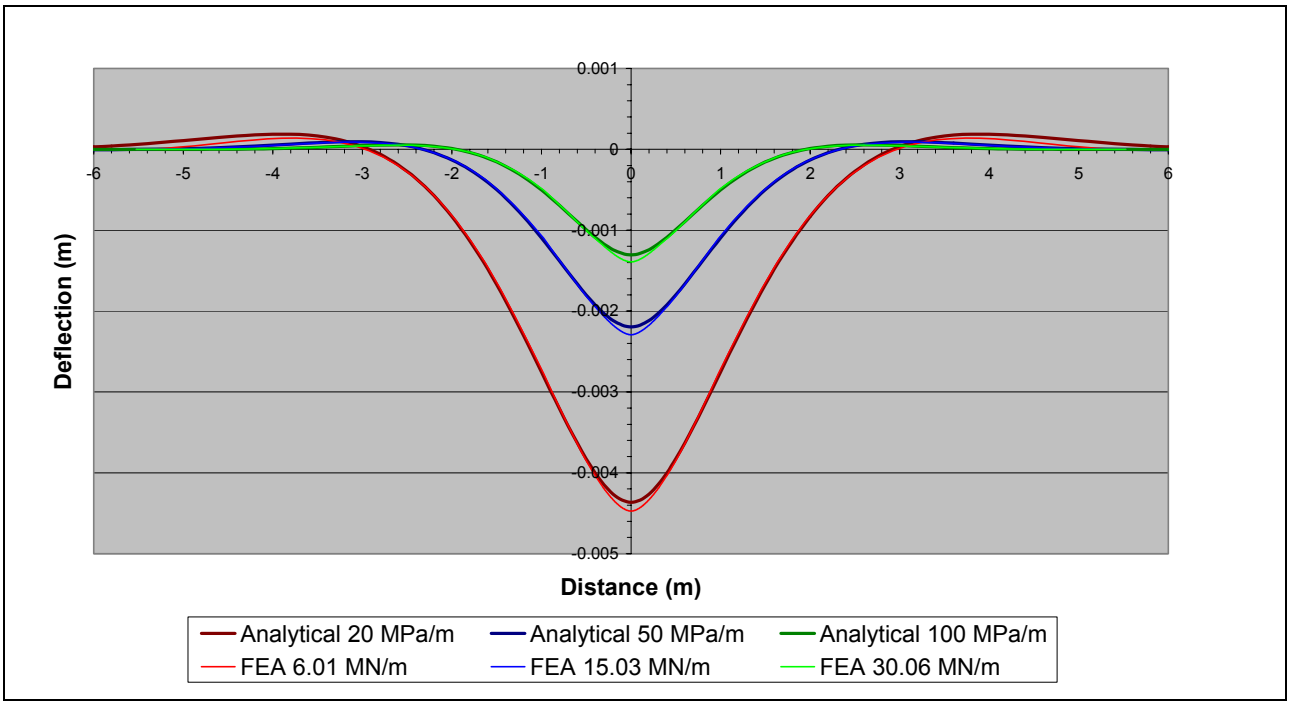

Figure 3-5: Deflection curve of FEA models and analytical methods

For the analytical results, a Foundation Modulus (C) of 20, 50 and 100*MPa/m* were used where the units (*MPa/m*) indicate the stress experienced by the foundation under a unit deflection. For the FEA models, the Foundation Modulus had to be converted to a spring stiffness with units in *MN/m*. According to Esveld (22, p. 59), the recommended conversion method is to multiply the Foundation Modulus (C) with half of the effective sleeper support area, thus

$$k = C.{}^{Ae}/_{2} \qquad (3.50)$$

For the case where $C = 20\ MPa/m$, and a PY or FY concrete sleeper is used:

$$k = 20.\frac{0.6012}{2} \qquad (3.51)$$

$$k = 6.012 MN/m \qquad (3.52)$$

Table 3-2 indicates a number of support stiffness values, which include those used by Spoornet in the analytical calculations, and those used in the FEA models. The deflections of a 57*kg/m* rail were then calculated with both the analytical and finite element methods under different support conditions and the results are tabulated in Table 3-2. With these three different support stiffnesses, two different load cases were applied to give a total of 6 different result sets. The first load case represented a 100*kN* centred vertical load (spread over an area of 20*mm* x 20*mm*) and the second represented an off-centred vertical load of 100*kN* with a simultaneously applied lateral load of 50*kN* over the same 20*mm* x 20*mm* area (see Figure 3-6). The actual loads and application area were halved since a symmetry plane was used in the model.

Table 3-2: Conversion of foundation modulus values to support stiffness

	Track support stiffness units	A		B		C	
		Stiffness	Maximum deflection	Stiffness	Maximum deflection	Stiffness	Maximum deflection
Analytical	Foundation modulus [*MPa/m*]	20	y=4.4*mm*	50	y=2.2*mm*	100	y=1.3*mm*
	Track modulus [*MPa*]	9.249		23.123		46.246	
FEM	Support stiffness 1 [*MN/m*]	6.012	y=4.5*mm*	15.03	y=2.4*mm*	30.06	y=1.4*mm*

From the deflection results it is clear that there is a strong correlation between the two methods.

The FEA stress results for the different support stiffnesses under a 100*kN* centred vertical load are indicated in Figure 3-7, overlaid on the results of the analytical model for the same load condition. The stress results for the different support stiffnesses under a 100*kN* off-centred vertical load and simultaneous 50*kN* lateral load are indicated in Figure 3-8 and Figure 3-9, overlaid on the results of the analytical model for the same load condition.

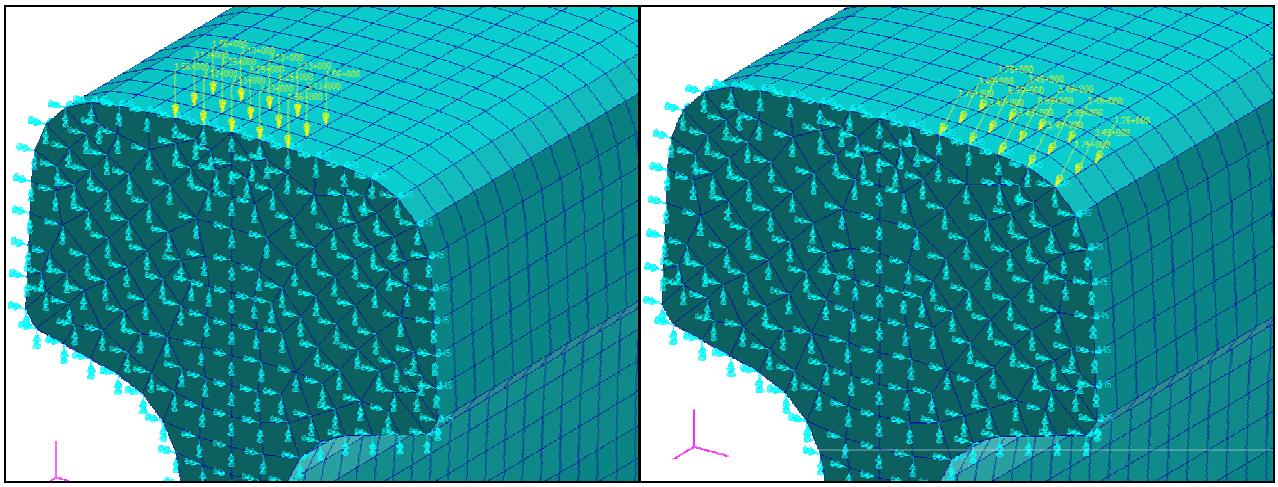

Figure 3-6: Centred and off-centred load cases

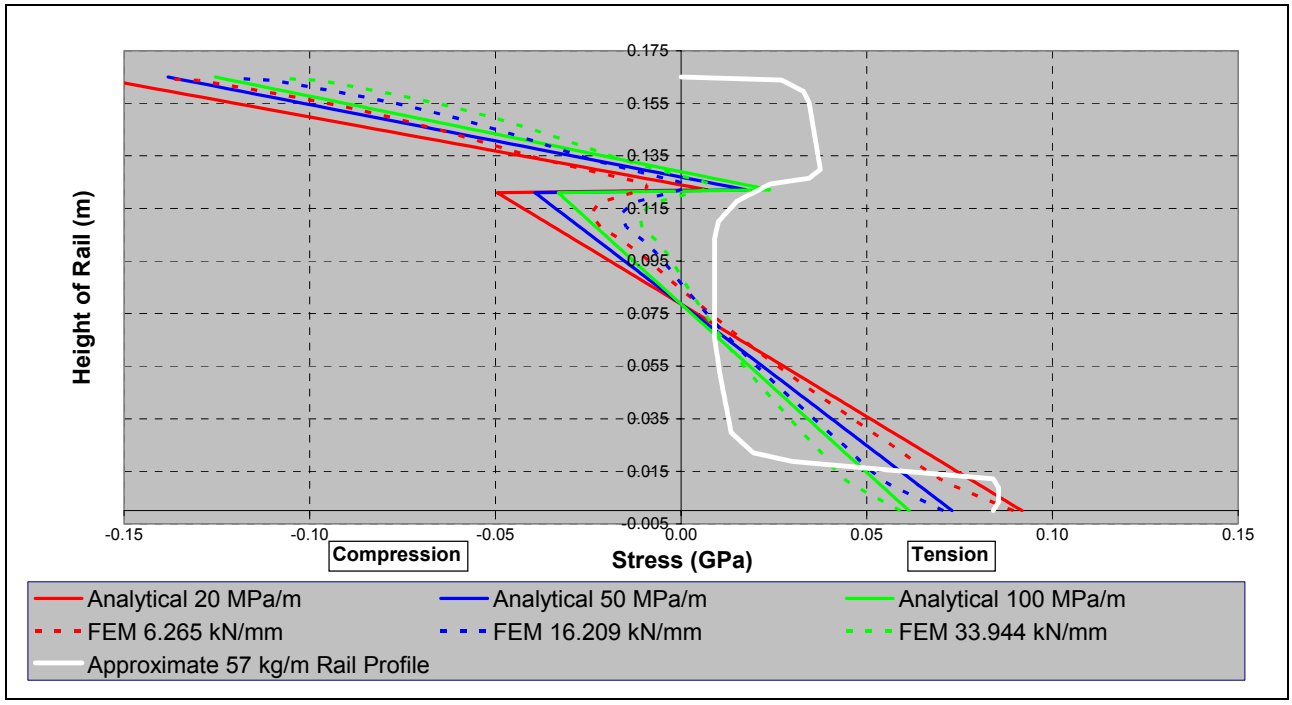

Figure 3-7: Axial stress results from analytical and FEM model with centred vertical load and different support stiffnesses

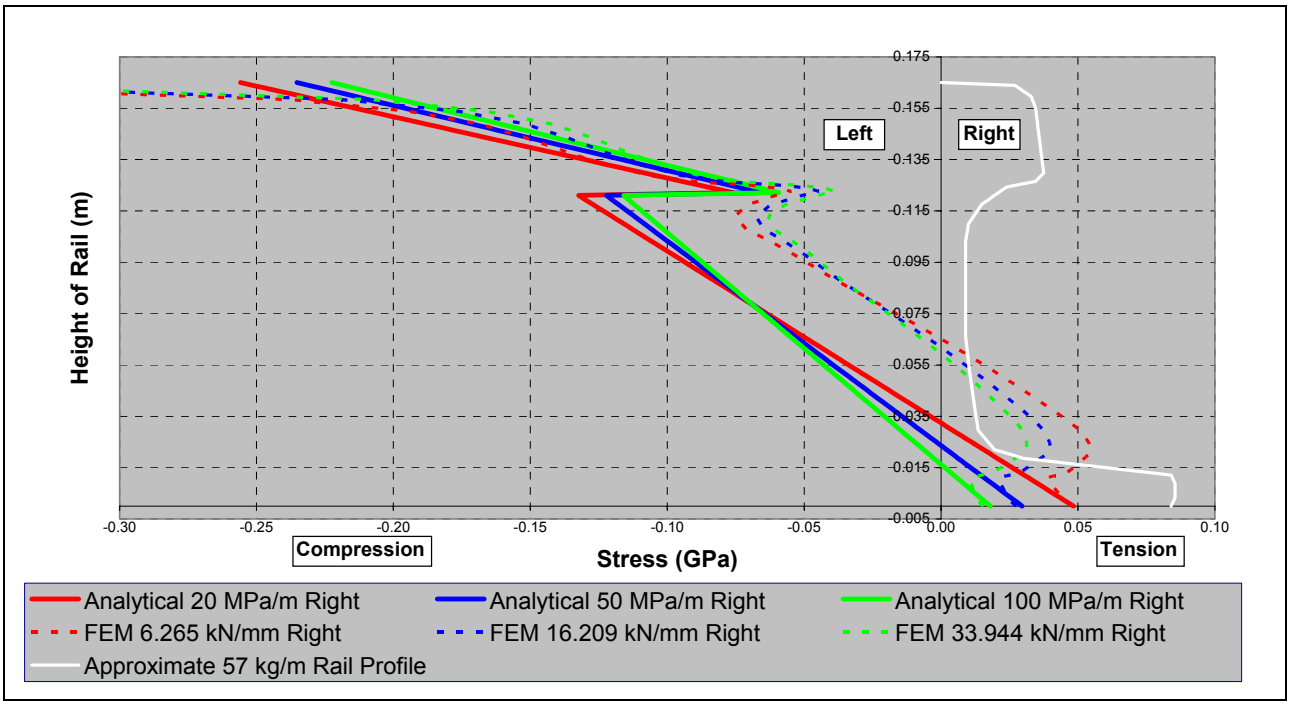

Figure 3-8: Axial stress results from FEM model with 100*kN* off-centre load and 50*kN* lateral load on different support stiffnesses of 20, 50 and 100*MPa/m* (right side of rail)

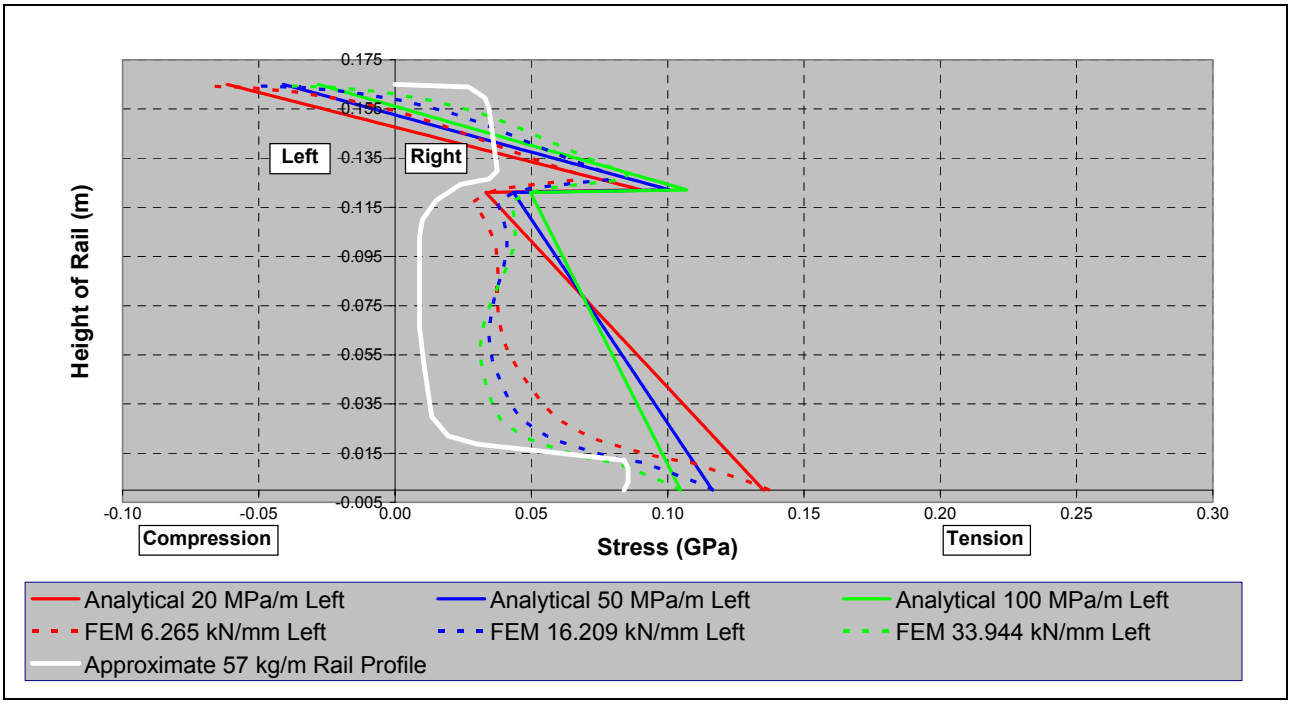

Figure 3-9: Axial stress results from FEM model with 100*kN* off-centre load and 50*kN* lateral load on different support stiffnesses of 20, 50 and 100*MPa/m* (left side of rail)

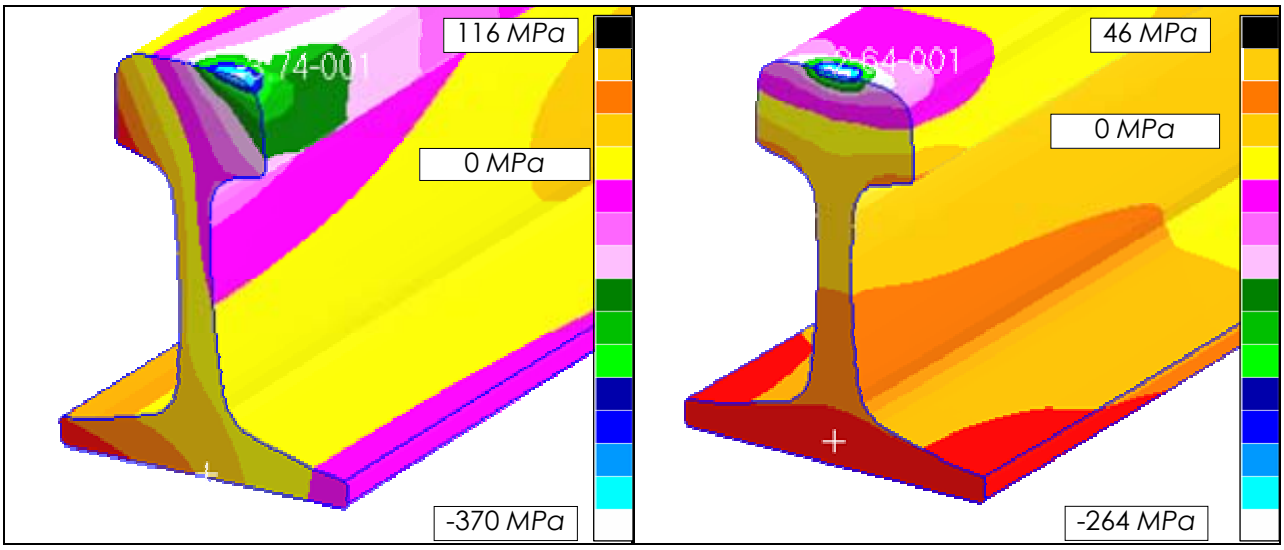

Figure 3-10: Graphical representation of typical stress results from a FEM model with an off-centre load with a simultaneous lateral load (left) and a centre load only (right)

The rail stresses of the finite element model and the analytical model were compared and are presented in Table 3-3.

The difference between the analytically determined stresses and those determined from the FEA, ranged from 2*MPa* to 106*MPa* for the different support stiffnesses under the centred load. For the off-centred load case, the difference ranged from 8*MPa* to 386*MPa* for the different support stiffnesses. The biggest difference is in the railhead area where the FEA model reported high stresses because of the close vicinity of the stress concentration under the applied load. It is clear from Figure 3-7 to Figure 3-9 that the stresses correlate well in the railhead area (below the top corner) and the so-called Timoshenko effect is also well represented.

The rail web area shows less correlation than the flange area since the analytical calculations do not account for the discontinuity between the web and flange and thus approximate a uniform stress distribution from below the railhead to the bottom of the flange.

It should also be noted that the overall stresses of the FEA and analytical model have the best correlation in the centred load case, whereas the off-centred load case presents higher differences in stresses. The overall correlation is, however, quite acceptable if the fundamental differences between the two methods are taken into account.

Table 3-3: Stress comparison between FEM and analytical model

	Maximum Rail Stress, type and location [*GPa*]	FEM [*MPa*]	Analytical [*MPa*]	Difference	
				[*MPa*]	[%]
Centre load 100*kN*	**20 *MPa/m***				
	Railhead compressive stress	-138	-159	-20	13%
	Railhead tensile stress	-9	7	16	229%
	Rail flange tensile stress	90	92	2	2%
	50 *MPa/m*				
	Railhead compressive stress	-118	-138	-20	15%
	Railhead tensile stress	2	17	16	91%
	Rail flange tensile stress	71	73	2	3%
	100 *MPa/m*				
	Railhead compressive stress	-106	-125	-20	16%
	Railhead tensile stress	8	24	16	66%
	Rail flange tensile stress	59	61	2	4%
Off-centre load 100*kN*	**20 *MPa/m* Right**				
	Railhead compressive stress	-386	-256	131	-51%
	Railhead tensile stress	-58	-76	-18	24%
	Rail flange tensile stress	47	48	1	3%
	50 *MPa/m* Right				
	Railhead compressive stress	-367	-235	132	-56%
	Railhead tensile stress	-48	-66	-18	27%
	Rail flange tensile stress	27	30	2	7%
	100 *MPa/m* Right				
	Railhead compressive stress	-355	-222	132	-60%
	Railhead tensile stress	-42	-59	-17	29%
	Rail flange tensile stress	15	18	3	14%
	20 *MPa/m* Left				
	Railhead compressive stress	-69	-62	8	-12%
	Railhead tensile stress	48	90	42	47%
	Rail flange tensile stress	137	135	-1	-1%
	50 *MPa/m* Left				
	Railhead compressive stress	-50	-41	9	-21%
	Railhead tensile stress	58	101	43	42%
	Rail flange tensile stress	117	116	-1	0%
	100 *MPa/m* Left				
	Railhead compressive stress	-38	-28	10	-34%
	Railhead tensile stress	64	107	43	40%
	Rail flange tensile stress	105	105	0	0%

It is important to re-emphasise the fundamental differences between the analytical method and the FEA method:

- The analytical method sees the rail as a infinite beam on a continuous elastic foundation whereas the FEA model has a finite length and is discretely supported.

- The analytical method simplifies the complex rail profile to a profile built up by 3 rectangular profiles (railhead, rail web and rail flange) whilst the FEA model uses the precisely defined profile in the area of highest stresses (solid elements) and simple beam elements in the rest of the model. In both cases the simplified profiles have the same areas and second moment of areas as the actual rail profile.
- In the analytical method the Timoshenko effect is taken into account by decomposing the model into firstly a beam with the same height as the rail profile and continuously supported by an elastic foundation, and secondly as a model where the railhead is continuously supported by the elastic rail web. The stress results from these two models are then again superimposed to produce the final stresses. In the FEA the profile geometry and material properties define the varying elasticity throughout the rail profile, with the resultant varying axial stresses throughout the profile.
- The deflection of the rail in both methods is a function of the rail properties and the support stiffness, although the calculations are derived from totally different avenues.

Apart from these fundamental differences between the analytical model and the finite element analysis, the results in Figure 3-7 to Figure 3-9 and Table 3-2 and Table 3-3 indicate that the two methods are in accord.

Another method to validate the results from the analytical method was a comparison with rail stress results from field measurements.

3.1.3.2. Rail stress results from field measurements

In preparation for field tests (23), several strain gauges were pasted onto a rail in track along the rail profile (Refer Figure 3-11). The rail stresses were then measured under passing trains. Unfortunately, the exact locations (eccentricity) of the loads are unknown, which makes it difficult to compare the results with those of the previous analyses. However, the vertical loads were measured, as well as the lateral loads. A summary of maximum rail stresses measured during the test is presented in Figure 3-12 for the two different load cases with vertical loads of 118kN and 108kN and lateral loads of 25kN and 19kN. From the results it became clear that the measured stresses are in the same order of magnitude as those of the previous analyses and that the stress patterns show similarities to those of the analytical results.

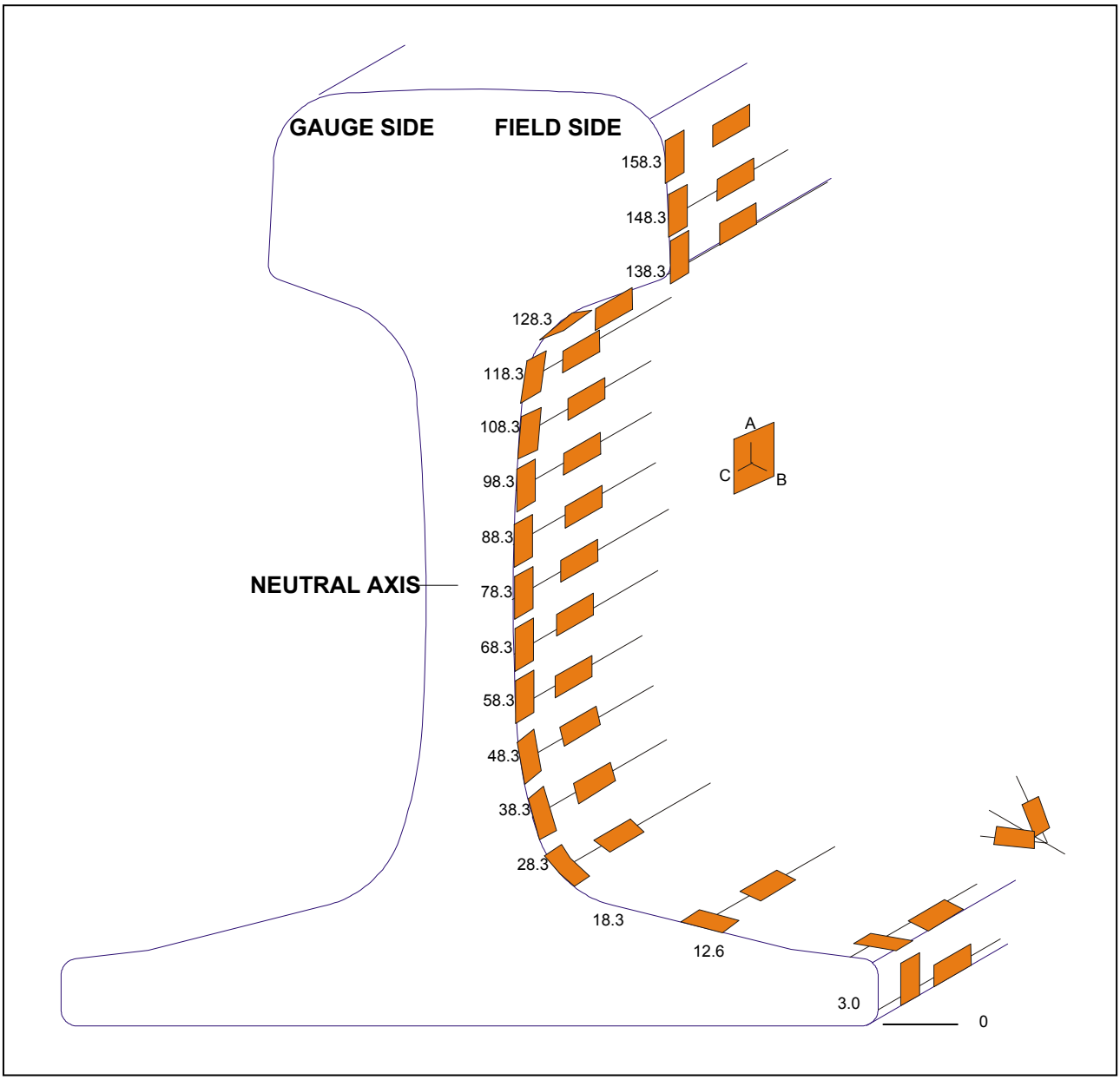

Figure 3-11: Strain gauge positions as pasted onto rail for field tests (23)

Although a number of assumptions were made in the derivation of the theory for calculating rail stresses, the results are in accord with finite element analyses and field measurements. Adjustments to the input will, however, be investigated to improve on the correlation.

The last section of the analytical method, the sleeper reaction force, is described in the next section.

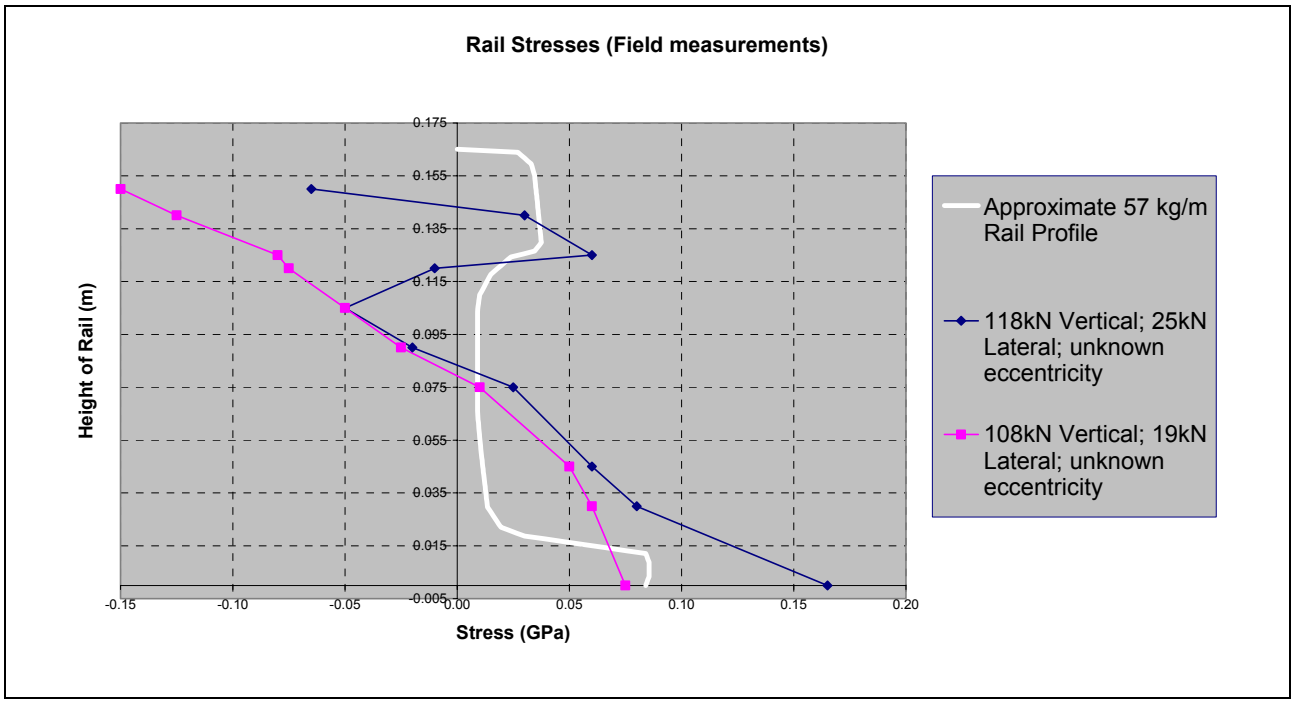

Figure 3-12: Rail stresses under different vertical and lateral loads (eccentricities unknown) (23)

3.1.4. Sleeper reaction force:

The sleeper reaction forces (20, p. B3.9) are the forces from the rail acting on the sleeper as the vertical wheel load is distributed from the rail to a number of sleepers. The sleeper reaction force in the analytical method is calculated by distributing the vertical wheel load from the rail to a number of sleepers. The sleeper reaction force is dependent on the stiffness of the rail, the sleeper spacing and the foundation modulus.

If the deflection of the sleeper is presumed to be proportional to the deflection of the rail, the force carried by the sleeper can be calculated by (20, p. B3.13)[‡]:

$$R' = \frac{a \cdot Q \cdot \lambda}{2} \cdot \eta \qquad (3.53)$$

with R' the sleeper reaction force $[kN]$, a the sleeper spacing $[m]$, Q the vertical dynamic wheel load $[kN]$ and η the influence factor of the adjoining wheels.
The formula for η is:

$$\eta = e^{-\lambda|x|} \cdot \left(\cos\left({|x|}/{\lambda} \right) - \sin\left({|x|}/{\lambda} \right) \right) \qquad (3.54)$$

[‡] Due to (20, p. B3.7) inverting the definition of λ, by using β instead of λ to define the characteristic length and defining λ as the inverse of β, equations 3.53 and 3.54 were modified to have λ in the nominator part of the fractions in order to keep the definition of λ constant throughout this document.

where x is the distance from the wheel. In the event of more than one wheel being calculated, η is replaced by η', with

$$\eta' = \eta(x_1) + \eta(x_2) + ... + \eta(x_n) \qquad (3.55)$$

and the distance to each wheel being x_1, x_2 *to* x_n respectively.

The mean contact pressure between rail and sleeper on the most heavily loaded sleeper can be approximated by:

$$\sigma_{rs} = \frac{F_0 + R'}{A_{rs}} \qquad (3.56)$$

with F_o being the pretension force of the fastening system and A_{rs} being the base plate area in contact with the rail or sleeper, whichever is the smallest.

According to (1, p. 91), the maximum permissible contact pressures between rail and sleeper are:

- Softwood sleepers: $\sigma_{rs} \leq 1.0 - 1.5MPa$
- Hardwood sleepers: $\sigma_{rs} \leq 1.5 - 2.5MPa$
- Concrete sleepers: $\sigma_{rs} \leq 4MPa$

The vertical stresses between the sleeper and ballast bed should be kept below $0.5MPa$, with the formula for the sleeper ballast stress (σ_{sb}):

$$\sigma_{rs} = \frac{R'}{A_{sb}} \qquad (3.57)$$

with A_{sb} being half the contact area between sleeper and ballast.

By investigating the theory behind the analytical model, its limitations have been identified and will be discussed in the next section.

3.2. Limitations of the analytical method

Preliminary investigations showed that important parameters such as curve radius and super elevation were not included in the analytical method and that some calculated values did not correlate well with measurements performed on Spoornet track (23). Tomas (23) thoroughly explained the manner in which the measurements did not correlate with the theoretical results. The most important unknown parameters were the vertical load positions (eccentricity) and track stiffness for which values had to

be chosen based on experience and good engineering judgment. Tomas further questions the assumption that the rail has only one rotation centre at the bottom of the rail web and proposes that the rail may actually have an additional rotation centre at the top of the rail web. Proving this theory, however, falls beyond the scope of this study.

The following areas for investigation into the analytical method have been identified:

- The calculation of the dynamic factor is performed with an empirical formula that was not developed or validated locally, although widely accepted.
- The formula for the dynamic factor does not include the effect of factors such as track cant or curve radius, nor does it include any suspension parameters of the rolling stock.
- The parameter indicating the running top condition is a subjective value and not uniquely specifiable.
- There is no indication which value for the running top condition will result in a "safer" result if the user is uncertain of the correct value to enter.
- There is no guideline on how the statistical confidence level should be chosen and how its choice will affect the results.
- The value for the track support condition is a subjective value and not easily determinable.
- There is no indication which value for the track support condition will result in a "safer" result if the user is uncertain of the correct value to use.
- The eccentricity of the vertical force is used as an input from the user and not as a function of the rail type, rail profile, wheel profiles, track geometry or steering and hunting characteristics of the vehicle.
- There is no specific guideline on typical eccentricity values of the vertical load.
- There is no indication which value for the eccentricity will result in a "safer" result if the user is uncertain of the correct value.
- The lateral load in the analytical method is calculated as a fixed percentage of the vertical force, which could not be the case since the lateral force is a function of a number of other parameters, such as track geometry, rolling stock steering ability and speed of the vehicle.
- The analytical method acknowledges the fact that an error is introduced with the assumption that the rail is continuously supported.

In order to prioritise and focus the investigation on the shortcomings of the analytical method, it was decided to perform a sensitivity study on the model to determine which parameters have the greatest effect on the results under the current relationships.

3.3. Sensitivity analyses

Sensitivity analyses help to focus the attention on the input parameters that have the greatest effect on the output by recording the range of results according to a predetermined range of input.

It is well understood that a sensitivity study will not highlight or indicate any incorrect relationships between parameters and thus any areas of concern in this regard will have to be dealt with in separate investigations by comparing results with empirical results or other established methods. It is thus also imperative that another sensitivity study should be performed on the model, after changes to the model have been introduced, to ensure that the final list of important parameters is well documented and guidelines for obtaining proper input are given.

Two independent sensitivity studies were performed on the analytical method namely a quantitative study and a qualitative study.

3.3.1. Quantitative sensitivity analysis

In this study, the rail stresses were monitored while each parameter in the model was set to a median (middle) value and each in turn was changed from its minimum to its maximum value. The results did not include the effect of combinations of high or low parameter values, but included the effect of a single parameter value on the rail stresses, with the other parameter values equal to their respective median values. The range of stresses of the rail was then noted for each parameter as indicated in Table 3-4.

Figure 3-13 indicates the information from Table 3-4 graphically where it is clear that the 'Static Wheel load', 'Lateral force factor', 'Max Temperature change', 'Eccentricity of Vertical force Q', 'Dynamic Factor', the 'Wheel distances' and the 'Rail section' are the most important parameters to investigate since the results are the most sensitive to changes in these parameters. Table 3-5 indicates the parameters from Table 3-4 in order of importance as a function of the sum of the railhead and rail flange stress ranges. The stress ranges for each parameter are also indicated as a percentage of the maximum value and used here as an indication of relative importance.

According to the result from Table 3-5 it can be concluded that the current model is most sensitive to the static wheel load and least sensitive to the type of sleeper used. One must keep in mind that, once the model is further developed, results from a sensitivity analysis on the updated model may differ from the results shown.

Table 3-4: Input parameter sensitivity analysis

Parameter	Parameter Value			Max Rail Head Tension (MPa) / Max Rail Flange Tension (MPa)			Band Width Max - Min	Sum Head & Flange Band width
	Min	Mid	Max					
	A	B	C	A	B	C		
Running Top Condition	0.1	0.2	0.3	233.23	248.16	263.1	29.87	64.21
				174.66	191.83	209	34.34	
Confidence Level	1	2	3	238.2	248.16	258.12	19.92	42.81
				180.38	191.83	203.27	22.89	
Speed (V)	60	90	120	242.89	248.16	253.43	10.54	22.66
				185.77	191.83	197.89	12.12	
Dynamic Factor	1.1	1.49	1.73	196.7	248.16	239	51.46	102.86
				149.9	191.83	201.3	51.4	
Static Wheel load	67.5	100	150	198.57	248.16	324.46	125.89	205.3
				160.54	191.83	239.95	79.41	
Foundation Modulus	20	50	100	239.48	248.16	250.17	10.69	30.5
				207.92	191.83	188.11	19.81	
Sleeper Spacing	500	600	700	241.98	248.16	254.27	12.29	36.79
				179.65	191.83	204.15	24.5	
Type of Sleeper	Wood	Concrete	Steel	247.85	248.16	247.96	0.31	0.88
				192.4	191.83	192.2	0.57	
Effective Area of Sleeper	0.4	0.48	0.6	247.14	248.16	249.05	1.91	5.45
				193.71	191.83	190.17	3.54	
E modulus rail	200	205	210	245.95	248.16	250.38	4.43	9.53
				189.28	191.83	194.38	5.1	
Poisson	0.289	0.3	0.33	247.99	248.16	248.62	0.63	1.42
				192.04	191.83	191.25	0.79	
Eccentricity of Vertical force Q	-0.022	0	0.022	281.14	248.16	215.18	65.96	107
				203.29	191.83	232.87	41.04	
Position of Lateral force below top	0	0.007	0.015	250.59	248.16	245.39	5.2	11.67
				188.81	191.83	195.28	6.47	
Rail section	48	57	S60	271.44	248.16	258.97	23.28	65.11
				218.95	191.83	177.12	41.83	
Wheel distances	1.56	1.91	10.06	250.4	248.16	220.79	29.61	84.5
				187.68	191.83	242.57	54.89	
Max Temperature change	30	42	55	220.86	248.16	277.74	56.88	113.77
				164.52	191.83	221.41	56.89	
Lateral force factor	0	0.4	0.8	166.45	248.16	329.88	163.43	194.16
				177.04	191.83	207.77	30.73	

This exercise should therefore be seen as an initial step to highlight important parameters in order to focus the attention on areas where the greatest impact can be made in the improvement of the current model. The quantitative sensitivity analysis can be regarded as a simplistic method for determining parameter sensitivity since it does not take the effect of different combinations of high and low parameter values into account. It was therefore decided to validate the findings of the quantitative sensitivity analysis with a qualitative sensitivity analysis where random combinations of parameter values are used in identifying sensitive parameters.

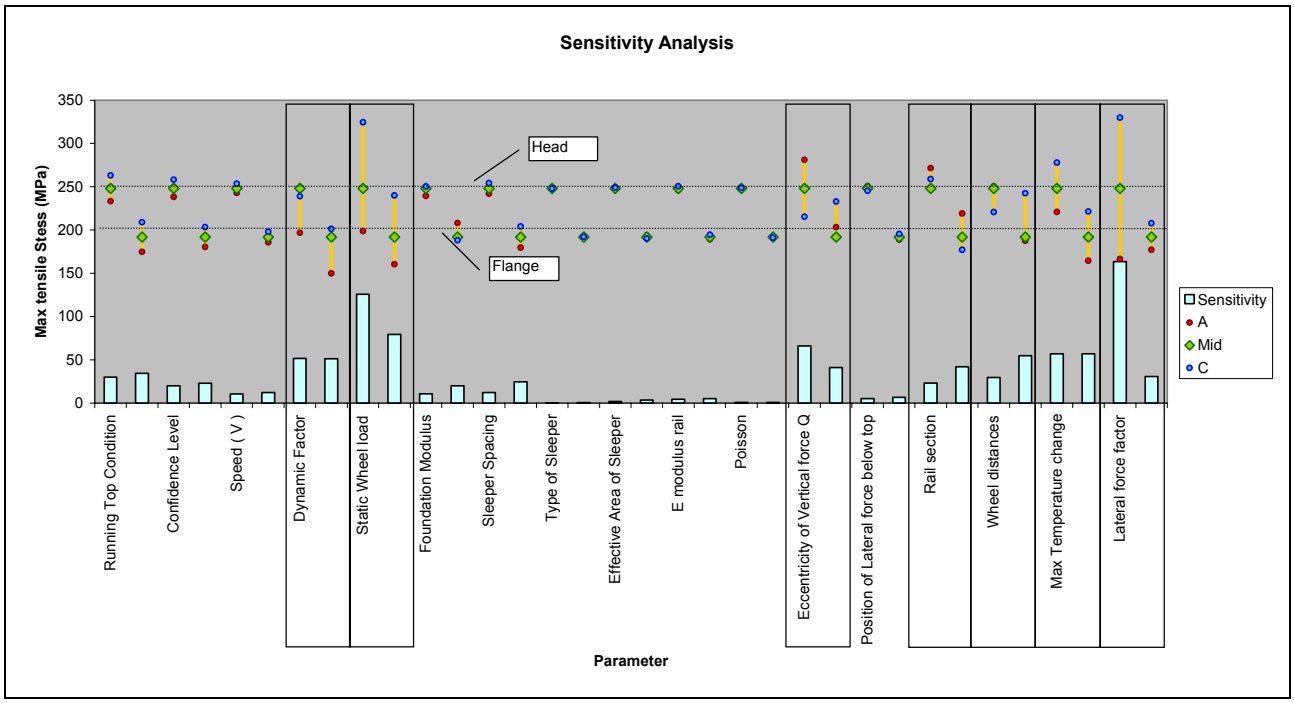

Figure 3-13: Sensitivity analysis of parameters in component stress calculation spreadsheet

Table 3-5: Order of sensitive parameters

Order of Importance	Parameter	Sum of Head & Flange Stress Band widths	Percentage of highest value
1	Static Wheel load	205	100%
2	Lateral force factor	194	95%
3	Max Temperature change	114	55%
4	Eccentricity of Vertical force Q	107	52%
5	Dynamic Factor	103	50%
6	Wheel distances	85	41%
7	Rail section	65	32%
8	Running Top Condition	64	31%
9	Confidence Level	43	21%
10	Sleeper Spacing	37	18%
11	Foundation Modulus	31	15%
12	Speed (V)	23	11%
13	Position of Lateral force below top	12	6%
14	E modulus rail	10	5%
15	Effective Area of Sleeper	5	3%
16	Poisson	1	1%
17	Type of Sleeper	1	0%

3.3.2. Qualitative sensitivity analysis

Marczyk's book, "Beyond Optimization in CAE (Computer Aided Engineering)" (12), inspired the use of his philosophy of stochastic simulation as an alternative method to evaluate the sensitivity of

the analytical method towards its input parameters. In this case, the input parameters of the analytical method were randomly changed between their lowest and highest values and the stress results of the rails evaluated accordingly for each random combination of parameters. Figure 3-14 indicates the railhead stresses vs. the rail flange stresses for a number of random combinations of input parameters. The tensile stresses at the railhead and flange were plotted against each other in Figure 3-14 to Figure 3-16, to investigate not a correlation between these two output parameters, but the spread of their values due to changes in the input parameters. Using such 2D plots creates a visual aid for investigating the effect of the changing input parameters on the output parameters chosen. Since each data point is generated from randomly changed input parameters, numerous graphs like this can be generated, with each graph displaying a unique data scatter. A point to note, however, is that the data form "point clouds" which are a phenomenon found in each generated graph. Additional graphs (iterations from the same model) are presented in Appendix A, which indicate not only the similarities between such randomly generated data points graphs, but also the possible changes in outliers.

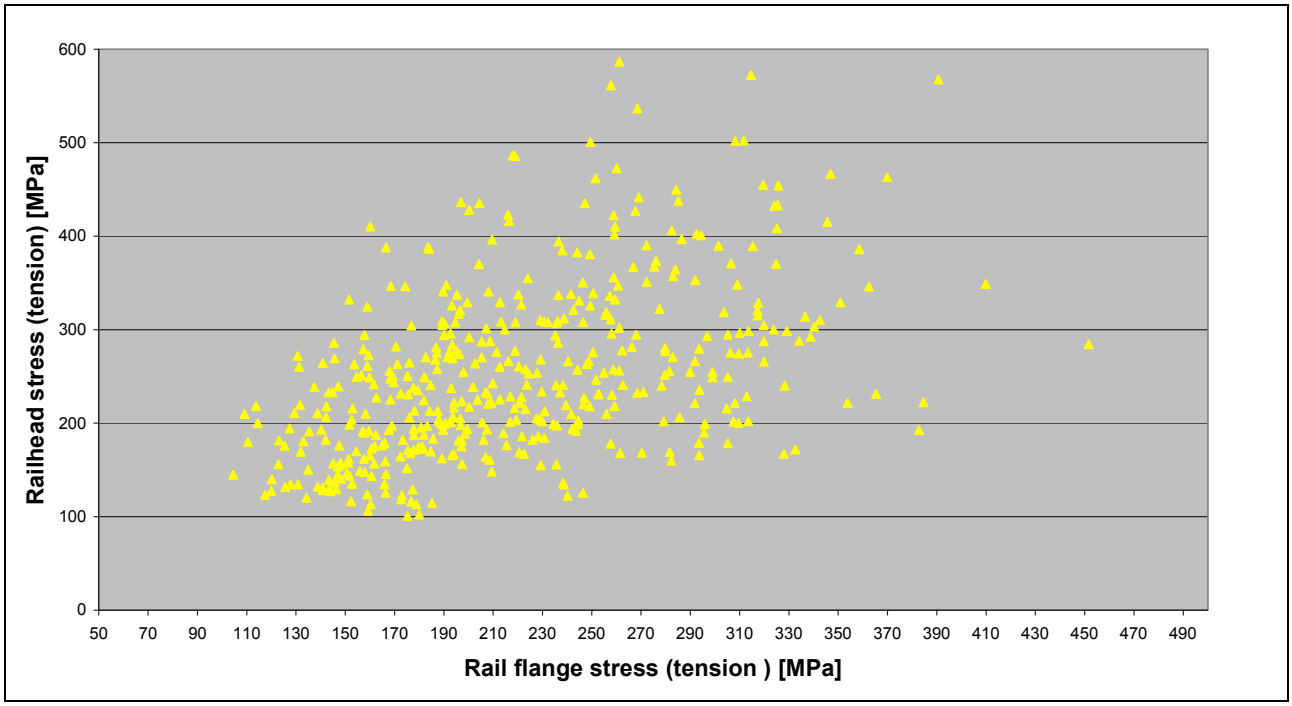

Figure 3-14: Stochastic distribution of rail stresses from the analytical method

The main objective of stochastic simulation is to get an impression of possible ranges of answers to a problem instead of focusing on only one answer. The data scatter produced in Figure 3-14 will collapse into one data point if each input parameters is changed to one specific value. Studying the patterns of the data scatter in these results therefore provides the engineer with a more holistic impression of the problem than studying only a few isolated data points or fixed combinations of input parameters.

The next step was to eliminate parameters by holding them constant in turn and evaluating the effect on the data scatter. In using this method, the sensitivity of the model towards the different parameters was thus qualitatively evaluated, instead of quantitatively as in the previous method.

Figure 3-15 indicates the data scatter when a number of input parameters are held constant as indicated in Table 3-6. Figure 3-16 indicates the resulting data scatter when the parameters, which were held constant in Figure 3-15, are changed randomly while the remaining parameters are held constant.

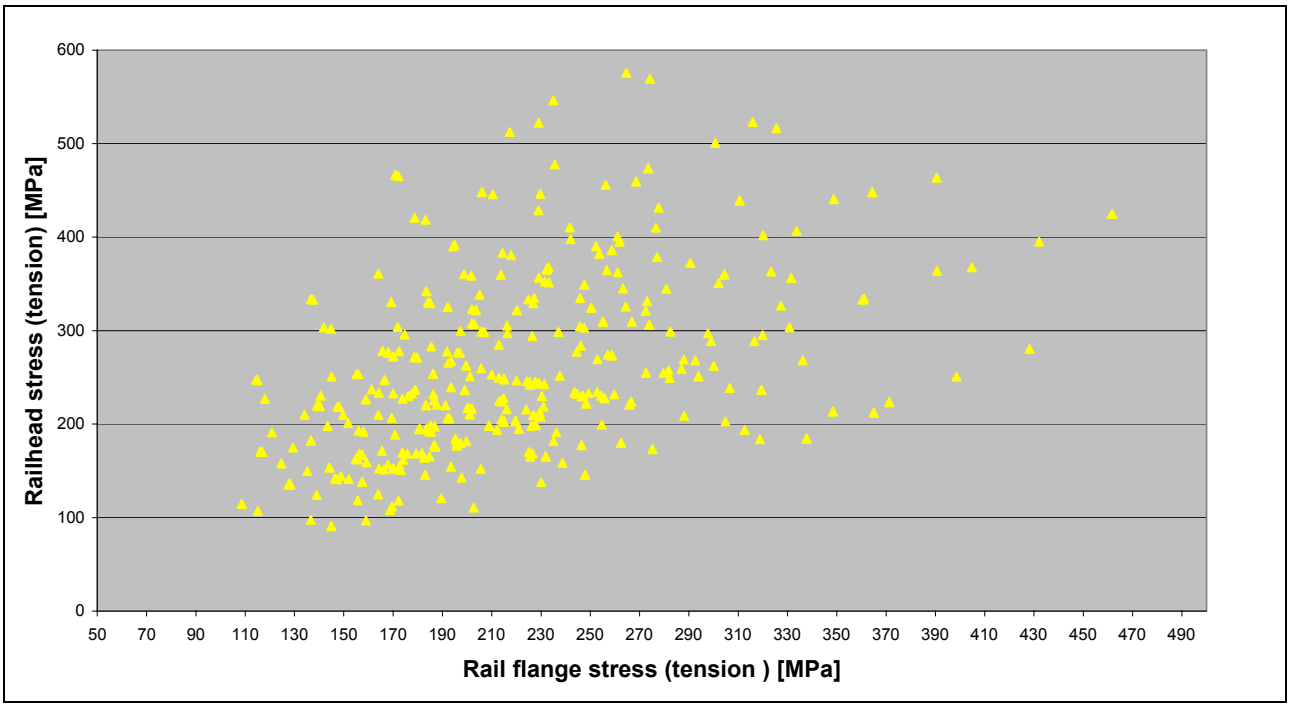

Figure 3-15: Stochastic distribution of rail stresses with a number of parameters held constant

The number of unique data points was subsequently reduced but the spread of data points (or rail stress ranges) was still similar to those of Figure 3-14 and Figure 3-15. Figure 3-16 indicates a dramatic reduction in data scatter due to the parameters as listed in Table 3-6 being held constant. From Figure 3-15 and Figure 3-16 it is clear that the parameters that affect the rail stresses the most are indeed those that were determined earlier and indicated here in Table 3-7.

Table 3-6: List of parameters modified in stochastic simulation results of Figure 3-15 and Figure 3-16

	Parameter	Held Constant?	
		Figure 3-15	Figure 3-16
1	Static Wheel load	No	Yes
2	Lateral force factor	No	Yes
3	Max Temperature change	No	Yes
4	Eccentricity of Vertical force Q	No	Yes
5	Dynamic Factor	No	Yes
6	Wheel distances	No	Yes
7	Rail section	No	Yes
8	Running Top Condition	Yes	No
9	Confidence Level	Yes	No
10	Sleeper Spacing	Yes	No
11	Foundation Modulus	Yes	No
12	Speed (V)	Yes	No
13	Position of Lateral force below top	Yes	No
14	E modulus rail	Yes	No
15	Effective Area of Sleeper	Yes	No
16	Poisson	Yes	No
17	Rail steel type	Yes	No
18	Type of Sleeper	Yes	No

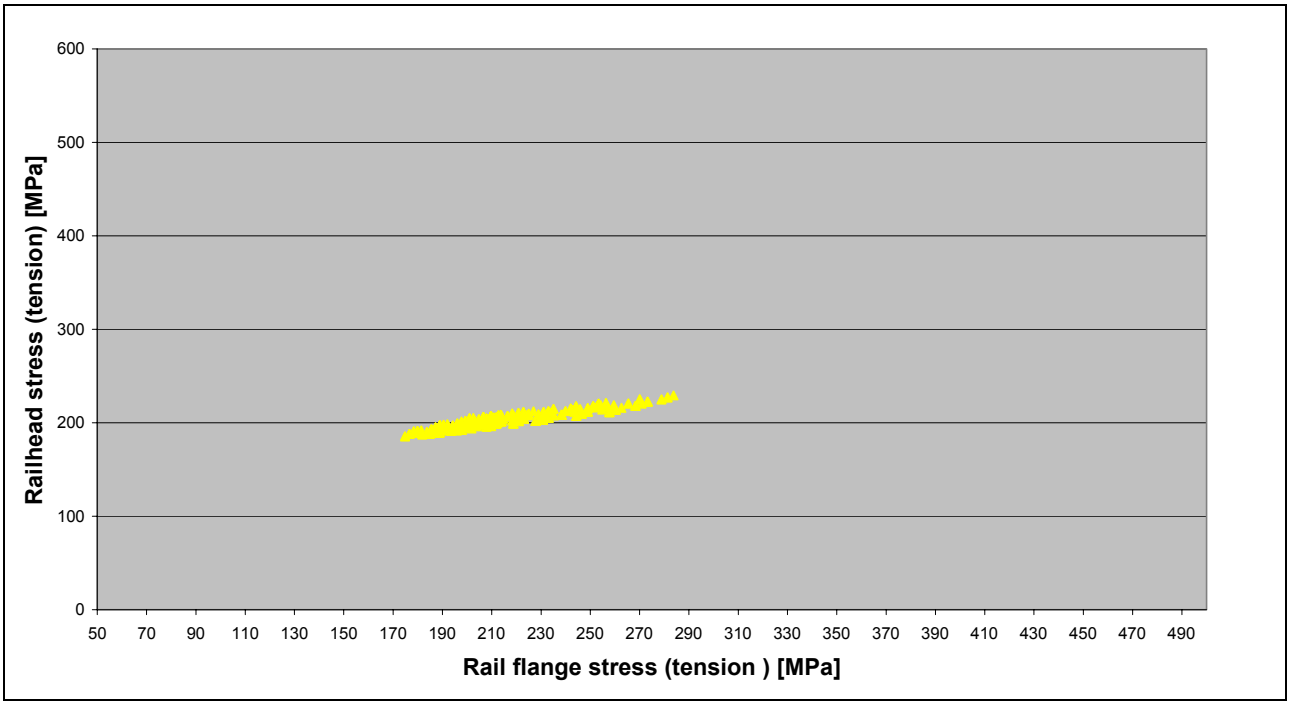

Figure 3-16: Stochastic distribution of rail stresses with a number of parameters held constant

Table 3-7: Most sensitive input parameters of the analytical method

	Most Sensitive Input Parameters	Uniquely Identifiable?
1	Static Wheel load	Yes
2	Lateral force factor	No
3	Max Temperature change	Yes
4	Eccentricity of Vertical force	No
5	Dynamic Factor	No
6	Wheel distances	Yes
7	Rail section	Yes

Table 3-7 also indicates whether or not the input parameter values are uniquely identifiable (or uniquely obtainable), which is of importance for the purpose of this study.

Because it is vitally important that the parameters, to which the model is most sensitive and for which confidence is lacking in the values used, are correctly entered, the following three parameters will be researched: dynamic factor, lateral force factor and the eccentricity of the vertical force.

3.4. Conclusion

The analytical method is a method utilised to calculate rail stresses under dynamic loading by factoring the static load with an appropriate amount and calculating track component stresses by means of a static analysis. This method employs input parameters, which describe the loading conditions and track design and then calculate track component stresses directly. The analytical method is fast and easy-to-use in evaluating different loading conditions or different track designs without having to modify the model and proved capable of providing results, which correlate well with other proven methods and empirical tests. For this reason, the shortcomings and limitations of the method were investigated in order to improve on them and further enhance the analytical method for calculating track component stresses.

4 IMPROVEMENTS TO THE ANALYTICAL METHOD

The analytical method has proven to be valuable in calculating track component deflections and stresses under vehicle loads with reasonable accuracy as validated with empirical and other well-established methods. It was, however, discovered that the current analytical method had its limitations. These limitations were mostly related to input parameters for which the user would have difficulty in supplying reasonable (or correct) values and to which the results were the most sensitive. It is the intention of this chapter to identify the shortcomings of the analytical method, to improve on it where possible and to provide the user with guidelines and some nominal values for input parameters that may be used in future stress calculations.

4.1. Investigations into the improvements of the analytical method

From the sensitivity analyses it was discovered that the dynamic factor, lateral force factor and the eccentricity of the vertical force were the three parameters that the analytical method was the most sensitive to and for which the user may have the greatest difficulty in obtaining reasonable (or correct) values. A number of empirical tests were conducted in separate studies which were utilised to determine the best practice approaches in obtaining these input parameter values. It will further provide the user with some nominal values and/or ranges of values to be used in the event that empirical testing is not possible.

The following section will focus on the dynamic factor which is an important parameter in the analytical method since it is the parameter to which the model is the most sensitive.

4.1.1. Dynamic Factor

The influence of moving loads on the track structure cannot be ignored since loads under dynamic conditions are higher than the same loads under static conditions (24, p. 107), (25, p. 1). This increase in load is referred to as the dynamic factor or dynamic amplification (26, p. 5), (10, p. 1-4) and is determined, either empirically or numerically, with appropriate models by comparing the static wheel loads on the rail or structure to the loads when the same wheels are moving over at speed.

Since the analytical method is the most sensitive towards the static load, which directly affects the dynamic factor, the dynamic factor will be investigated here under the assumption that the static load is known. The loads affecting the track can be divided into horizontal and vertical forces. The vertical forces are a function of the static wheel load and wheel load shifting due to the slanting and swaying

of the vehicle (25, p. 1). The slanting of the vehicle is affected by the radius of the curve (27), the amount of super elevation of the track, the travelling speed, and the height of the centre of gravity of the vehicle. Timoshenko (21, p. 412) introduced a further possible cause to the magnifying effect of moving loads, namely, the vibration of the rails under moving loads. Wilson (24, p. 125), however, regards this contribution as negligible under low speeds. Dynamic loads are not only higher than static loads because of the above-mentioned factors, but also because of impact loads. According to Wang (17), there are two kinds of factors that cause high impacts between wheel and rail, namely, those resulting from the vehicle, and those resulting from the track. Impacts resulting from the vehicle include: wheel abrasion, wheel ovality, flat wheels and wheel eccentricity. The impacts due to the track include: track geometry irregularities, rail joints and track defects underneath the rail such as slacks. The support condition therefore also causes moving loads to be higher than static loads.

Figure 4-1 indicates a skid mark on a rail, which causes impact forces under moving loads. Skid marks are caused by locomotive traction wheelsets that slip and “burn” the rail metal away. Figure 4-2 indicates a flat wheel (skid mark on a wheel thread) that causes impact forces when the wheel rolls over the rail. Wheel flats are the result of excessive braking or brakes that fail to release the wheel, when the vehicle is pulling away. Surface defects on the rail have a detrimental effect on the track structure, and, with the presence of water, may cause "mud holes" such as the one indicated in Figure 4-3. In an investigation on the Sishen Saldanha line, Spoornet found that there is a linear relationship between the vertical track profile and the depth of dip joints (flash butt welds that developed local soft zones) (28). This indicates that the impact due to the surface defects has a detrimental effect on the track geometry, which in turn affects the dynamic loading of the track. Figure 4-4 and Figure 4-5 indicate typical dip joints.

Figure 4-6 indicates an attempt to relate track vertical alignment to the resulting dynamic vertical forces. The results show that there exists no definite relationship for this specific data set, which were measured in Sweden by the Spoornet Engineering team (29).

The results in Figure 4-6 underline the statement in the UIC Code 518 OR (30, p. D-1) which states that"*...it is difficult to draw a simple relation between track-geometry and vehicle response. As a result, it is not possible either to relate a geometrical value to a track geometric quality or a given track geometrical error to a vehicle-response.*"

One of the options of calculating a dynamic factor using a quasi-static calculation is to use an empirically determined formula. Many such formulas have been developed in the past and will be discussed in the next section.

Figure 4-1: Skid mark on rail running surface

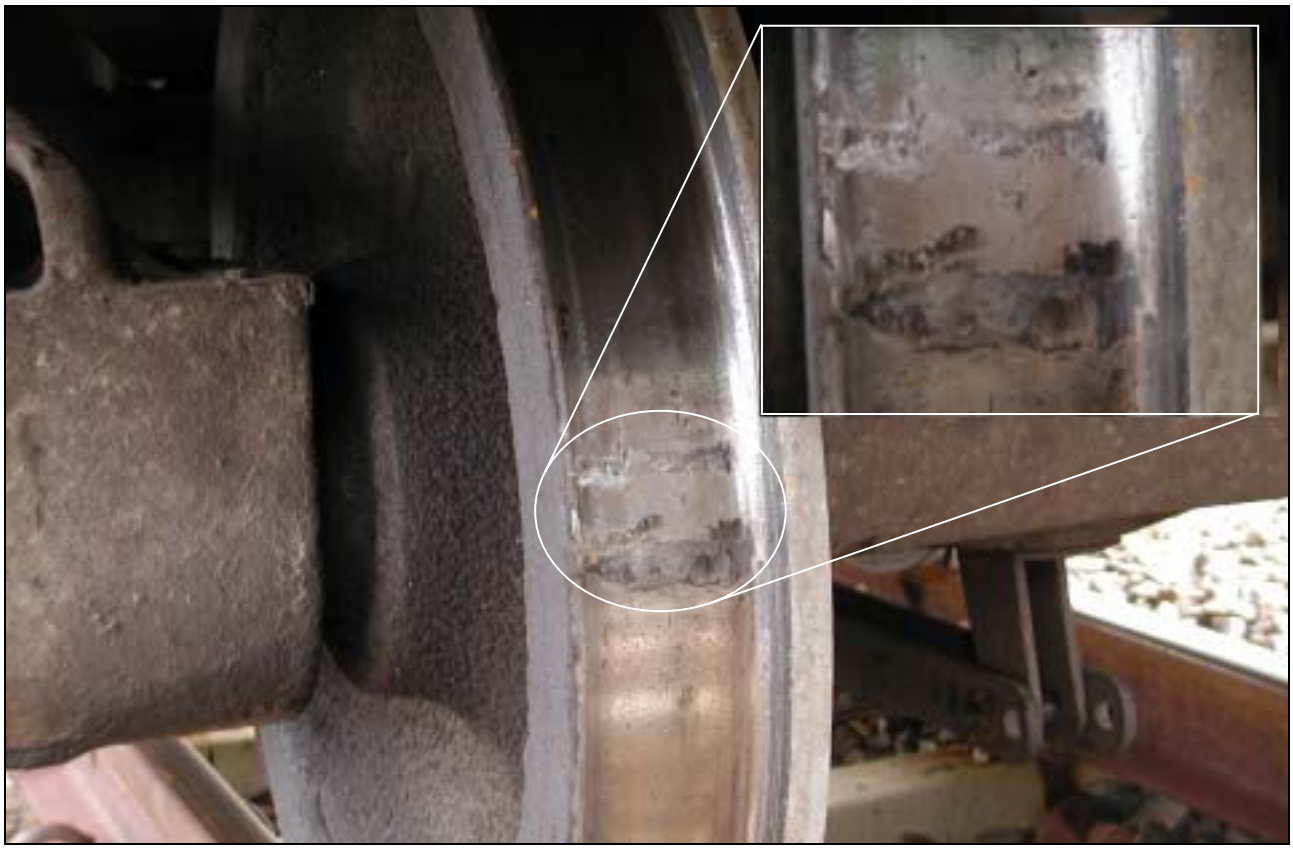

Figure 4-2: Skid mark on wheel tread ("flat wheel")

Figure 4-3: The presence of water and excessive track deformation pump mud to the surface

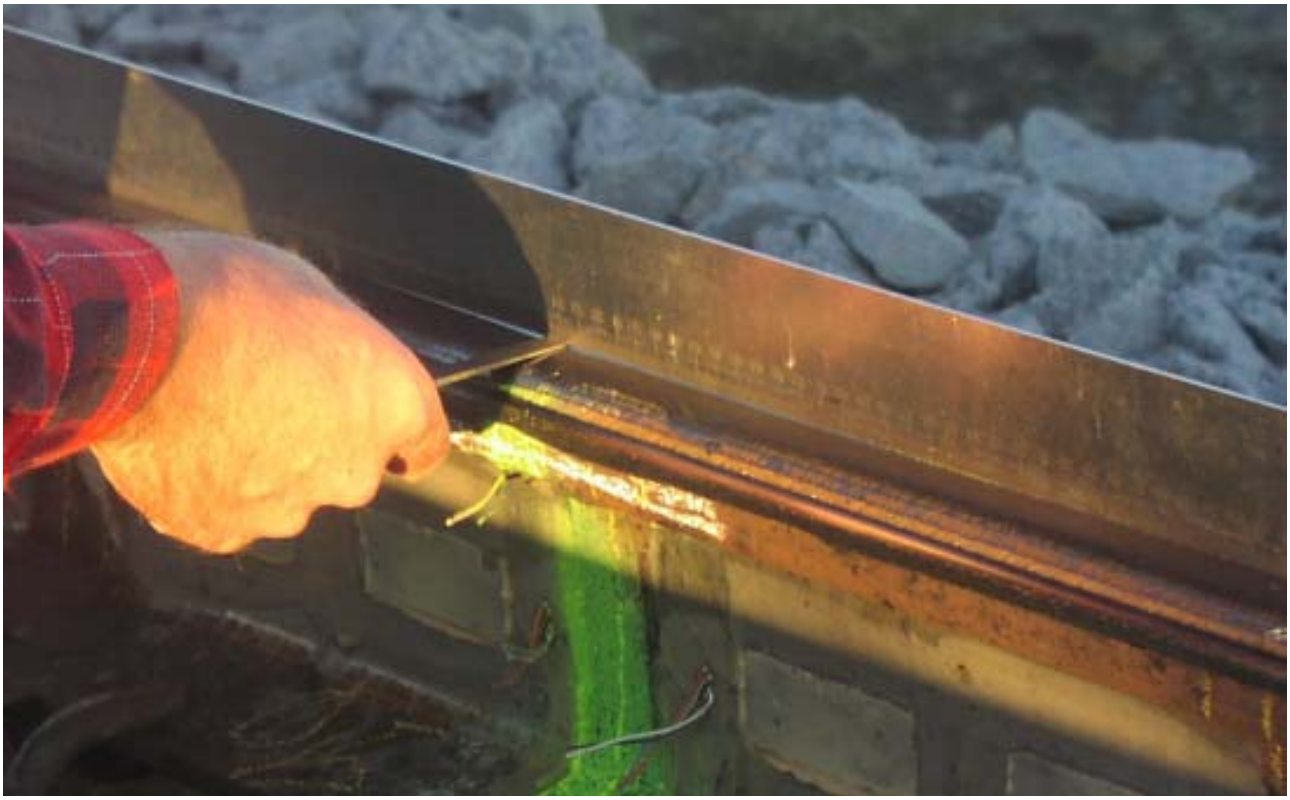

Figure 4-4: Measuring the depth of a dip joint (soft flash butt weld)

Figure 4-5: Dip joint identified by two wider patches on the contact band

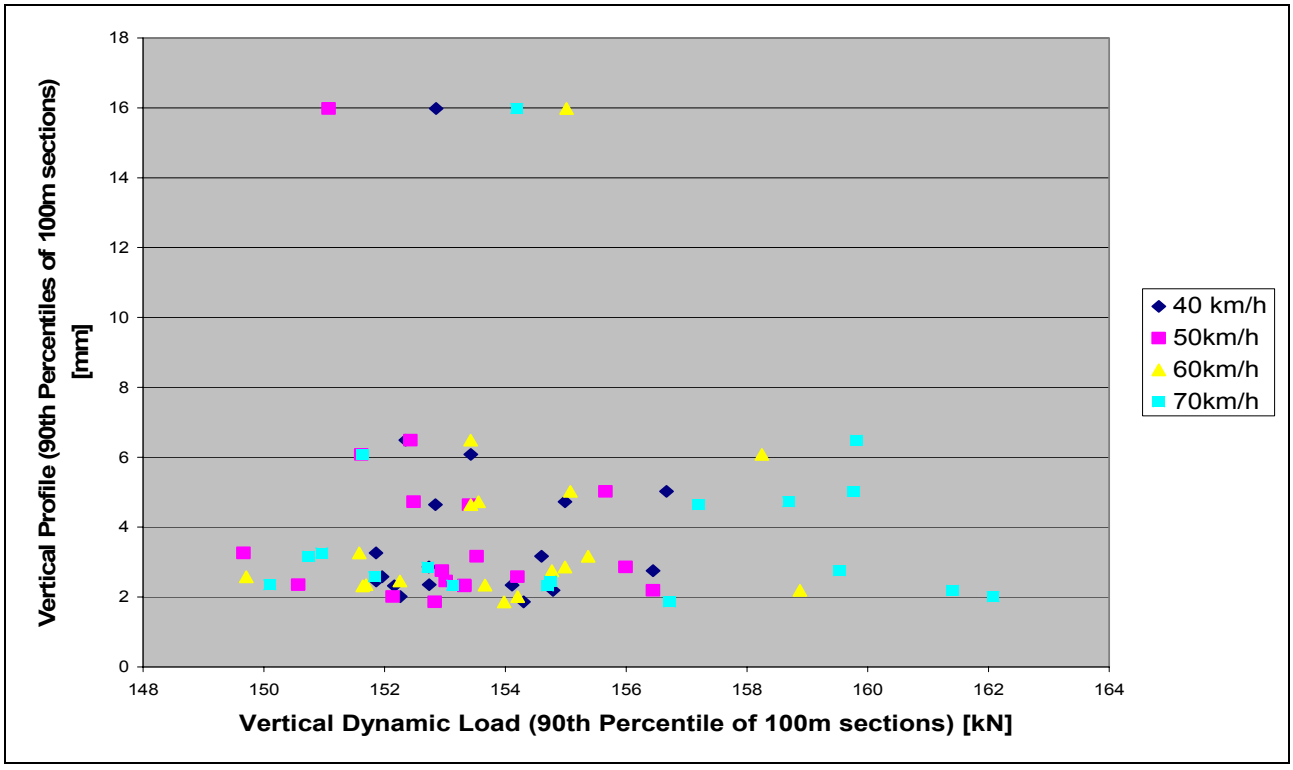

Figure 4-6: Track geometry vertical alignment vs. dynamic loads

4.1.1.1. Empirical Formulas

In order to investigate the magnitude of typical dynamic factors, current widely accepted empirical formulas were investigated and compared to measurements. According to Esveld (1, p. 83), it is common practice to carry out strength or fatigue calculations for a static system in which the dynamic effects are taken into account by a speed coefficient or a dynamic amplification factor. Researchers over the world have investigated the magnifying effect of dynamic loads and produced various empirically determined formulas. According to Lombard (31), various researchers demonstrated that the average results obtained from extensive track measurements are in accord with theoretical predictions using static wheel loads as input. A number of empirical formulas were investigated, namely, that of Eisenmann (19), Schramm (25), Klöckner (25), Clintock (25), ORE and AREA as summarised by Wang (17) and listed in Table 4-1.

Table 4-1: List of empirical formulas for the calculation of a dynamic factor

1.	Eisenmann	$\phi = 1 + \delta \cdot \left(1 + \frac{V - 60}{140}\right) \cdot t'$
2.	Schramm	$\varphi = 1 + 45 \cdot 10^{-6} \cdot V^2 + 15 \cdot 10^{-8} \cdot V^3$
3.	Klöckner (Light traffic)	$\varphi = 1 + 20 \cdot 10^{-4} \cdot V - 5 \cdot 10^{-6} \cdot V^2$
4.	Klöckner (Heavy traffic)	$\varphi = 1 + 25 \cdot 10^{-4} \cdot V - 7 \cdot 10^{-6} \cdot V^2$
5.	AREA	$\varphi = 1 + 5.21 \cdot V/D$
6.	ORE	$\varphi = 1 + 0.04 \cdot \left(\frac{V}{100}\right)^3 + \frac{V^2(2 \cdot h + c)}{127 \cdot R} - \frac{2 \cdot c \cdot h}{g^2} + \left(0.1 + 0.017\left(\frac{V}{100}\right)^3\right) a_0 \cdot b_0$
7.	ORE (V<140km/h)	$\varphi = 1.29 + 0.04 \cdot \left(\frac{V}{100}\right)^3$

Figure 4-7 and Table 4-1 indicate a comparison by Wang (17) of empirical formulas which calculate dynamic factors. A number of results from the Eisenmann formula are indicated in Figure 4-7 and Table 4-2. The results are distinguished by two numbers in the legend, which relate to the track geometry condition and statistical confidence. These factors are not included in the other empirical formulas. In Figure 4-7 and Table 4-2, "Eisen 1 0.1" indicates the results from the Eisenmann formula for a good track geometry {0.1}, and a low statistical confidence {1}, whereas "Eisen 3 0.3" indicates the results from the Eisenmann formula with a bad track geometry {0.3} and high statistical confidence {3}.

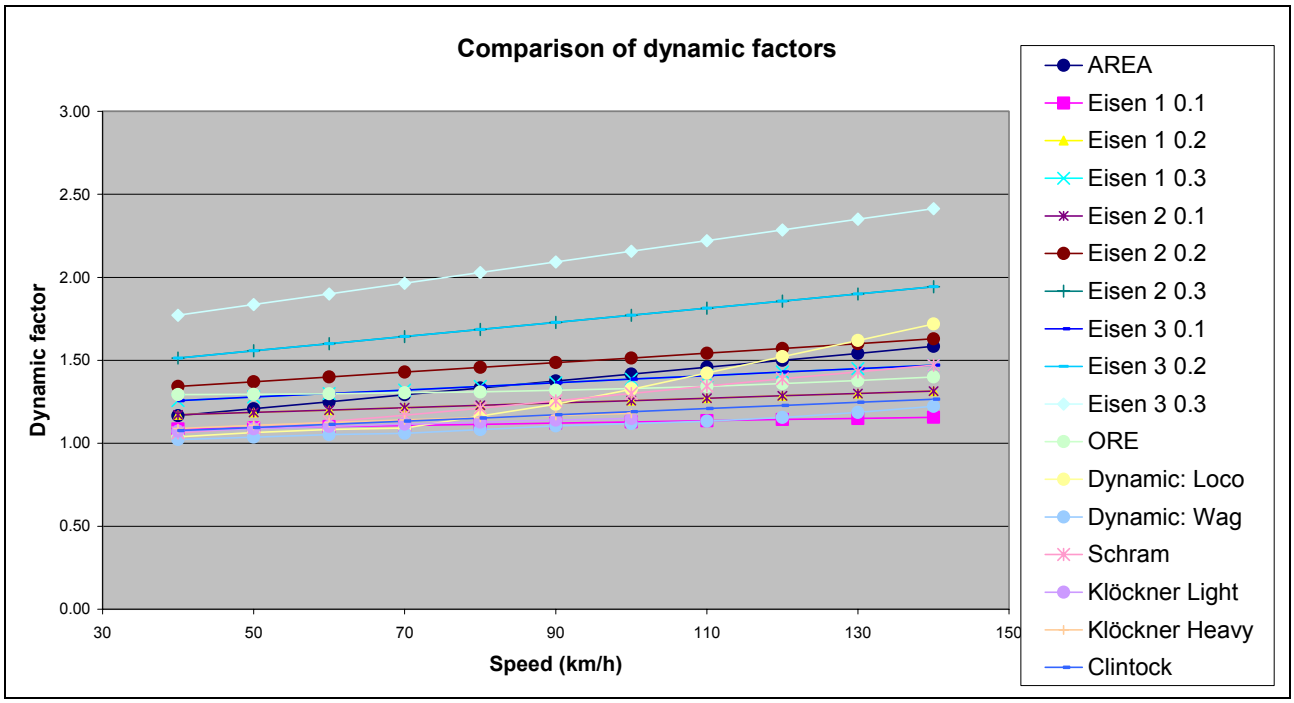

Figure 4-7: Comparison of dynamic factors from different empirical formulas

Table 4-2: Comparison of dynamic factors from different empirical formulas

Speed (km/h)	40	50	60	70	80	90	100	110	120	130	140
AREA	1.17	1.21	1.25	1.29	1.33	1.38	1.42	1.46	1.50	1.54	1.58
Eisen 1 δ=0.1	1.09	1.09	1.10	1.11	1.11	1.12	1.13	1.14	1.14	1.15	1.16
Eisen 1 δ=0.2	1.17	1.19	1.20	1.21	1.23	1.24	1.26	1.27	1.29	1.30	1.31
Eisen 1 δ=0.3	1.26	1.28	1.30	1.32	1.34	1.36	1.39	1.41	1.43	1.45	1.47
Eisen 2 δ=0.1	1.17	1.19	1.20	1.21	1.23	1.24	1.26	1.27	1.29	1.30	1.31
Eisen 2 δ=0.2	1.34	1.37	1.40	1.43	1.46	1.49	1.51	1.54	1.57	1.60	1.63
Eisen 2 δ=0.3	1.51	1.56	1.60	1.64	1.69	1.73	1.77	1.81	1.86	1.90	1.94
Eisen 3 δ=0.1	1.26	1.28	1.30	1.32	1.34	1.36	1.39	1.41	1.43	1.45	1.47
Eisen 3 δ=0.2	1.51	1.56	1.60	1.64	1.69	1.73	1.77	1.81	1.86	1.90	1.94
Eisen 3 δ=0.3	1.77	1.84	1.90	1.96	2.03	2.09	2.16	2.22	2.29	2.35	2.41
ORE	1.29	1.30	1.30	1.30	1.31	1.32	1.33	1.34	1.36	1.38	1.40
LOCO *2	1.04	1.07	1.08	1.09	1.16	1.24	1.33	1.42	1.52	1.62	1.72
WAGON *3	1.02	1.04	1.05	1.06	1.08	1.10	1.12	1.13	1.16	1.19	1.22
Schram	1.06	1.09	1.13	1.17	1.21	1.26	1.30	1.34	1.39	1.43	1.47
Klöckner Light	1.07	1.09	1.10	1.12	1.13	1.14	1.15	Only valid for V<=100km/h			
Klöckner Heavy	1.09	1.11	1.12	1.14	1.16	1.17	1.18				
Clintock	1.08	1.09	1.11	1.13	1.15	1.17	1.19	1.21	1.23	1.25	1.27

The average value of the dynamic factors listed in Table 4-2 is equal to 1.38, with the minimum being 1.086 as calculated at 40 km/h with the Eisenmann formula (with an excellent track geometry and a 68.3% statistical confidence) and a maximum of 2.414 as calculated at 140 km/h with the Eisenmann formula (with a bad track geometry and 99.7% statistical confidence).

The majority of empirical formulas is in agreement with values between 1 and 1.5, the exception being the Eisenmann formula (values of 1.7 to 2.4) when a statistical confidence of 99.7% is chosen. Esveld (1, p. 84) suggests the use of a statistical confidence of 99.7% when investigating rail stresses and a lower statistical confidence when investigating ballast and sub-formation stresses.

Because of uncertainty regarding the validity of these empirical formulas for local track and rolling stock conditions, data from field tests were investigated to determine typical dynamic factors

4.1.1.2. Empirical Tests

Data from empirical tests are useful when determining dynamic factors since they represent local track and operating conditions. Dynamic factors can be determined from field measurements where static loads from vehicles are known and are then compared to their measured load under dynamic conditions. These tests can be performed with wayside (weigh-in-motion) measurements or with instrumented wheelset measurements.

(i) Weigh-in-motion weighbridges

The weighbridges on Spoornet track measure the load of each passing truck wheel at operational speed. These weighbridges are specially calibrated to determine the static loads of each passing wheel by utilising a dynamic factor to convert the vertical force of the wheel to a static load value. Thus, extracting the dynamic factors used in the weighbridges provides representative dynamic factors applicable for local track and rolling stock conditions. The weighbridges are firstly statically calibrated at installation with a load cell rig, which is used to load the track to a known value and calibrate the system accordingly. After this is performed, the software analyses the signals as a train passes and reports the measured values. These values are not the static loads of the vehicles but the dynamic loads as measured by the weigh-in-motion system. The system is calibrated with the use of a test train, with wagons which were measured at an SABS certified static weighbridge. The calibration is done at various speeds and in both directions. The dynamic factors are then calculated by comparing the measured values with the known static wheel loads. If the weighbridge is installed in track where operating conditions permit trains to pass without tractive or braking effort from the locomotives, the measured weight of the locomotives can be compared to design loads as an additional method for calibration. Unfortunately, when the locomotives apply braking or traction while travelling over the weigh bridges, weight transfer takes place on the locomotive bogies and a dynamic or calibration factor cannot be calculated.

Figure 4-8: A complete unmanned weigh-in-motion weighbridge.

At the Saaiwater weigh-in-motion weighbridges, there are three railway lines, each with its own independent weighbridge. Each weighbridge has a number of calibration curves for each direction of travel and for different weight groups of the vehicles. It was found that vehicles from different weight groups (static loads) need different calibration curves since light vehicles tend to have higher dynamic loads in relation to their static loads than heavier vehicles. This is due to a higher undamped mass to damped mass ratio in unloaded vehicles. Because the coal export line is a dedicated line with a closed fleet and only a small amount of general freight traffic, vehicles of similar mass are normally of the same type, which would also contribute to the fact that the different groups have different dynamic factor calibration curves. The following graphs in Figure 4-9 to Figure 4-11 indicate the dynamic calibration factor curves for the three weighbridges at Saaiwater.

The results from the calibration curves indicate dynamic factors of less than 1.2 for the whole range of vehicles and speeds, which is less than the dynamic factors calculated with the empirical formulas. This could, however, be due to the high standard of track maintenance in these areas.

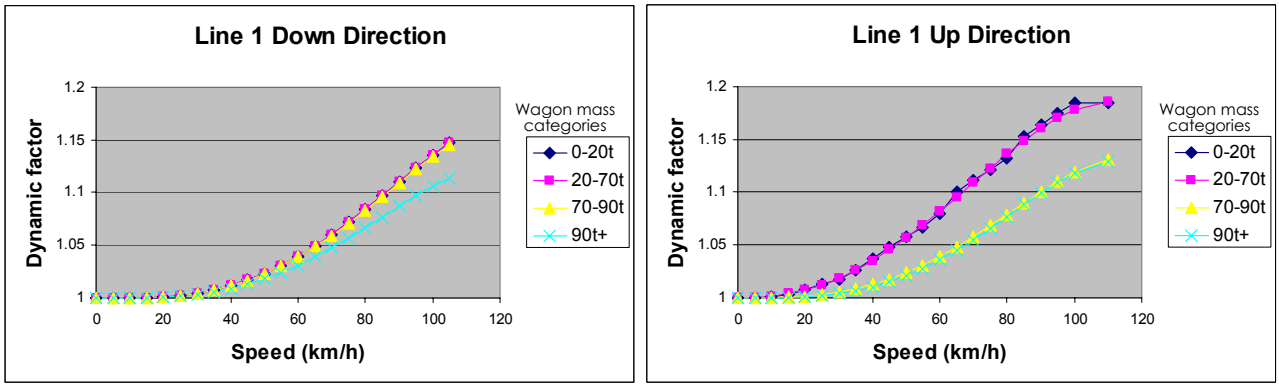

Figure 4-9: Calibration curves for weighbridge on No1. line at Saaiwater

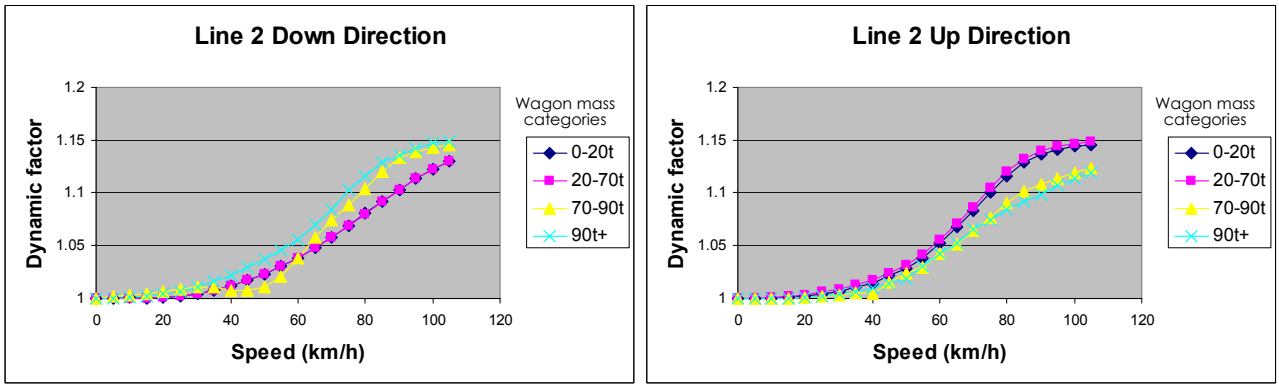

Figure 4-10: Calibration curves for weighbridge on No2. line at Saaiwater

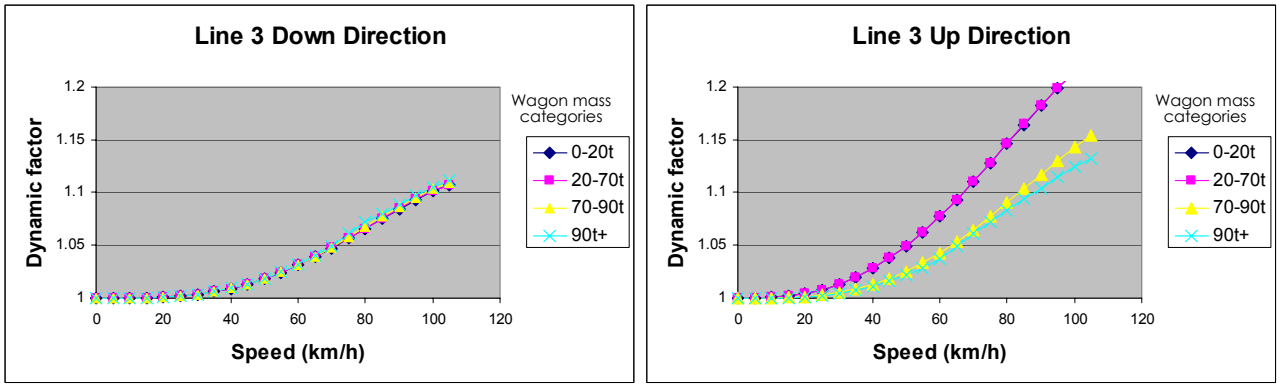

Figure 4-11: Calibration curves for weighbridge on No3. line at Saaiwater

Table 4-3: Track setup at Saaiwater weighbridges

Track setup	Line 1	Line 2	Line 3
Rail type	57*kg/m*	57*kg/m*	S60*kg/m*
Sleeper spacing	700*mm*	700*mm*	650*mm*

As mentioned before, wheel irregularities may also cause high impact loads on the track, resulting in loads higher than the static wheel loads.

Figure 4-12 indicates a typical wheel load signal as captured by a weigh-in-motion weigh bridge. As the wheel rolls along the track, the wheel load is recorded and should, under perfect circumstances, follow the 'pink' line as portrayed by the "perfectly round wheel" data series. If the wheel however has a flat spot or any other imperfection, the captured data may look like the 'blue' data series portrayed by the "Wheel with a flat spot" data series. The impact load is clearly distinguishable from the nominal wheel load since it occurs within a short distance compared to the wheel circumference.

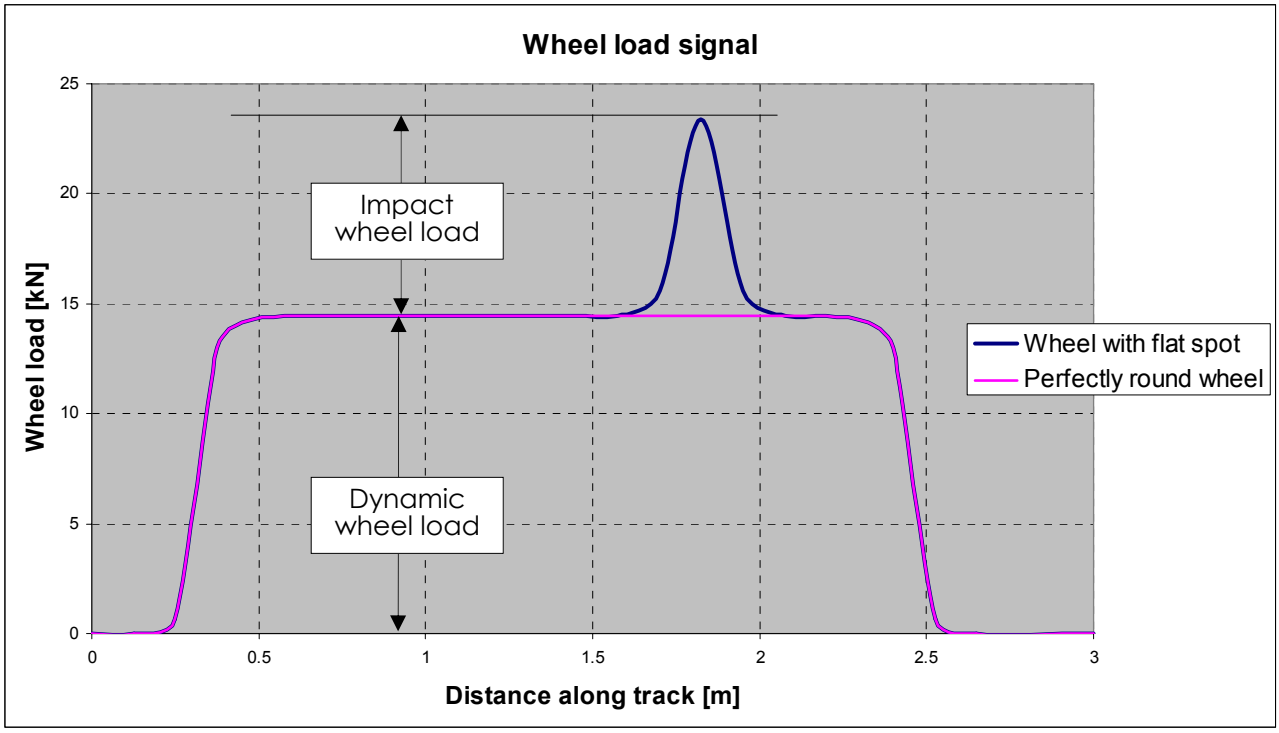

Figure 4-12: Wheel impact load presentation

Figure 4-13 to Figure 4-15 indicate the distribution and magnitude of significant impact loads (higher than 5 tons) as identified at the Saaiwater weigh-in-motion stations. However, these impact loads, although substantially higher than the static wheel loads (up to 44 tons in one instance), only occurred on 0.3% of 1.9 million wheels (Line 1), 0.03% of 1.8 million wheels (Line 2) and 0.06% of 2.6 million wheels (Line 3) respectively. It is important to take note of these high impact loads when designing railway track, but, due to their rare occurrences, it would be uneconomical to design the track to be able to carry an infinite number of these high loads.

The cumulative percentages of wheel impact loads indicated in Figure 4-13 to Figure 4-15 (secondary vertical axes) indicate the contribution of significant wheel impact loads (higher than 5 tons) to the

total number of wheel impact loads. The distributions of impact loads are only indicated for impact loads up to 31 tons.

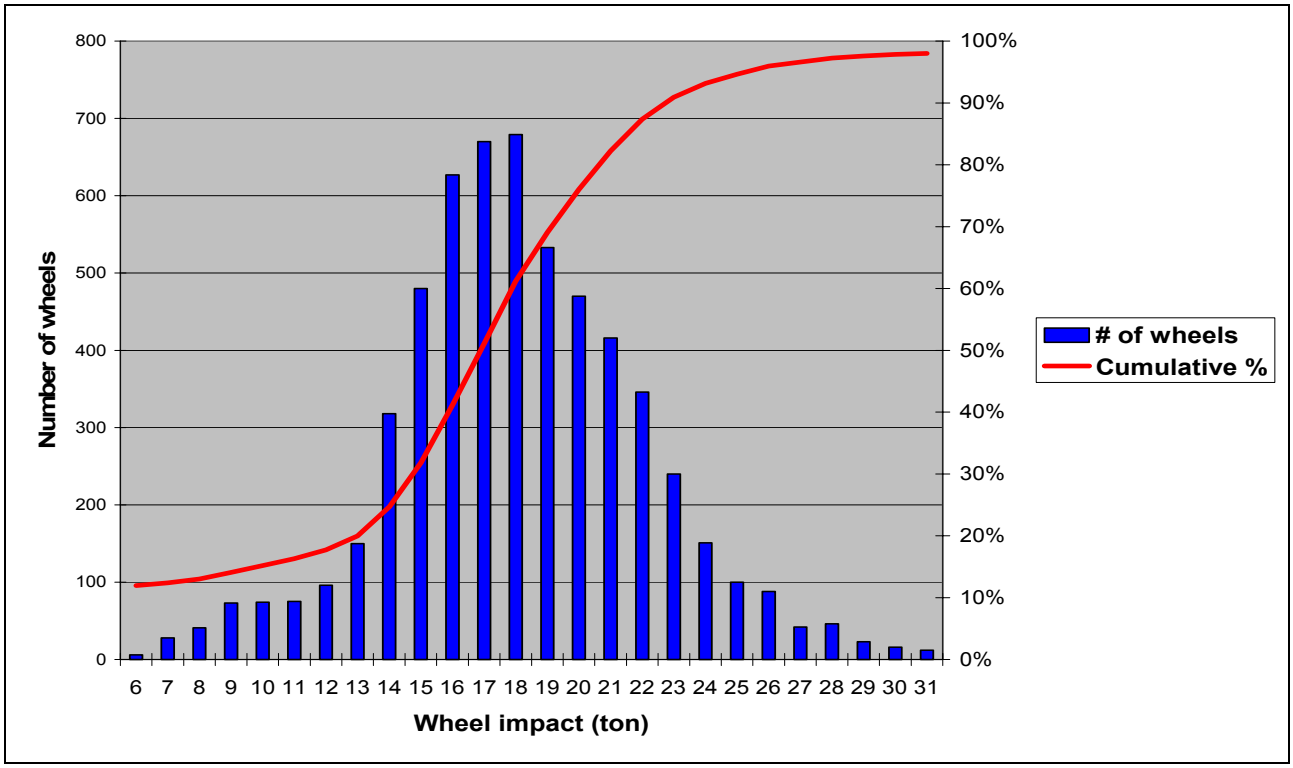

Figure 4-13: Dynamic impact loading distribution (number of wheels) – Line 1

The impact loads from the above figures represent the whole fleet travelling over the Saaiwater weigh bridges (coal export line) which could be much lower than impact loads on other less maintained fleets. Such information should therefore be obtained from weighbridges from the area of interest, if an area specific design is sought, and from weighbridges across the country, if a design is necessary for the worst-case scenario.

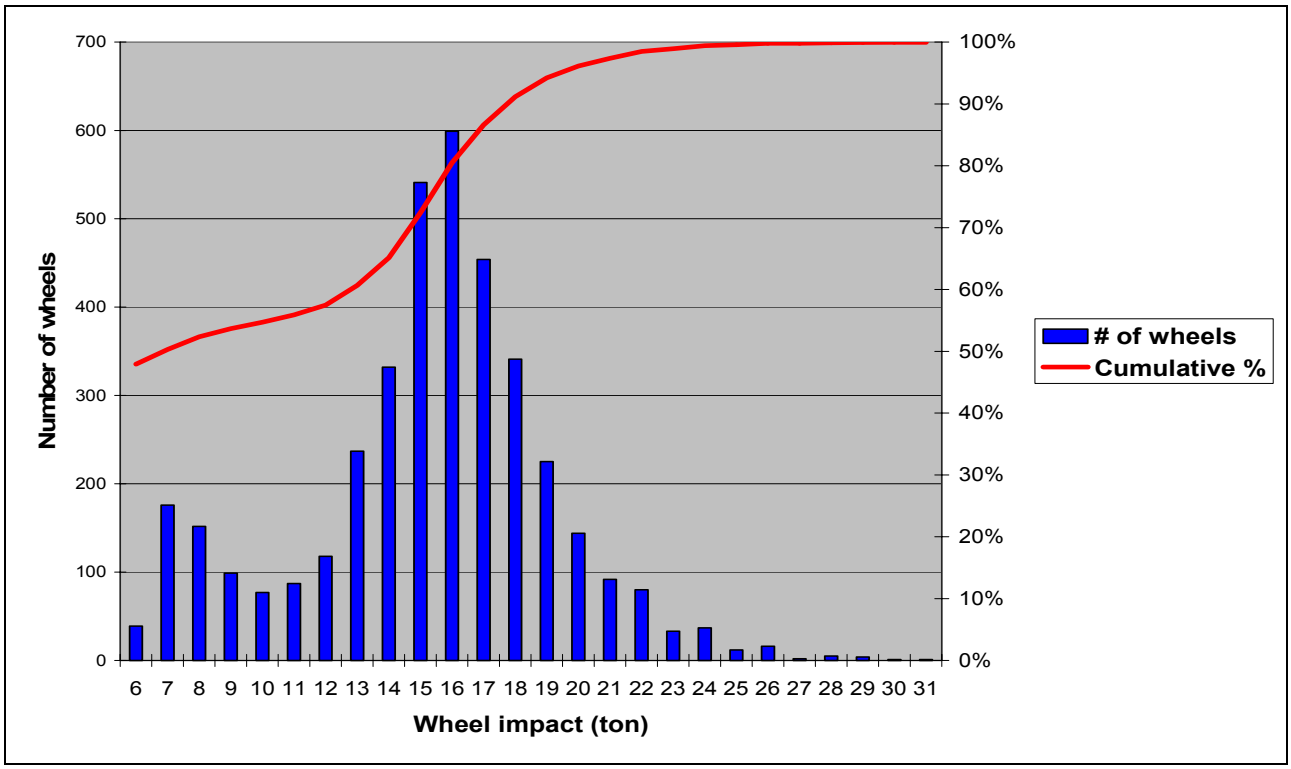

Figure 4-14: Dynamic impact loading distribution (number of wheels) – Line 2

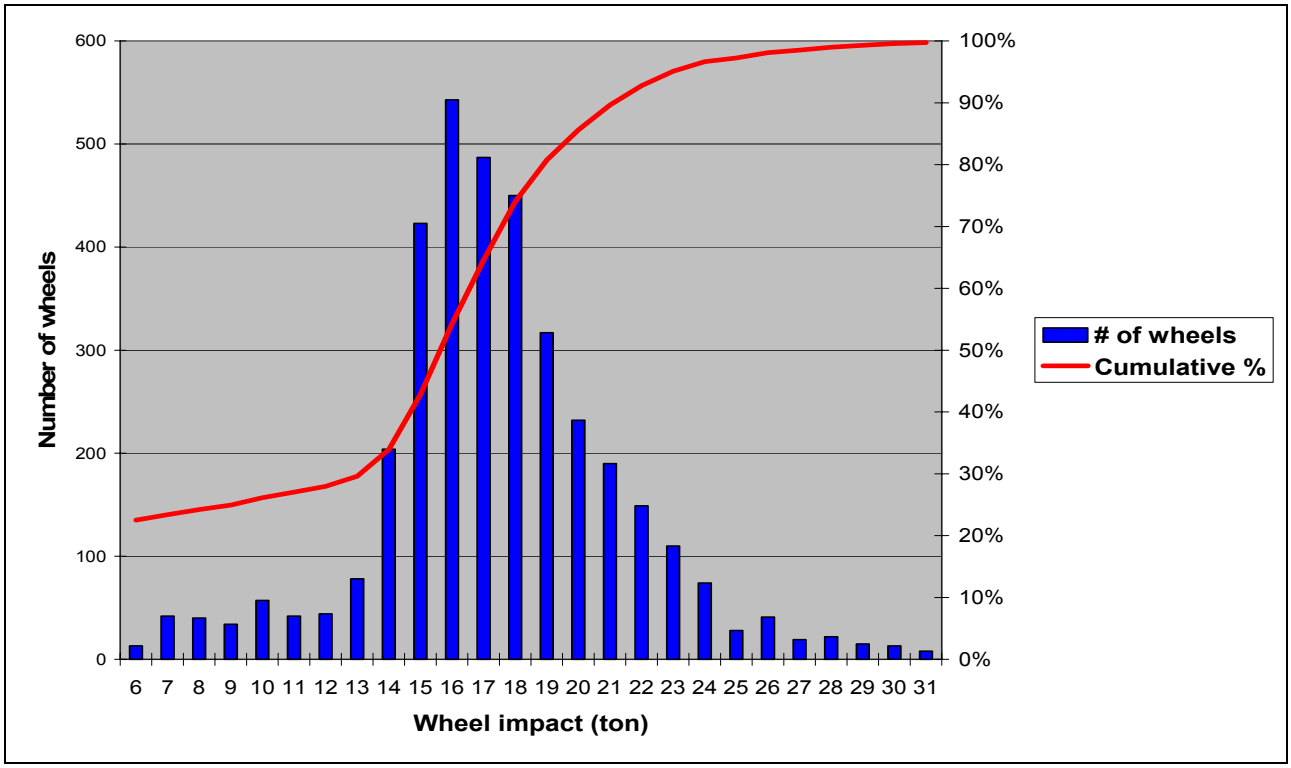

Figure 4-15: Dynamic impact loading distribution (number of wheels) – Line 3

(ii) Way-side measurement tests

The way-side measurement tests use the technology developed for the weigh-in-motion bridges to measure vertical and lateral loads of passing trains, as well as deflections or accelerations of track components. The only difference in the way-side measurements is that the mobile laboratory is used to capture and analyse the data and that the equipment is removed after testing. Figure 4-16 indicates the mobile laboratory with which temporary tests sites can be set up to measure strains, deflections or accelerations of track components.

Figure 4-16: Spoornet mobile laboratory for measuring strains, deflections and accelerations.

(iii) Instrumented wheelset

Another method that can be utilised to determine dynamic loads is the instrumented wheelset. With the instrumented wheelset installed in a rolling stock vehicle, dynamic wheel loads can be measured for both vertical and lateral loads. Figure 4-17 indicates the instrumented wheelset as installed on a 30ton per axle iron ore wagon. Figure 4-35 indicates the train setup. The wheelsets as well as the

vehicle body and bogie are instrumented to measure strains, deflections and accelerations. The wheel strains are analysed to produce vertical and lateral loads at any desired speed, which can then be compared to the static wheel loads in order to calculate dynamic factors under different conditions.

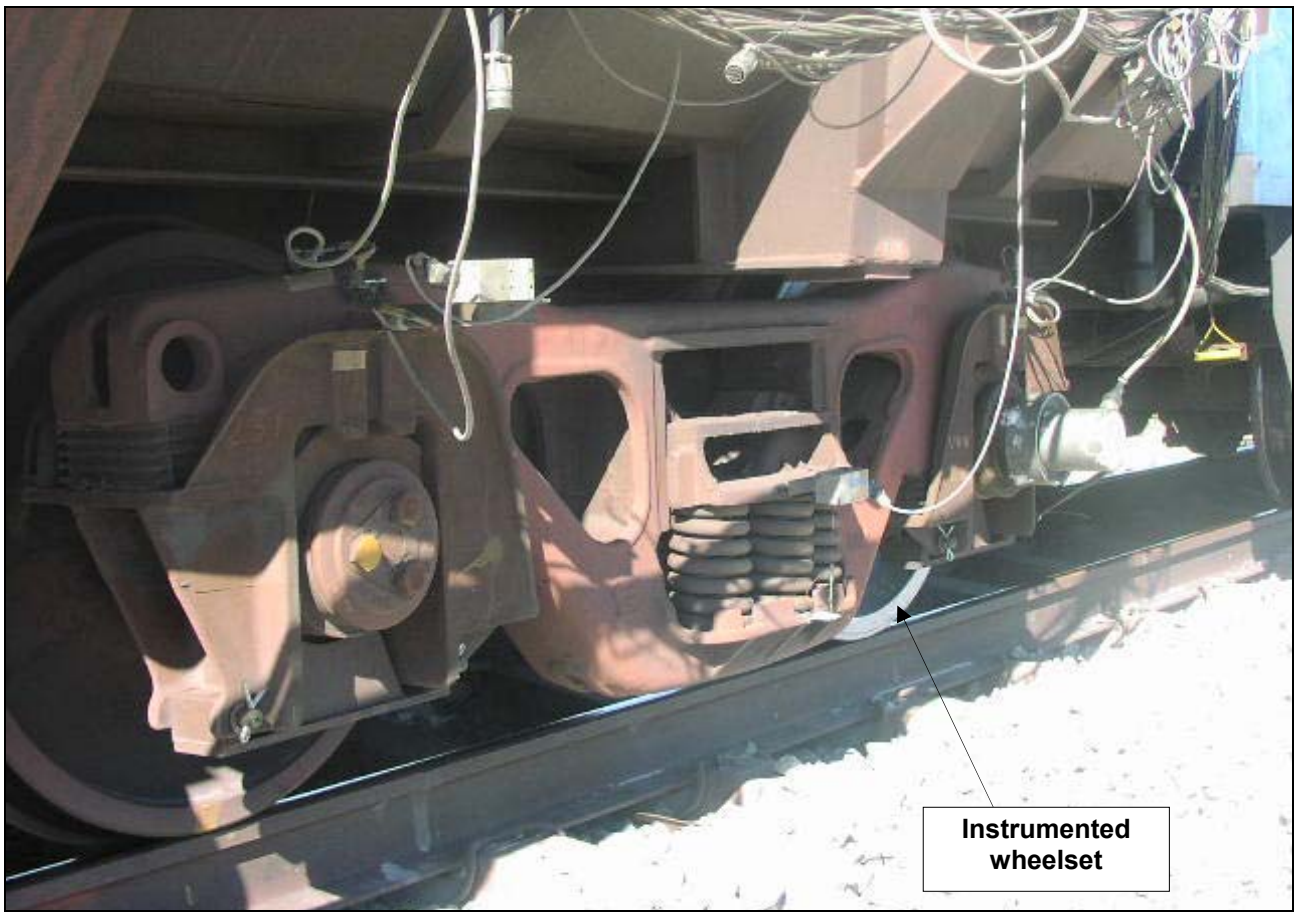

Figure 4-17: Instrumented wheelset installed in 30t per axle iron ore wagon

Results from tests (28) on the Iron Ore Export line indicated that the dynamic factor at 70km/h could typically be 1.13 for a 30ton axle load and 1.43 for a 26-ton axle load. Possible reasons for the lower dynamic factor associated with the higher axle load include the following: the suspensions of the vehicles behaved differently at that particular speed, or the unsprung mass (wheels, axles and bogies[§]) for a heavier loaded vehicle is lower in relation to its sprung mass (bogies[§], wagon body and load) than for a lighter loaded vehicle. In each case the sprung mass acts as a shock absorber to accelerations of the unsprung mass.

Another test was executed at Leandra on the Springs-Bethal line. Figure 4-18 indicates the track layout at the test site and Figure 4-19 indicates the measured track alignment in terms of the curve radius for the 800*m* length of track at Leandra on the Springs-Bethal line. It is clear that the test

[§] Depending on the bogie design, parts of it can be unsprung (i.e. unsupported by the suspension), and the other parts can form part of the sprung mass (i.e. supported by the suspension).

section consists of two adjacent curves. The first curve has a radius of ±950*m* for 200*m* and the second a curve of ±800*m* radius. In between the curves exists a piece of track which is almost straight (large radius) and is immediately followed by a sharp curve with a radius of 600*m*. The sharp transition from a straight track to a 600*m*-radius track is evidence that the track is moving in the direction of the ruling traffic over time.

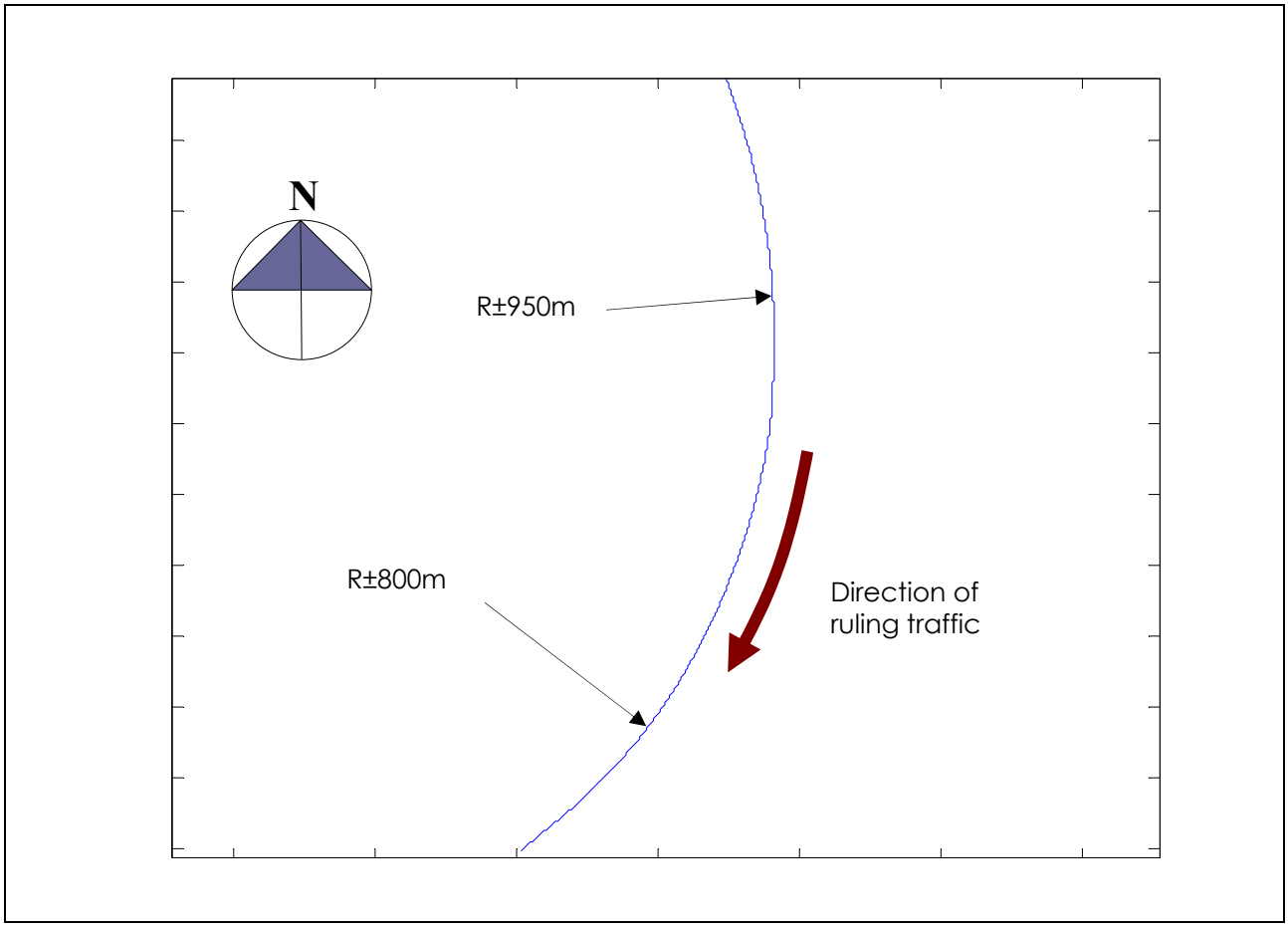

Figure 4-18: Leandra test site track layout

Eight runs of data were obtained over an 800*m* length of track. Measurements were taken at 20, 30, 40 and 60 km/h in one direction only and two tests were conducted at each speed.

A reflective plate triggered a "red eye", which is an optical instrument, as the train passed over to indicate the start and end of the test section for comparison purposes. The position of the red eye is as indicated in Figure 4-20 on the wagon body and reflects a beam from the stationary reflective plates at the start and end of the test section. The impulse from the red eye was recorded in the measured data as a peak or “spike” and was used to superimpose data from different runs.

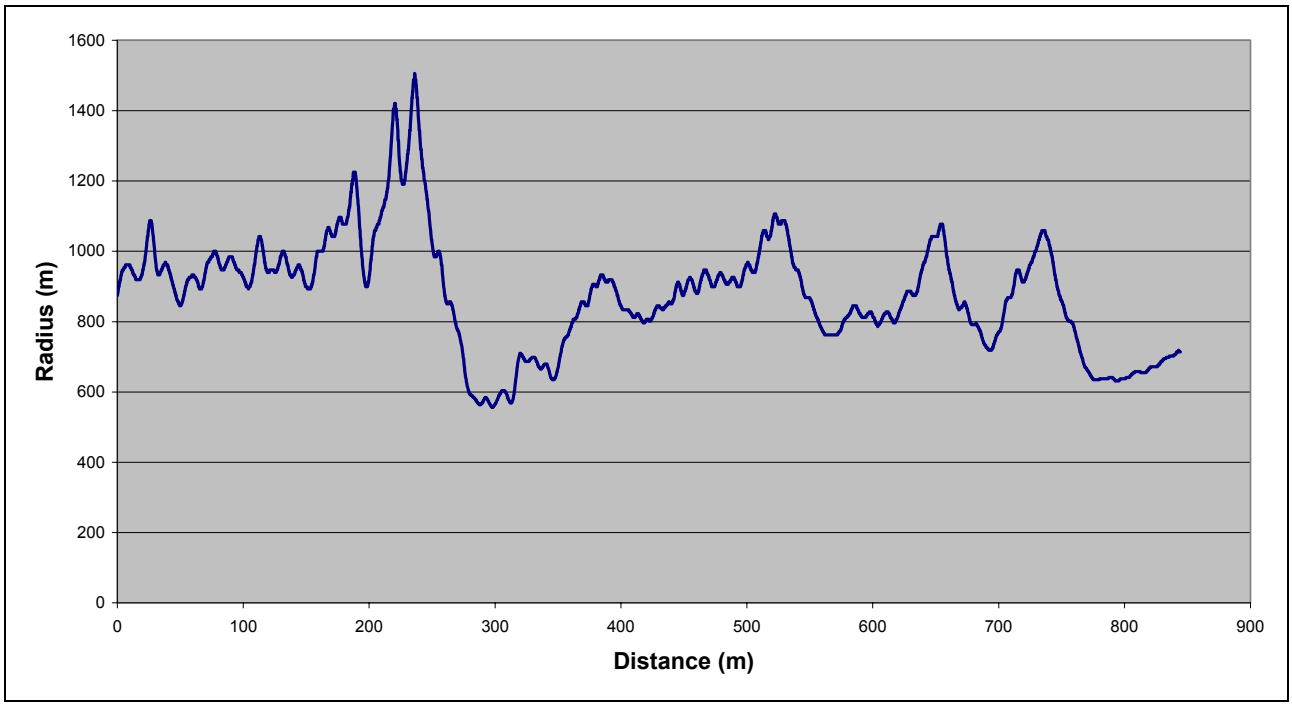

Figure 4-19: Leandra test site track geometry (curve radius)

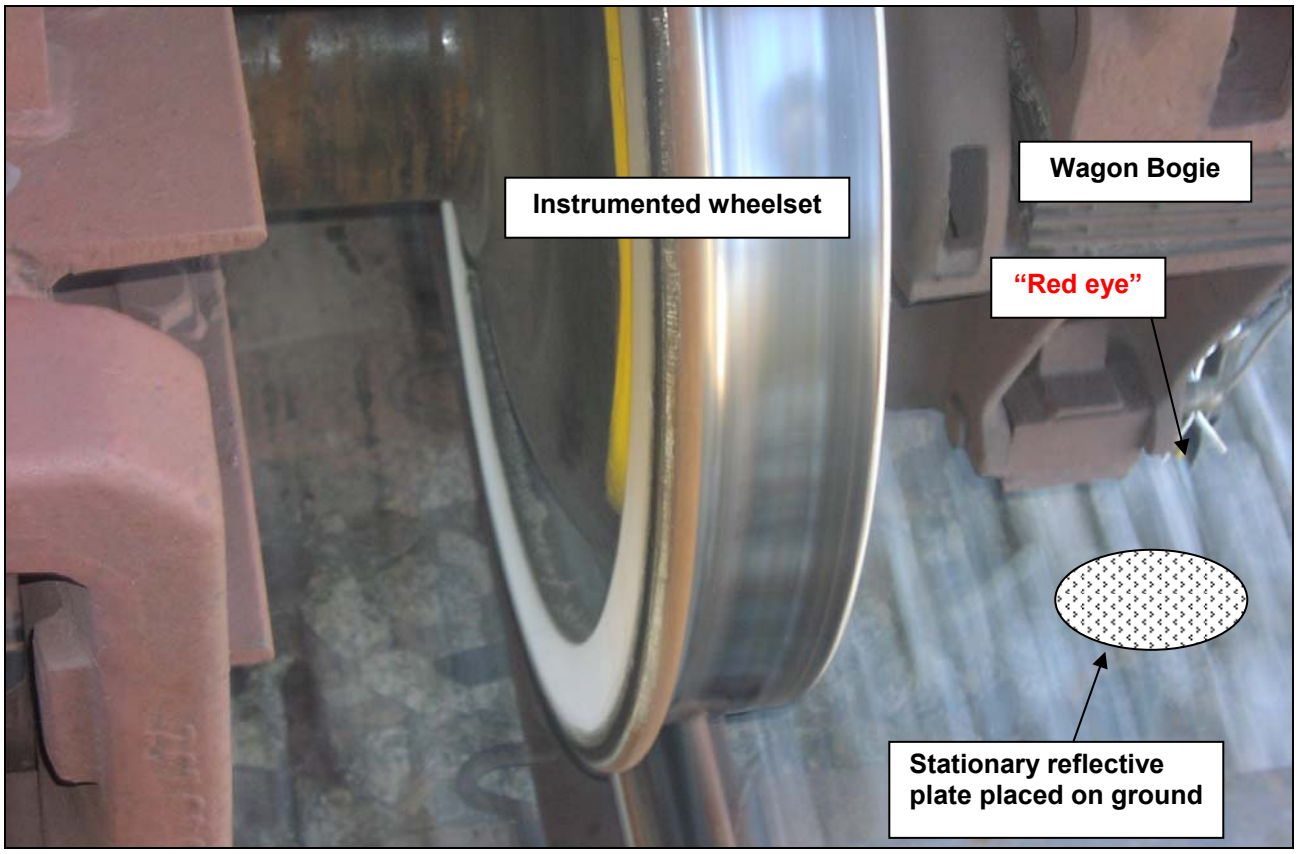

Figure 4-20: Instrumented wheelset with "red eye"

It is important to note that the only difference between the tests was the operating speed. Figure 4-21 and Figure 4-22 indicate the vertical forces between wheel and rail as measured with the instrumented wheelset under a 15 ton /axle load. The results from Figure 4-21 were measured whilst travelling at 20km/h. Due to the super elevation of the track (the test section was in a curve), there is a difference between the average left and right wheel loads. The data from the left leg are the outside leg of the curve, also referred to as the high leg. It is clear from the results that the low leg (right rail) carries the highest vertical load due to the excessive super elevation of the track which shifts the centre of the train mass at this low speed to the inside leg. The results from Figure 4-22 indicate the same test section and measuring wheelset at 60km/h. The results indicate the increase in loads on the high leg (left rail) and decrease of loads on the low leg (right leg). The average load on the right leg is still, however, higher than the load on the high leg due to the excessive super elevation of the track and the relatively low speed of the vehicle. From the data, the difference in the dynamic vertical forces from the static 75*kN* wheel load can clearly be seen. Local geometry errors and vehicle dynamics cause the measured loads to vary about the mean values of 60*kN* for the left wheel and 90*kN* for the right wheel. The shift of the average from 75 to 60 and 90*kN* in Figure 4-21 can be attributed to the super elevation of the track, possible skew loading of the vehicle or suspension defects. In Figure 4-22 the value of 90*kN* decreases to 80*kN* on the right rail (low leg) due to the increase in speed that shifts some of the weight to the outside leg (left rail).

Turnouts also present areas of high dynamic impact, as is seen from the data at approximately 240*m* and at 800*m* into the test section. This effect is greatly enhanced by the increase in speed (Compare Figure 4-21 and Figure 4-22).

One of the shortcomings of the analytical model is the fact that the macrotrack geometry is not accounted for in the determination of the dynamic factor. These results clearly indicate the effect of the track geometry on the vertical track forces. It is therefore suggested that the super elevation of the track should be considered, together with the speed and centre of mass of the vehicle, when calculating the dynamic factor. Esveld (1, p. 58) suggested the use of an additional factor to include the effect of excess cant or cant deficiency.

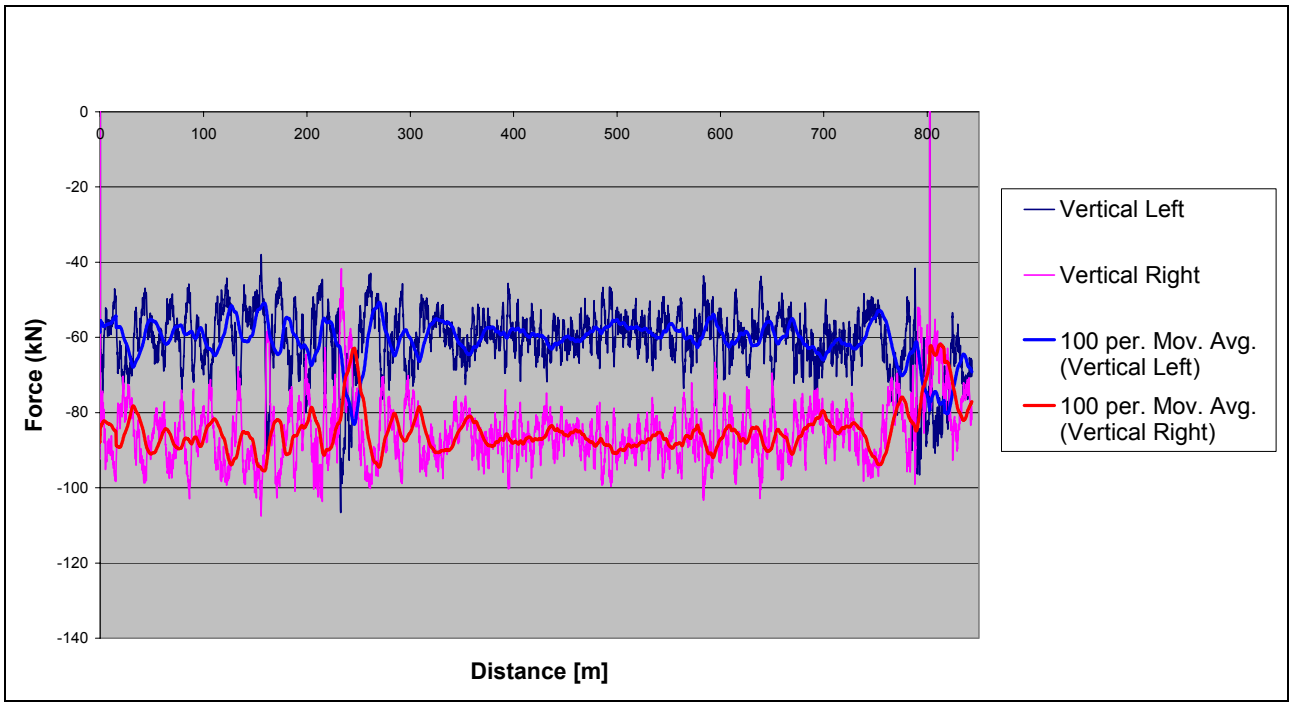

Figure 4-21: Vertical forces measured at 20km/h with instrumented wheelset and 15t axle load

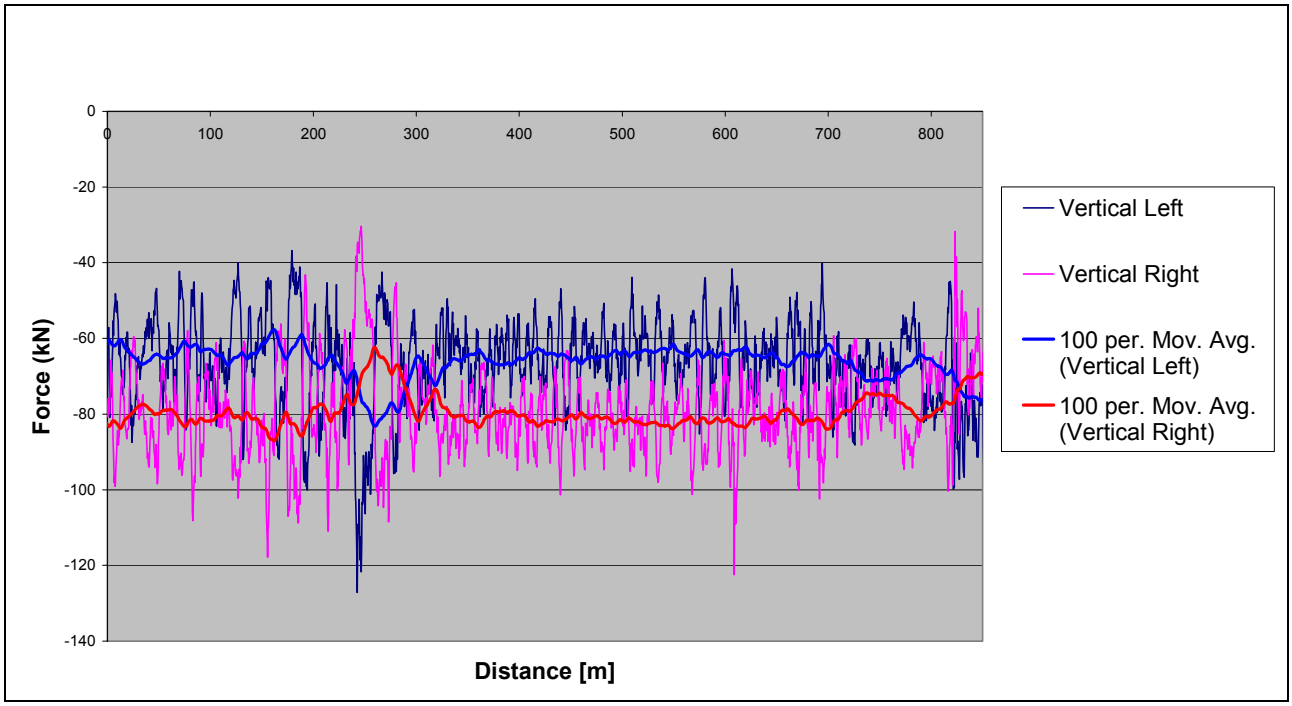

Figure 4-22: Vertical forces measured at 60km/h with instrumented wheelset and 15t axle load

The reason for using only one factor to account for both excess cant and cant deficiency is:

- In the first instance, the low leg is loaded with a higher load than the static wheel load, due to the centre of gravity being closer to the low leg, and the centrifugal forces are being overcompensated for
- In the second instance, the centrifugal forces are not being compensated for and thus the high leg will experience a higher load than the static wheel load.

The factor Q_c to account for excess cant and cant deficiency may be calculated by

$$Q_c = 1 + \frac{p_c \cdot \left(\frac{s \cdot v^2}{g \cdot R} - h' \right)}{s^2} \qquad (4.1)$$

where p_c is the vehicle centre of gravity distance (vertical) from the track, s is the track gauge (width), v is the speed, g is gravitational acceleration, R is the curve radius and h' is the track cant. According to Esveld, Q_c are normally in the order of 1.1 to 1.25 which correlates well with the empirical data that showed an increase of 1.18 on the low leg at 20km/h.

The results of the lateral forces on these tests are presented in Section 4.1.2.1 and are shown in Figure 4-28 to Figure 4-31.

4.1.1.3. Calculating the dynamic factor

When executing a track stress analysis, one normally has one of two objectives in mind: to design a new track that does not currently exist or to evaluate an existing track (e.g. for increasing wheel load or speed capacity).

These two mainstream design objectives would result in different methods of obtaining the necessary information to calculate the track stresses. When designing a new track, typical track parameters such as sleeper spacing and rail size would be design parameter variables and dynamic factors would be obtained from formulas such as the empirically determined Eisenmann formula. The other design objective, to evaluate an existing track, would provide the opportunity to measure the track quality as well as to determine the dynamic factors for the relevant conditions and rolling stock.

With the availability of the instrumented wheelset, it is possible to empirically determine a dynamic factor from the vertical loads. A methodology is henceforth provided on how to use the instrumented wheelset to determine a vertical dynamic factor.

In order to determine the dynamic factor from the instrumented wheelset results, there are two possible approaches to follow:

- The first approach ignores the existence of a moving average (i.e. there is no distinction made between straight and curved track) and calculates the dynamic factor from the 99.85th percentile (3 times the standard deviation) of the whole track, including irregularities such as turnouts. This method is preferred when the railway line is designed as a whole, without distinguishing between straight and curved track (and even turnouts).
- The second approach is based on the procedure specified in UIC Code 518 (30, p. 28) for testing and accepting railway vehicles based on their dynamic behaviour. The dynamic factor is calculated for short sections of the whole track individually. This method is preferred when evaluating shorter sections of track, where the macrogeometry is taken into account by other means like additional force factors etc.

When determining a dynamic factor that includes macrogeometric deviations (first approach), the dynamic factor should be calculated as follows:

1. A piece of representative track should be measured with the instrumented wheelset at different speeds (up to and including the maximum line speed). It is, however, seldom possible to find a short section of track which is sufficiently representative of the track as a whole and it is thus preferred to measure the whole track under consideration.
2. Calculate the dynamic factor with either of the following equations:

$$\varphi = \frac{3 \cdot \text{Standard Deviation}\,(\text{Vertical Forces}) + \text{mean}(\text{Vertical Forces})}{\text{mean}\,(\text{Vertical Forces})} \qquad (4.2)$$

or

$$\varphi = \frac{99.85^{th}\ \text{Percentile}\,(\text{Vertical Forces})}{\text{mean}\,(\text{Vertical Forces})} \qquad (4.3)$$

With currently available calculation tools, both formulas could easily be utilised and the results evaluated to determine which value would be more appropriate to use. Using 3 times the Standard Deviation of the vertical forces could present a less realistic result, when a short piece of track is measured, if the maximum values are a result of localised geometry defects (which would result in a high deviation from the mean). If a sufficiently long piece of track is measured and a Gaussian distribution is present, the results of equations 4.2 and 4.3 should be the same.

When determining a dynamic factor that does not include the effect of macrogeometric deviations (second approach), the dynamic factor should be calculated as follows:

1. The test section should be divided into three zones (30, p. 28), namely:
   - tangent track and large radius curves ($R>1200m$),
   - large radius curves ($600m<R<1200m$),
   - small radius curves ($R<400m$).

The procedure in (30, p. 30) specifies that each zone should have a total of at least 10km, since it is seldom possible to find a short section of track which is sufficiently representative of the track as a whole.

2. Each of these zones should then be divided into sections with a maximum length as indicated in Table 4-4 (for this purpose, the transient curves may be included in the curve sections).

Table 4-4: Test section lengths for statistical analysis

Test Zones		Section Lengths
Tangent track and large radius curves (R>1200*m*)		250*m*
Large radius curves (600<R<1200*m*)		100*m*
Small radius curves	(400<R<600*m*)	100*m*
	(R<400*m*)	70*m*

3. For each of these sections, the following should be calculated: Mean value, Standard Deviation and 99.85th percentile of the measured vertical loads.
4. A dynamic factor is then calculated for each section with the use of equations 4.2 and 4.3 and then calculated for the line as a whole by taking the average of all the values calculated (for either the standard deviation method or the percentile method).

4.1.1.4. Worked out example on Sweden test data (dynamic factor)

As an example, test results from Sweden, measured by Spoornet Engineering (29), were analysed with this method to determine the dynamic factor of this line. The dynamic factors from the Iron Ore Export line data as well as for the Leandra data were also calculated and are presented here. The available data from the Sweden line were for a 5km section of track, consisting of straight and curved track as indicated in Figure 4-23. The curvature can be related to curve radius *R* by the following relationship[**]:

$$R = \frac{10000}{0.875 \cdot Curvature} \qquad (4.4)$$

where curve radius *R* is in metres and *Curvature* is measured by the IM2000 track geometry car as the lateral deviation of the track to the vehicle wheelbase in millimetres.

Figure 4-24 indicates the vertical wheel rail forces measured at 40km/h. An indication is also given of the 99.85th percentile and 3*Standard Deviation values for each section, as well as the average and the

[**] This formula is specific to the IM2000 track geometry vehicle from Plasserrail which measures curvature as a function of the IM2000's wheelbase. Modifications to the vehicle wheelbase or measuring system will result in a different formula.

99.85th percentile and 3*Standard Deviation values for the measured track as whole. From the results it is clear the 3*Standard Deviation value is somewhat higher than the 99.85th percentile for both approaches. The 99.85th percentile and 3*Standard Deviation for the whole line are much larger than the averages of the sections' values. This clearly indicates how the one approach can be used to include the effect of the moving average or vice versa.

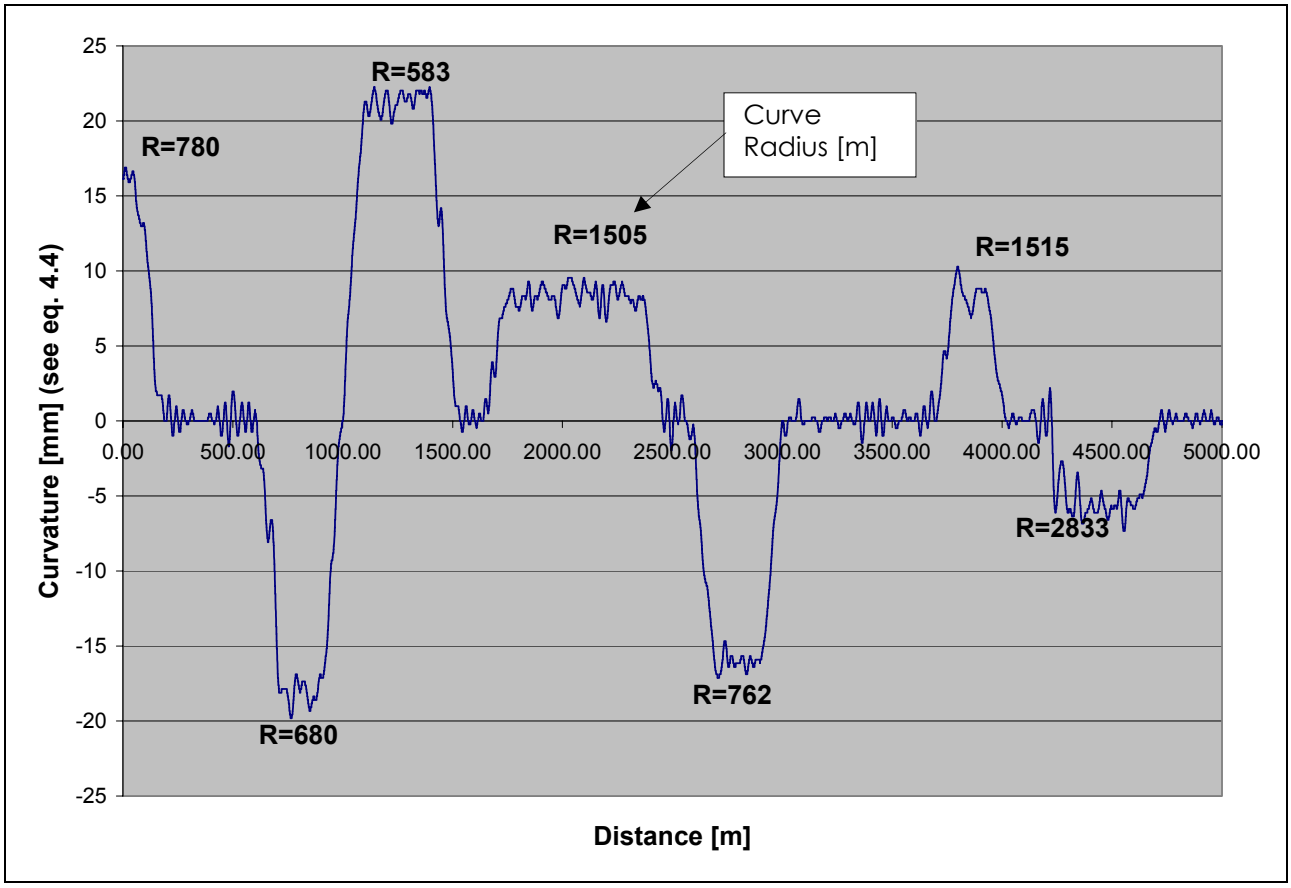

Figure 4-23: Sweden test track geometry (curvature)

Table 4-5 and Figure 4-25 indicate the calculated dynamic factors for the Sweden, Leandra and Iron Ore Export line data as calculated by the two different approaches. From the results in Table 4-5 it is clear that the standard deviation method versus the percentile method provided similar answers on the long tracks (Sweden and Iron Ore Export line) but not on the short track (Leandra data) due to local force peaks in the Leandra data that influenced the results.

The dynamic factors, as calculated for the tests conducted at higher speeds, sometimes show lower values than the trend set by the lower speeds. It is therefore not safe to extrapolate dynamic factor values at speeds for which values were not measured from these results since the test vehicle's body motions could influence the data at particular speeds.

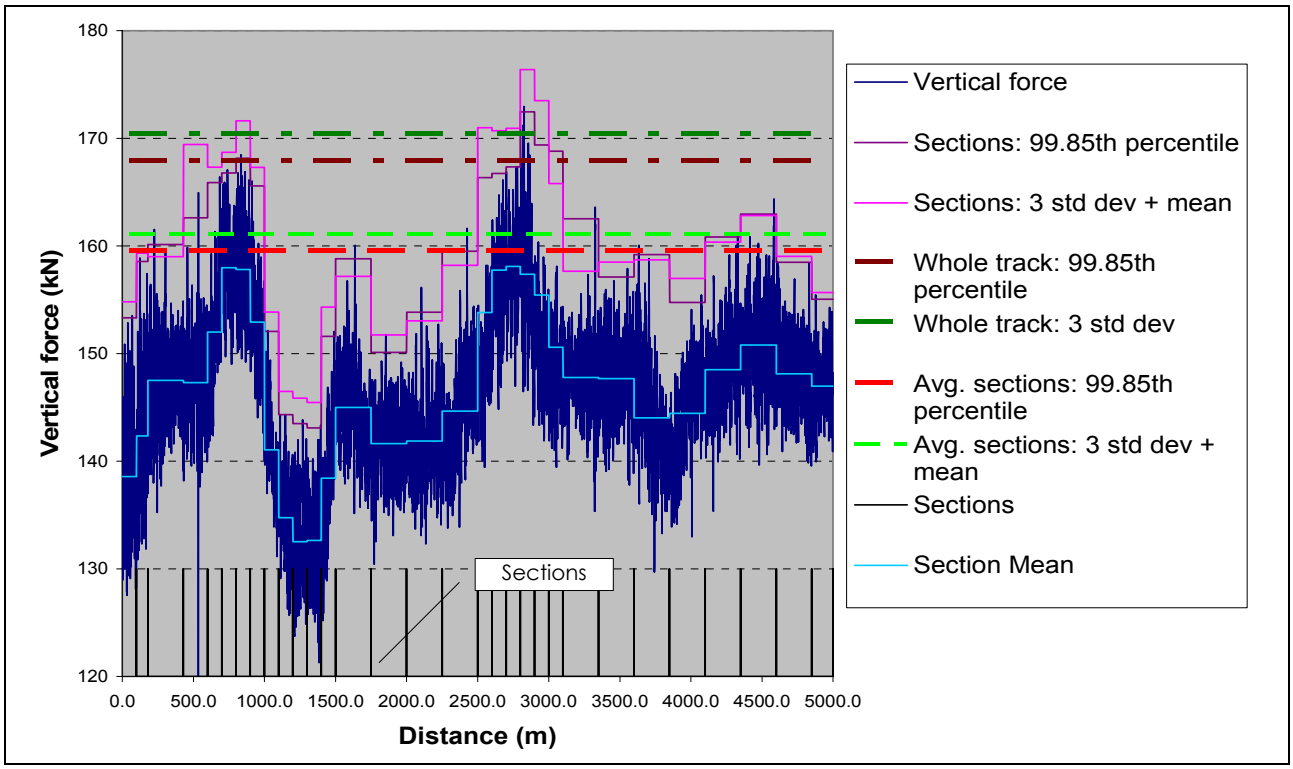

Figure 4-24: Sweden wheel-rail vertical forces @ 40km/h.

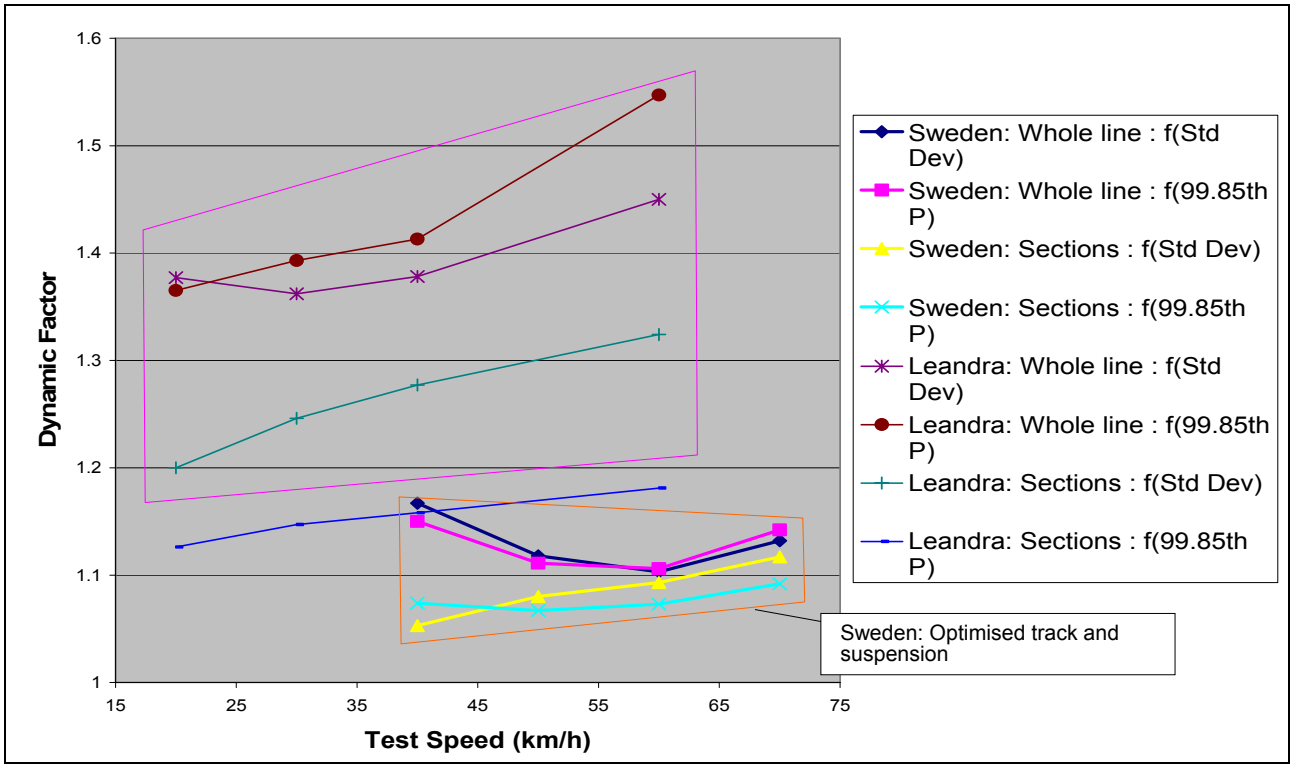

Figure 4-25: Dynamic factors from tests at Leandra and Sweden with different methods

Table 4-5: Dynamic factors as calculated with different methods

Tests		1st Approach (whole line)		2nd Approach (average of sections)	
		φ=f(3*Std Dev)	φ=f(99.85th Percentile)	φ=f(3*Std Dev)	φ=f(99.85th Percentile)
Sweden	40km/h	1.167	1.150	1.053	1.074
	50km/h	1.118	1.111	1.080	1.067
	60km/h	1.103	1.106	1.093	1.073
	70km/h	1.132	1.142	1.117	1.092
Leandra	20km/h	1.377	1.365	1.200	1.126
	30km/h	1.362	1.393	1.246	1.147
	40km/h	1.378	1.413	1.277	1.158
	60km/h	1.450	1.547	1.324	1.181
Iron Ore Export line 15t	30km/h	1.167	1.146	1.163	1.132
	40km/h	1.188	1.161	1.186	1.152
	50km/h	1.196	1.174	1.192	1.160
Iron Ore Export line 26t	30km/h	1.131	1.115	1.123	1.104
	40km/h	1.155	1.137	1.149	1.125
	50km/h	1.179	1.157	1.170	1.143
	60km/h	1.183	1.162	1.177	1.151
	70km/h	1.196	1.178	1.192	1.163
Iron Ore Export line 30t	30km/h	1.166	1.149	1.161	1.132
	40km/h	1.187	1.164	1.181	1.148
	50km/h	1.195	1.171	1.188	1.153
	60km/h	1.223	1.195	1.216	1.174
	70km/h	1.252	1.223	1.246	1.196

4.1.1.5. Dynamic factor overview

A dynamic factor cannot always be empirically determined, for example, when a new track and or rolling stock is designed and simulation resources are limited. It is therefore worth evaluating the range of possible values in order to be able to make an educated guess or use a suitable formula.

For this purpose, all the calculated dynamic factors, be it from empirical formulas or measured wheel–rail forces, are indicated in Figure 4-26. Some of the dynamic factors were grouped together and only the envelopes were presented (e.g. the Eisenmann formulas which are dependent on a number of factors beside speed). The ungrouped dynamic factors are presented in Appendix D.

From the processed data, although limited in scope, it is evident that the Eisenmann formula might be too conservative for local conditions and should not be used without the insight gained from this study.

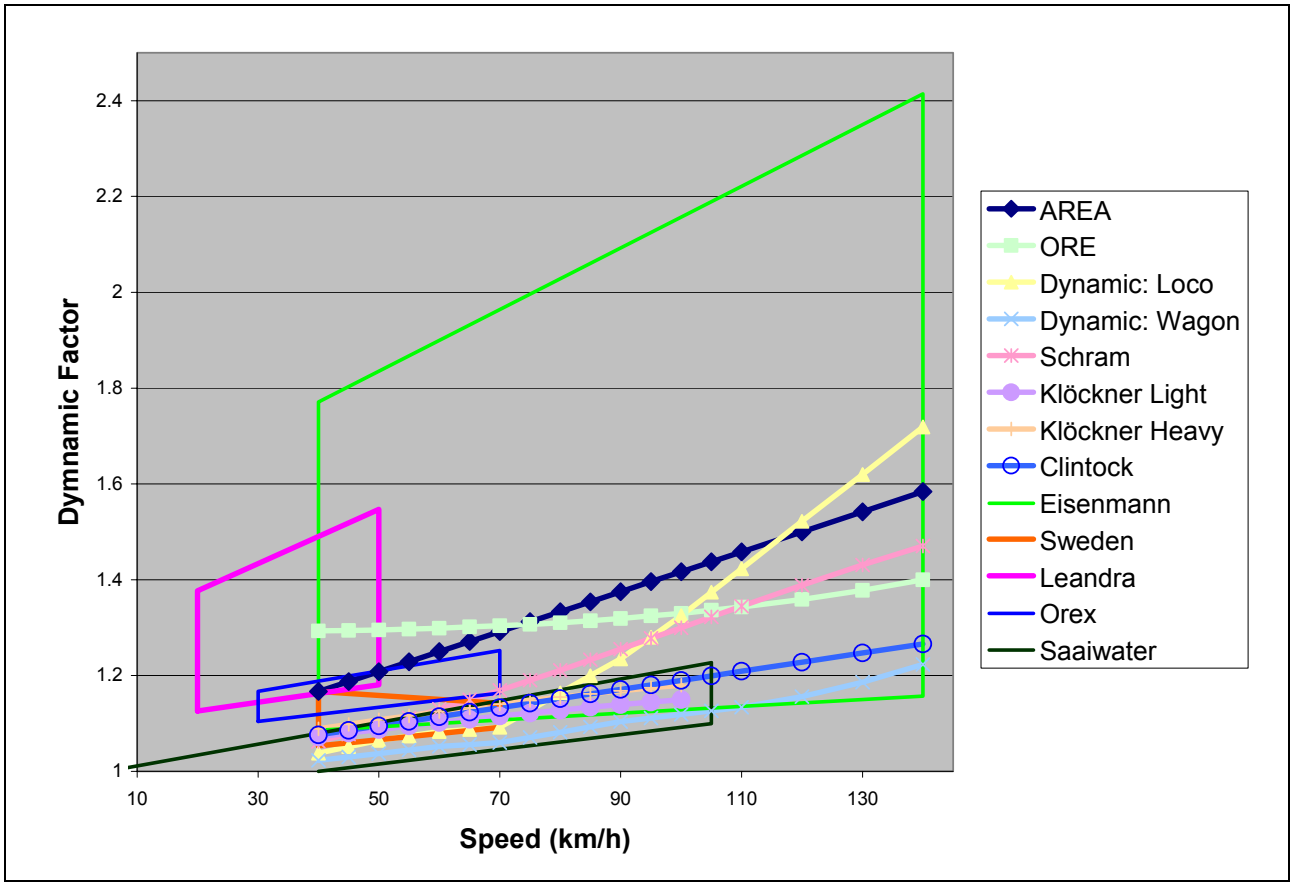

Figure 4-26: Summary of all dynamic factors from this study

It is important to realise that the empirically determined dynamic factors (Saaiwater, Leandra, Iron Ore Export line and Sweden), as displayed in Figure 4-26, are relevant only to the conditions under which they were determined.

The dynamic factors from the wayside measurements (Saaiwater) represent the entire COALlink fleet but the condition of the track at the measured site is of a very high standard, which might not be representative of the whole track. The Leandra, Iron Ore Export line and Sweden data, on the other hand, represent different conditions of track quality but again may only be characteristic of the type of vehicle utilised for the measurements.

The next section will investigate lateral wheel-rail forces.

4.1.2. Lateral Force

The lateral load parameter from the analytical method is the parameter to which the rail stresses are the second most sensitive, as indicated in Table 3-5. Ironically, the lateral load is also the parameter to which the least attention is given in the analytical method and was taken only as a fixed percentage of the vertical force.

Figure 4-27 indicates an attempt to relate lateral track geometry to lateral loads and shows that no definite relationship exists for this dataset measured in Sweden (29) as was the case with the vertical loads – see paragraph 4.1.1.

The lateral force is not only a function of the vertical load but also of a number of parameters such as the curve radius, the speed of the vehicle, the steering ability of the vehicle and the rigidity of the fastening system (31). Lombard (2, p. 57) specified the use of a lateral load of $40kN$, with no indication of whether or not this may be used with any vertical load. In the program "Moment", the lateral force was calculated as 40% of the vertical force. It is unknown whether this was done intentionally or in error, since Lombard used a $100kN$ vertical force in his worked-out example, which could possibly have led to this relationship, conveniently taken to be linear for higher vertical loads.

In this study, the lateral forces will be determined statistically from field measurements and compared to the simultaneous vertical forces at various speeds.

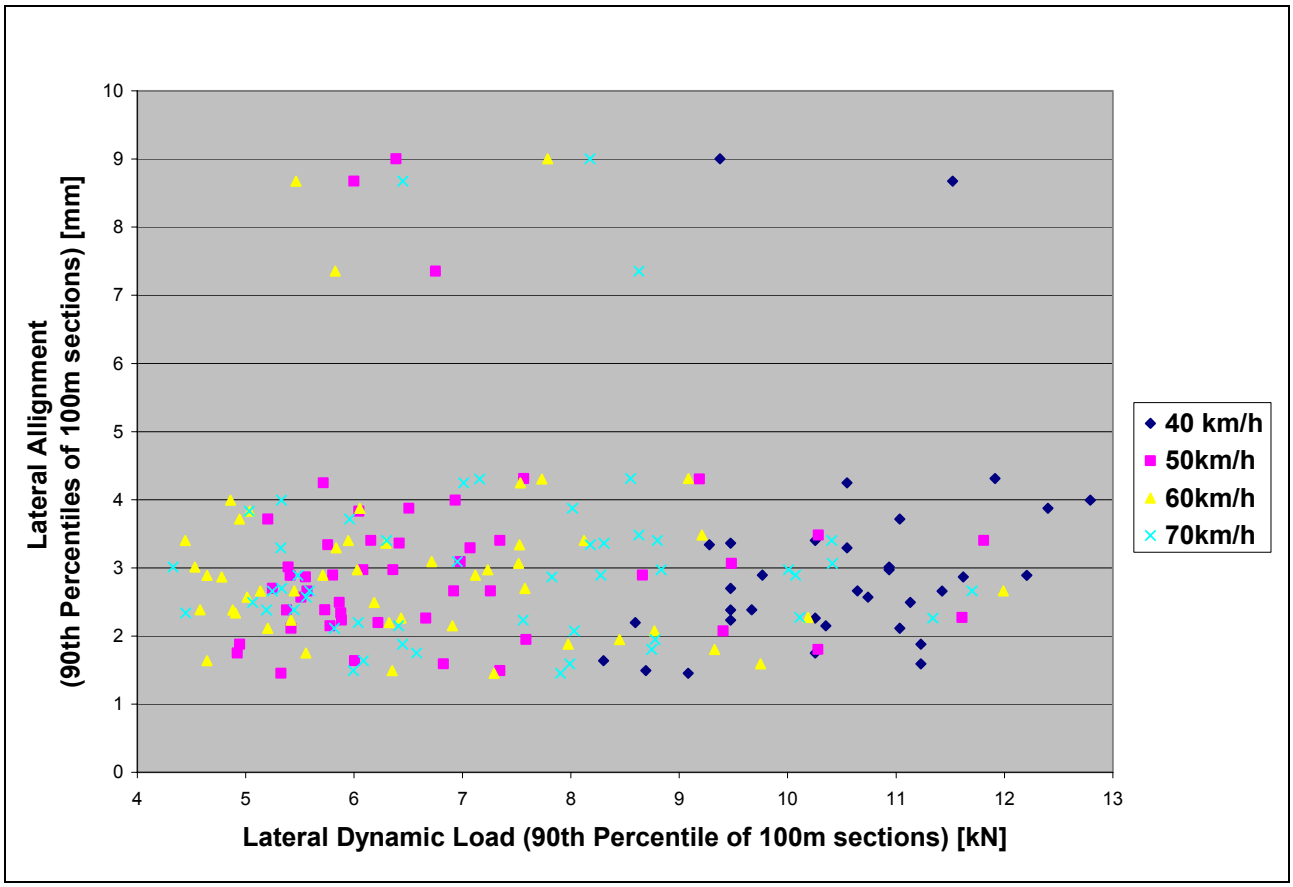

Figure 4-27: Track geometry lateral alignment vs. dynamic loads

4.1.2.1. Empirical test results

Lateral wheel loads will be investigated empirically in order to determine typical values under local conditions.

Lateral force measurements were obtained from the instrumented wheelset from three different test sites, namely, Leandra (General Freight Line), Loop 12 (Iron Ore Line) and from measurements performed in Sweden. The instrumented wheelset data from Loop 12 were available on three different vehicles, each with a different axle load.

(i) Leandra Test site

For the tests at Leandra, eight runs of data were available. Figure 4-18 indicates the track layout at the test site and Figure 4-19 indicates the measured track alignment in terms of the curve radius for the 800*m* length of track. Wheel load measurements were taken at 20, 30, 40 and 60 km/h in one direction

only. Two tests were conducted at each speed. Figure 4-28 and Figure 4-29 indicate the lateral forces on the instrumented wheelset at the Leandra test site at different speeds. Positive lateral loads are from the inside of the rail towards the outside. When comparing the test results, the change in lateral force can mostly be attributed to the change in speed, although the lateral position of the wheelset changes and plays a part in the magnitude of the lateral forces (see paragraph 4.1.3 on page 85). The negative lateral force peaks in the presented graphs indicate impulses due to the discontinuity of the rails at turnouts, which introduces large forces onto the wheelsets.

In order to study the effect of the vehicle speed on the magnitude of the lateral forces, statistical indexes have been determined for each test.

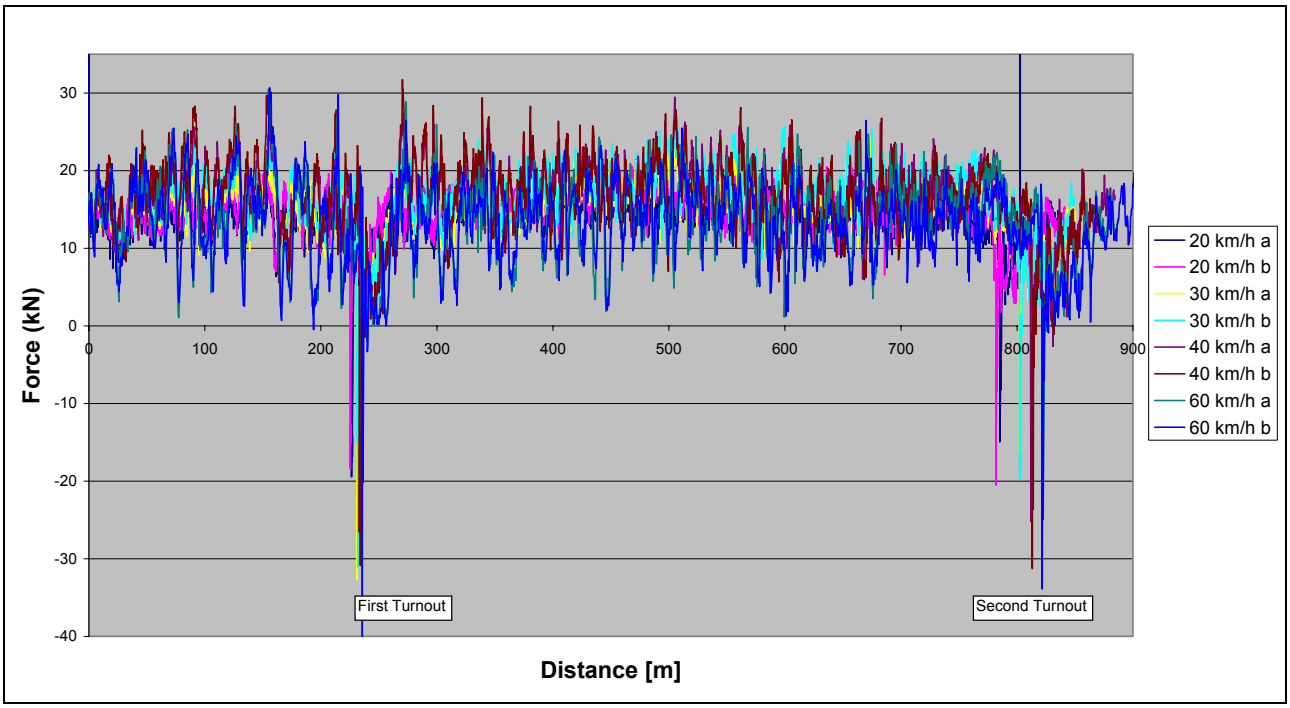

Figure 4-28: Lateral left wheelset force at different speeds [km/h]

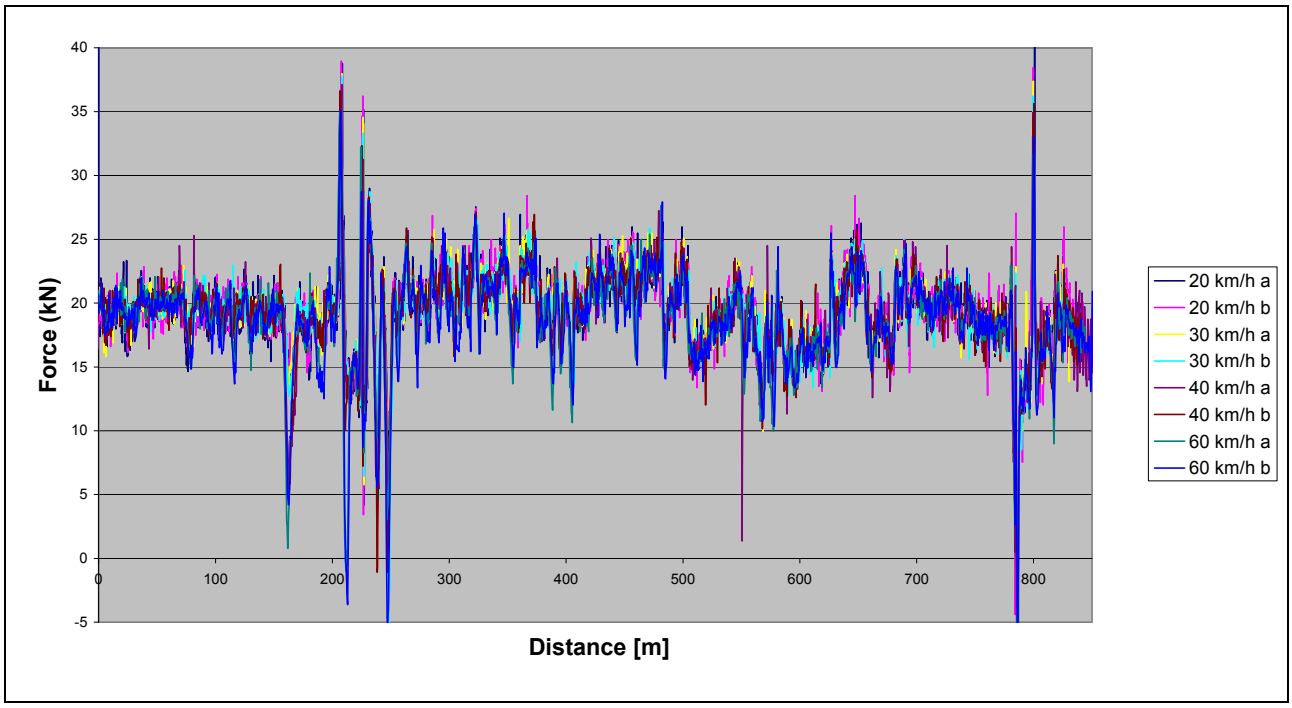

Figure 4-29: Lateral right wheelset force at different speeds [*km/h*]

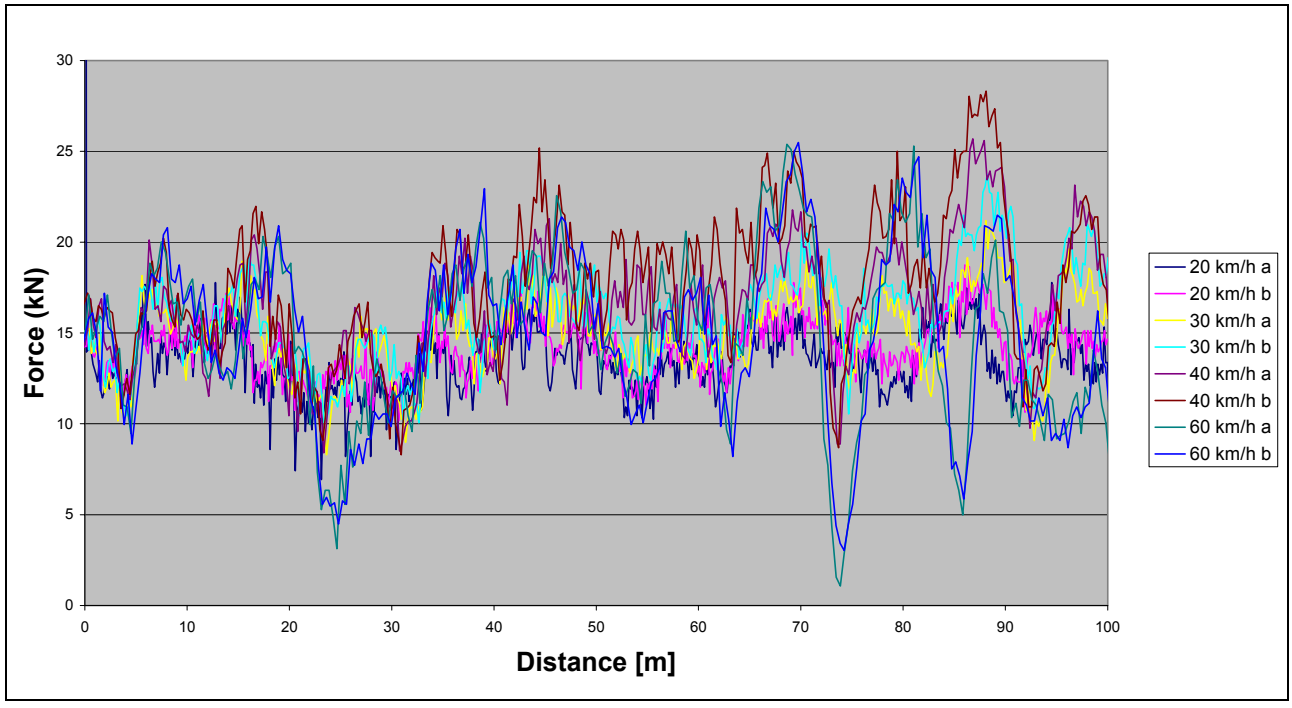

Figure 4-30: Lateral left wheelset force of 1st 100*m* at different speeds [*km/h*]

Figure 4-30 and Figure 4-31 present the data from Figure 4-28 and Figure 4-29 for the first 100m. At this scale, patterns in the results are easier to identify. At first glance there seems to be some correspondence between peaks and valleys of the different runs.

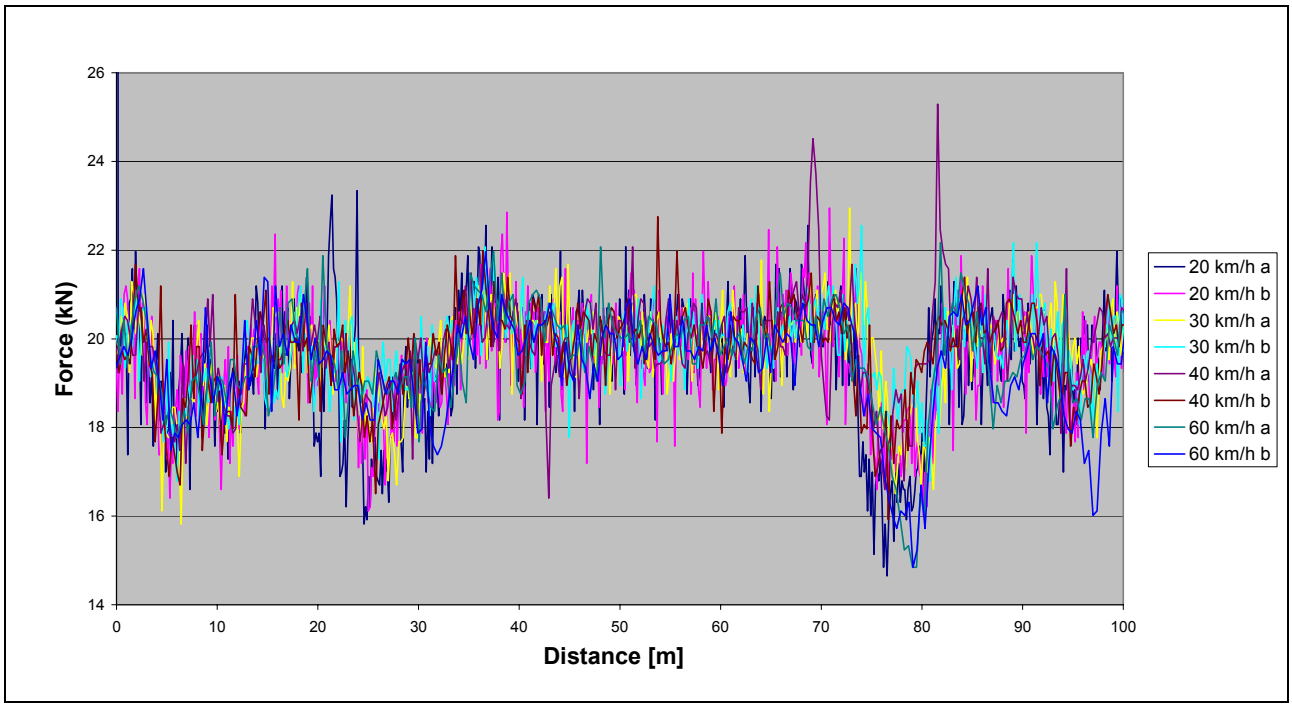

Figure 4-31: Lateral right wheelset force of 1st 100*m* at different speeds [km/h]

At closer inspection, there is a phase shift noticeable in the lateral force patterns of the different speeds. It seems that the lateral dynamics of the vehicle systems are a contributing factor in this case. In order to investigate other trends in the data that could be related to the speed of the vehicle, the data were analysed statistically. Table 4-6 indicates the statistical results of the lateral left forces and Table 4-7 indicates the results of the lateral right forces.

Table 4-6: Statistical results from lateral left forces [kN] of Leandra test data

	20km/h	20 km/h	30 km/h	30 km/h	40 km/h	40 km/h	60 km/h	60 km/h
Mean	13.61	14.65	14.91	15.71	15.80	15.73	13.19	12.80
Median (50th percentile)	13.96	15.04	15.23	16.02	15.92	15.72	13.38	13.18
Range	40.14	42.68	56.93	57.23	56.64	62.99	60.25	74.22
Minimum	-19.43	-20.51	-32.71	-31.15	-27.15	-31.25	-29.98	-43.55
Maximum	20.70	22.17	24.22	26.07	29.49	31.74	30.27	30.66
Standard deviation	2.59	2.93	3.68	4.18	4.67	5.00	5.12	5.10
Sample variance	6.73	8.61	13.55	17.50	21.81	25.05	26.17	25.98
99.85th percentile	18.76	20.80	23.14	25.25	27.39	29.82	28.84	29.15
3*standard deviation + mean	26.30	23.46	25.95	28.25	29.81	30.74	28.54	28.09

Table 4-7: Statistical results from lateral right forces [kN] of Leandra test data

	20km/h	20 km/h	30 km/h	30 km/h	40 km/h	40 km/h	60 km/h	60 km/h
Mean	19.19	19.37	19.28	19.16	19.04	18.89	18.45	18.01
Median (50th percentile)	19.24	19.53	19.43	19.34	19.24	19.04	18.65	18.36
Range	48.73	49.61	47.46	46.88	44.63	46.09	41.41	41.02
Minimum	-9.96	-10.64	-9.47	-9.08	-7.52	-9.47	-6.45	-5.96
Maximum	38.77	38.96	37.99	37.79	37.11	36.62	34.96	35.06
Standard deviation	3.07	3.17	3.10	3.17	3.15	3.21	3.21	3.61
Sample variance	9.44	10.06	9.62	10.07	9.94	10.31	10.30	13.00
99.85th percentile	35.78	34.65	34.02	34.20	33.37	33.50	31.89	30.21
3*standard deviation + mean	32.91	28.88	28.58	28.68	28.50	28.53	28.08	28.83

The same data are also indicated in Figure 4-32 and Figure 4-33, which indicate the difference between the patterns of the left and right wheel forces.

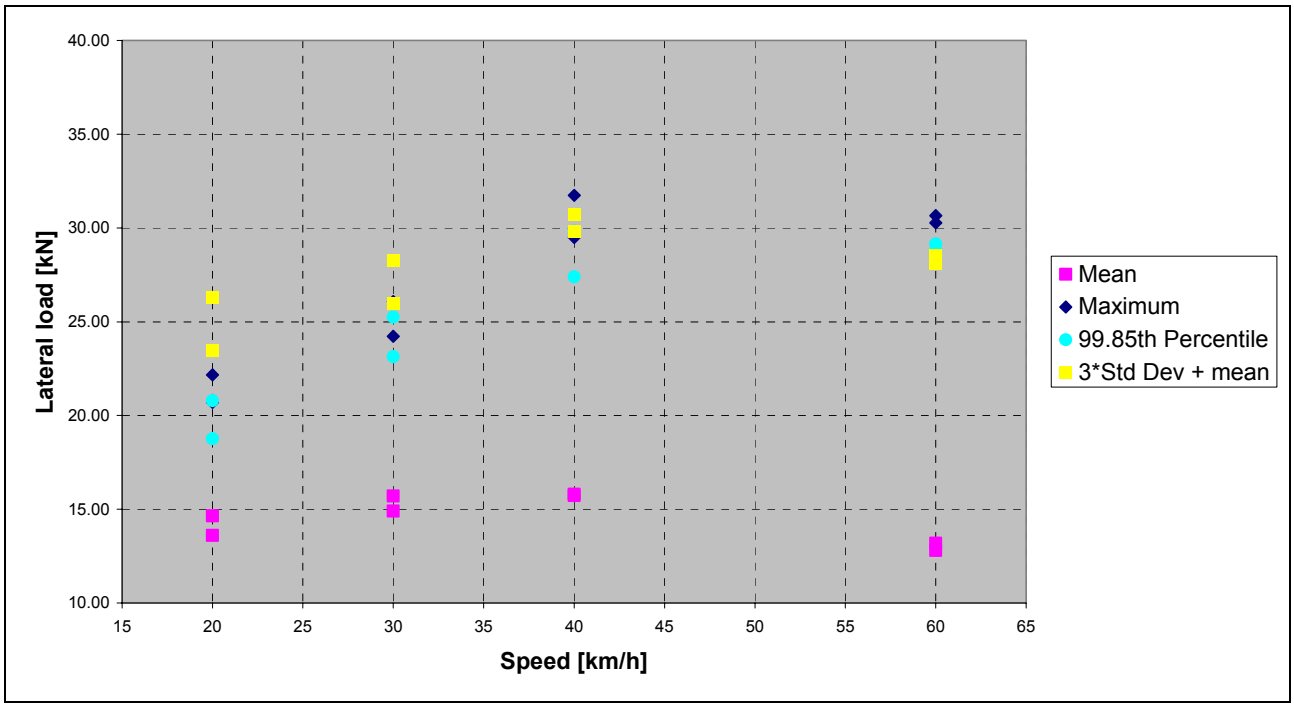

Figure 4-32: Statistical summary of lateral left forces at Leandra test site

Figure 4-32 clearly indicates an increase in lateral force with an increase in speed while Figure 4-33 indicates a reduction in forces with an increase in speed. As was the case with the vertical force (paragraph 4.1.1.2(iii)), the excess super elevation of the track caused an excess weight shift to the right leg (low leg) which increased the lateral towards the outside of the rail. As the speed increased, the centrifugal forces of the vehicle increased the lateral forces to the outside of the left rail (high leg) while reducing the right lateral forces. At the maximum speed of 60km/h, however, the results from the left and right leg converged and did not follow the trend set by the results from the lower speeds.

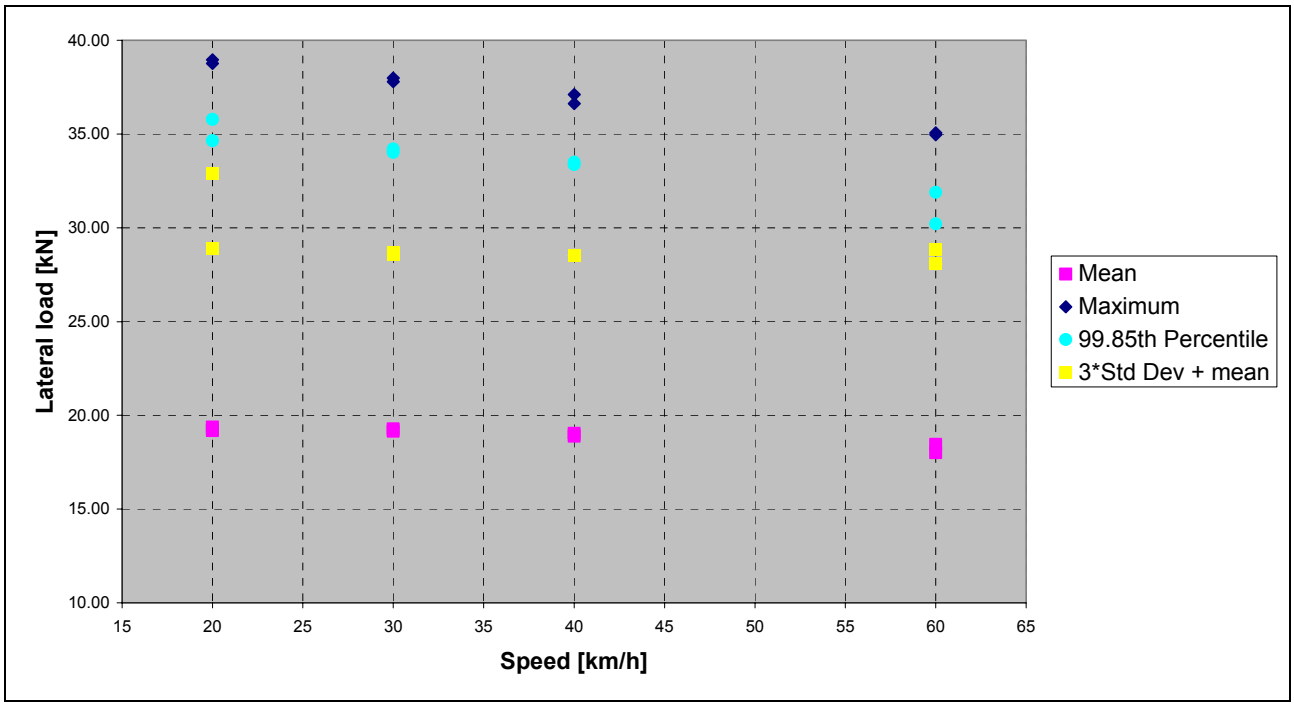

Figure 4-33: Statistical summary of lateral right forces at Leandra test site

Force distribution graphs have been drawn up for each test and are indicated in Appendix B to indicate the spread of lateral forces.

In order to establish whether or not a relationship exists between the lateral and vertical forces, the data from the different runs are presented in Figure 4-34. For each of the scatters, a linear fit was performed to quantify a possible relationship between the vertical and lateral forces.

It is evident that the data points about the linear fits are widely scattered and therefore the statistical correlation between the vertical and lateral forces had to be determined to provide an indication of confidence in a linear relationship. The correlation values are presented in Table 4-8.

From the correlation data in Table 4-8 it is clear that there is a 60% probability of a linear relationship between the vertical and lateral forces on the left but only about an 8% probability of a linear fit on the right. The negative correlation of the left data indicates a decreasing lateral load for an increasing vertical load.

From the results in Table 4-8 it is evident that no definite relationship exists between the vertical and lateral wheel-rail forces. It may be concluded that the suggestion by Lombard (2, p. 57) to use a constant lateral force of $40kN$ is a better option than trying to predict the lateral force as a function of the vertical force or the speed of the vehicle.

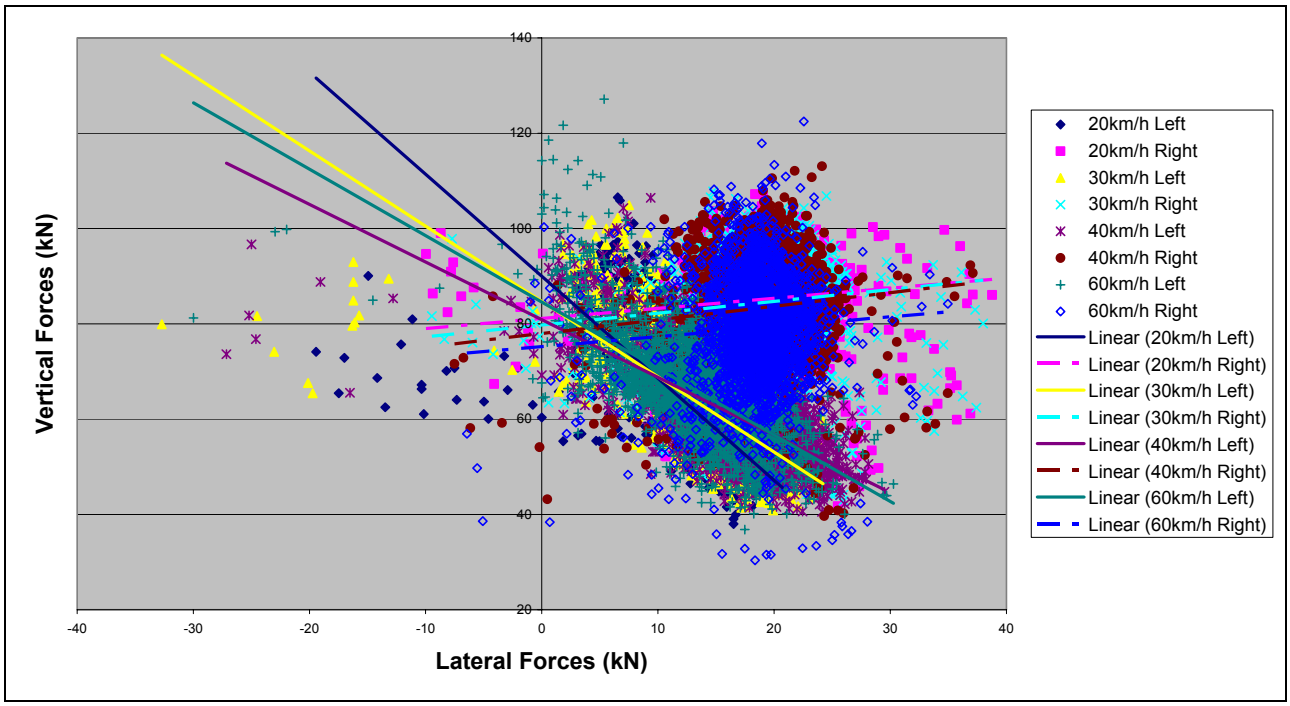

Figure 4-34: Leandra test data: Vertical vs. Lateral Forces

Table 4-8: Correlation between vertical and lateral force data

Speed [*km/h*]	Correlation	
	Left	Right
20	-0.678	0.080
30	-0.665	0.087
40	-0.626	0.097
60	-0.654	0.061

Lombard's proposal of 40*kN* is too high in this case for the left leg forces but is acceptable for the right leg when including the maximum lateral force at 40km/h. As will become clearer from following results, this measured piece of track is too short to make any definite decisions since the measured portion does not represent the whole line.

According to the limit prescribed by the International Union of Railways (UIC) (30, p. 23) when evaluating railway vehicles for acceptance on track, the sum of the guiding (lateral) forces over 2*m* of track should not exceed the following:

$$\sum Y = \alpha\left(10 + P/3\right) \qquad (4.5)$$

where Y is the lateral forces and P is the vertical axle load, both in kN and $\alpha = 1$ for traction units and $\alpha = 0.85$ for wagons. This results in a total lateral force limit of $57kN$ for a locomotive and $48kN$ for a wagon under a $140kN$/axle load. It is, however, also mentioned that these values may be exceeded by agreement between the infrastructure manager and railway operator. It is further stated under the heading of track fatigue that the quasi-static lateral force limit for small radius curves (Radius < $600m$) is $60kN$.

It should be made clear that these limits are not per rail, but the total lateral forces (both left and right rails) over a distance of $2m$, which is in contrast to the limit set by Lombard (2, p. 56) where each rail is evaluated separately.

The reason why the UIC states a lateral load limit per $2m$ track and not per rail is that its values are primarily based on empirically determined values, governed by track maintenance (alignment) strategies, and not individual rail stresses. When these limits are thus exceeded, track maintenance should be adjusted accordingly.

It can therefore be concluded that in the case of the limits set by the UIC, the maintenance of the track alignment is determined by the force limits and not the rail stresses.

(ii) Iron Ore Export line Test site

The instrumented wheelset tests conducted on the Sishen – Saldanha line (iron ore export line) consisted of three instrumented wheelsets on three different wagons. Figure 4-35 indicates the test train setup with the three instrumented wheelsets under 15, 26 and 30ton axle loadings. The tests were conducted on a $3km$ section of the line at speeds of 30, 40, 50, 60 and 70km/h and the vertical and lateral forces for each wheelset were investigated. Figure 4-38 and Figure 4-39 indicate the wheel rail forces for the tests at 30 and 70km/h. The force results from each test were analysed statistically and the results are tabulated in Table 4-9 and Table 4-10.

The data from Table 4-9 and Table 4-10 are also indicated in Figure 4-36 and Figure 4-37, which indicate the difference between the patterns of the left and right wheel forces. The vertical scale of Figure 4-36 was purposefully set to match the vertical scale of Figure 4-37 in order to highlight the difference between the left and right lateral forces.

From the results there is a clear discrepancy between the lateral loads of the 26ton/axle results and the rest of the results. In order to investigate this phenomenon, the lateral loads are displayed graphically in Figure 4-38 (30km/h tests) and Figure 4-39 (60km/h tests).

Figure 4-35: Test train setup with three instrumented wheelsets at Iron Ore Export line tests

Table 4-9: Statistical results from lateral left forces [*kN*] of Iron Ore Export line test data

	15t/axle				26t/axle					30t/axle				
Speed [km/h]	30	50	60	70	30	40	50	60	70	30	40	50	60	70
Mean	-0.77	-0.52	-0.56	-0.58	-18.24	-17.83	-19.70	-19.36	-19.33	0.21	0.34	0.62	0.45	0.58
Median	-0.78	-0.58	-0.58	-0.58	-17.96	-17.48	-19.53	-19.14	-18.94	0.00	0.19	0.58	0.39	0.58
Range	5.96	6.24	6.43	6.54	22.41	25.63	26.84	26.01	25.74	41.56	44.46	49.02	34.97	20.79
Minimum	-3.81	-3.61	-3.80	-3.71	-32.19	-33.73	-36.01	-34.79	-34.72	-30.69	-33.55	-37.99	-24.52	-10.05
Maximum	2.15	2.63	2.63	2.83	-9.79	-8.10	-9.17	-8.77	-8.98	10.87	10.91	11.03	10.45	10.74
Sample Variance	0.81	1.11	1.23	1.29	13.15	16.17	18.81	18.48	21.70	15.88	17.50	20.14	18.31	17.95
Standard Deviation	0.90	1.05	1.11	1.14	3.63	4.02	4.34	4.30	4.66	3.98	4.18	4.49	4.28	4.24
99.85th Percentile	1.76	2.34	2.34	2.44	-10.54	-9.08	-9.86	-9.66	-9.57	9.57	10.25	10.35	9.96	10.24
3*Std Dev +mean	1.94	2.64	2.76	2.83	-7.36	-5.77	-6.69	-6.46	-5.35	12.16	12.89	14.08	13.29	13.29

Table 4-10: Statistical results from lateral right forces [*kN*] of Iron Ore Export line test data

	15t/axle				26t/axle					30t/axle				
Speed [km/h]	30	50	60	70	30	40	50	60	70	30	40	50	60	70
Mean	-0.34	-0.16	-0.18	-0.47	-8.81	-10.19	-6.38	-8.05	-8.86	5.72	5.96	6.80	5.69	5.73
Median	-0.39	-0.19	-0.19	-0.48	-10.64	-12.10	-7.61	-10.15	-10.83	5.07	5.27	6.05	5.27	5.46
Range	6.41	6.62	6.83	7.40	31.14	31.78	39.06	37.47	43.07	24.70	31.51	37.06	25.68	23.13
Minimum	-3.68	-3.51	-3.61	-4.10	-18.65	-18.56	-18.35	-18.45	-18.84	-5.35	-6.33	-5.10	-5.57	-4.75
Maximum	2.73	3.11	3.22	3.30	12.48	13.23	20.71	19.02	24.23	19.36	25.18	31.96	20.12	18.38
Sample Variance	0.93	1.28	1.50	1.53	38.48	32.01	57.12	51.94	43.84	18.71	21.83	30.58	21.01	20.35
Standard Deviation	0.97	1.13	1.22	1.24	6.20	5.66	7.56	7.21	6.62	4.33	4.67	5.53	4.58	4.51
99.85th Percentile	2.34	2.73	2.83	2.83	9.37	8.78	13.08	13.08	13.96	17.67	19.23	27.73	18.85	17.57
3*Std Dev +mean	2.56	3.23	3.50	3.25	9.80	6.78	16.29	13.57	11.00	18.70	19.97	23.39	19.44	19.26

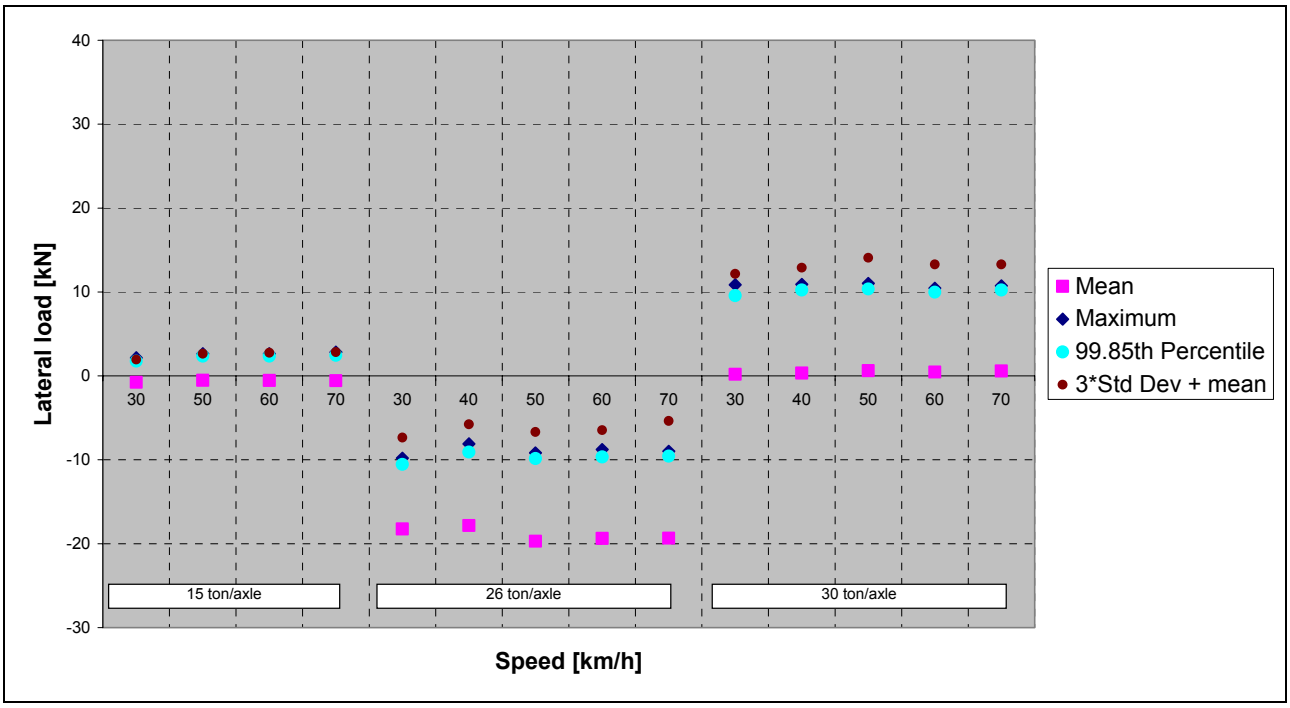

Figure 4-36: Statistical summary of lateral left forces at different speeds and axle loads

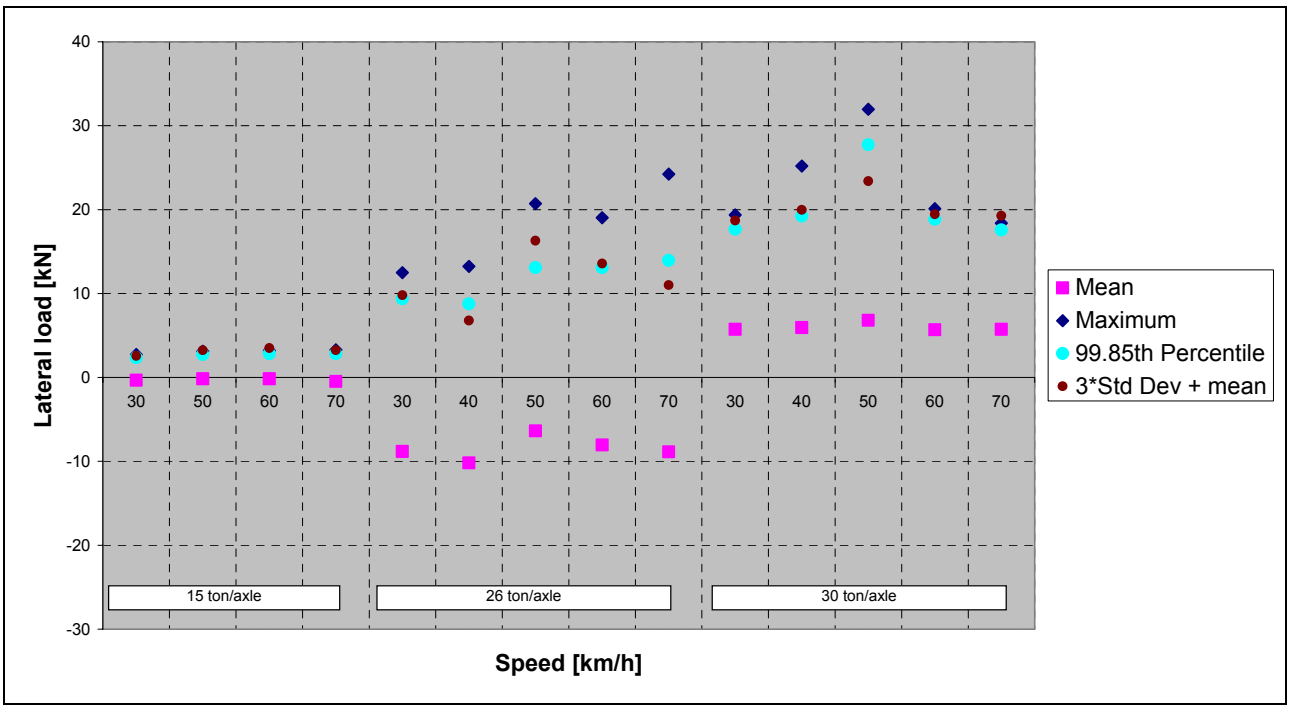

Figure 4-37: Statistical summary of lateral right forces at different speeds and axle loads

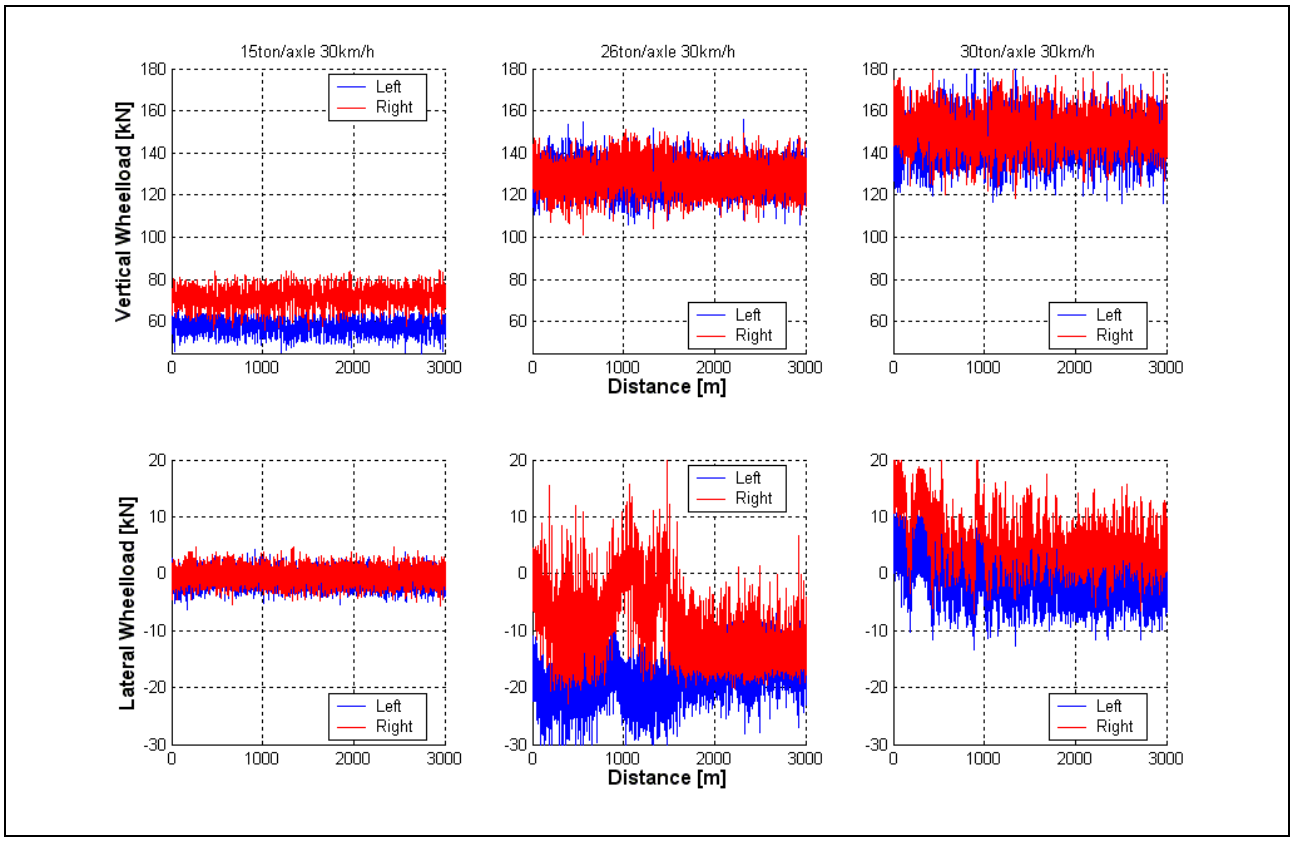

Figure 4-38: 30km/h test results of vertical and lateral loads (Iron Ore Export line tests)

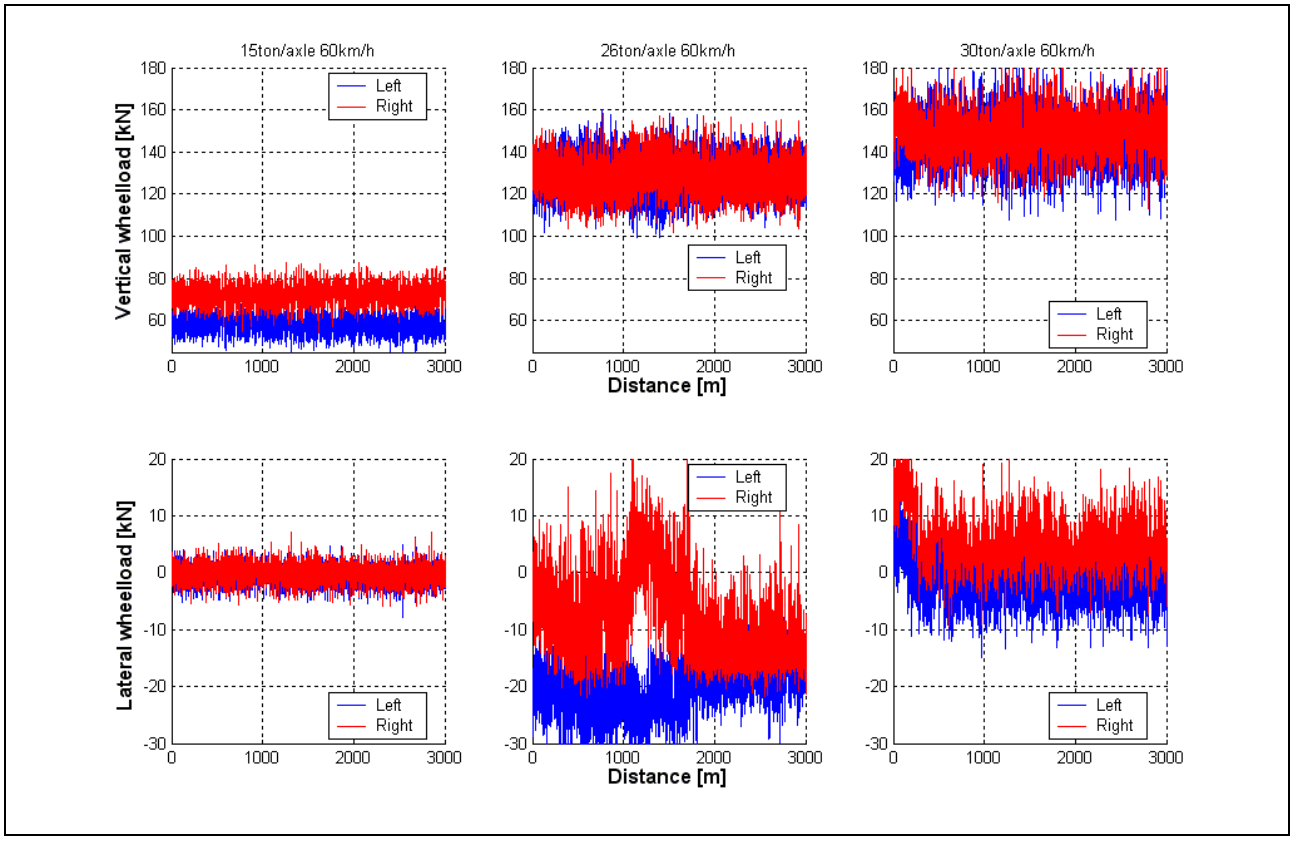

Figure 4-39: 60km/h test results of vertical and lateral loads (Iron Ore Export line tests)

From the above lateral load results, it is evident that the 26on/axle wagon results do not follow the trend set by the 15ton/axle and 30ton/axle results. It is also evident from Figure 4-38 and Figure 4-39 that the axle loads have greater effects on the lateral loads than a change in speed. In comparison with the Leandra lateral load results (paragraph 4.1.2.1 (i)), which were measured in an 800*m* curve, the 26ton/axle results are of the same order of magnitude, although being measured on straight track and large radius curves (R>1200*m*).

It was concluded that this particular wheelset or wagon bogie was faulty and can be described as a "skew" bogie which means that the wagon steers as if it is in a curve, even though it is travelling on a straight track. As described earlier in the document, this could be due to a wheel diameter difference between the left and right wheels of either axle.

Figure 4-40 and Figure 4-41 indicate the vertical vs. lateral forces for the 15ton/axle and 30ton/axle loads respectively as measured on the Iron Ore Export line line. Linear curve fits through the data scatter are also indicated. The correlations for each of the data sets have been calculated and are presented in Table 4-11.

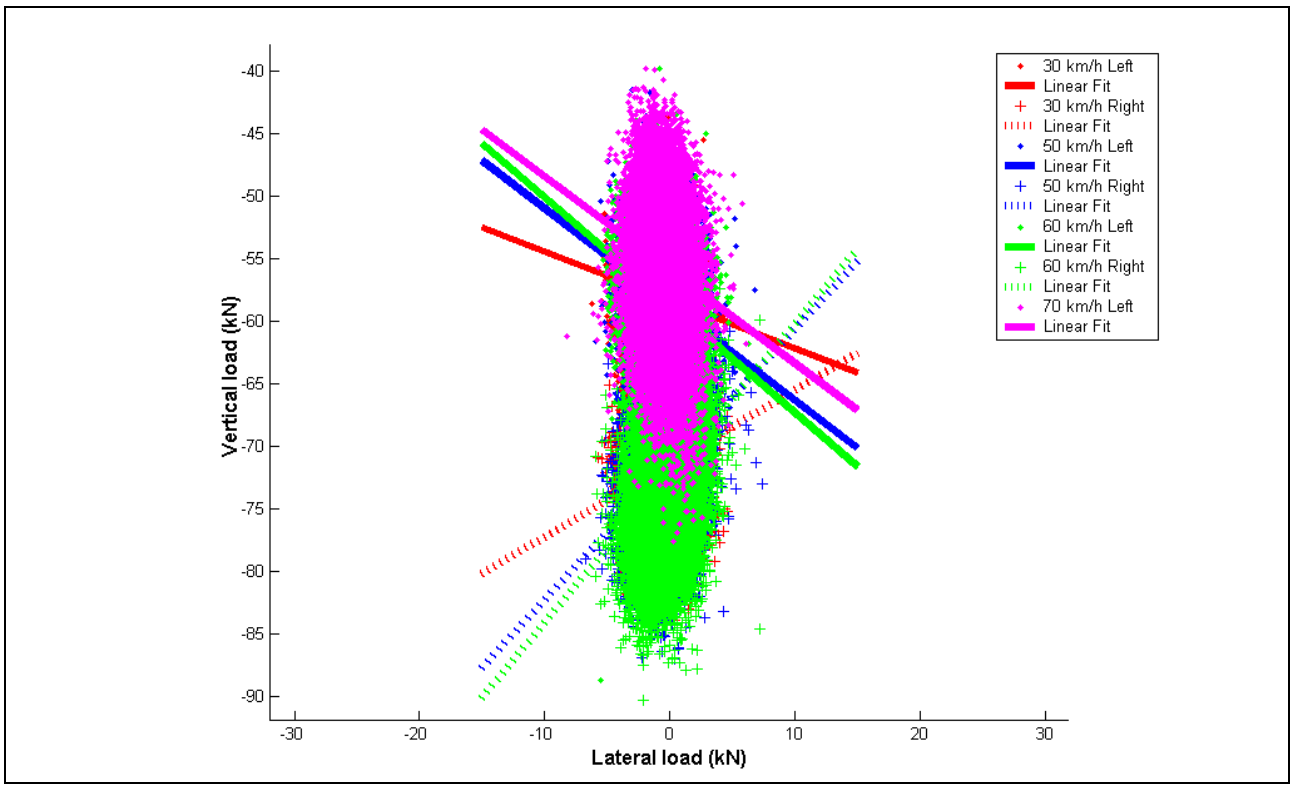

Figure 4-40: Iron Ore Export line vertical rail-wheel forces vs. lateral rail-wheel forces for 15t/axle tests

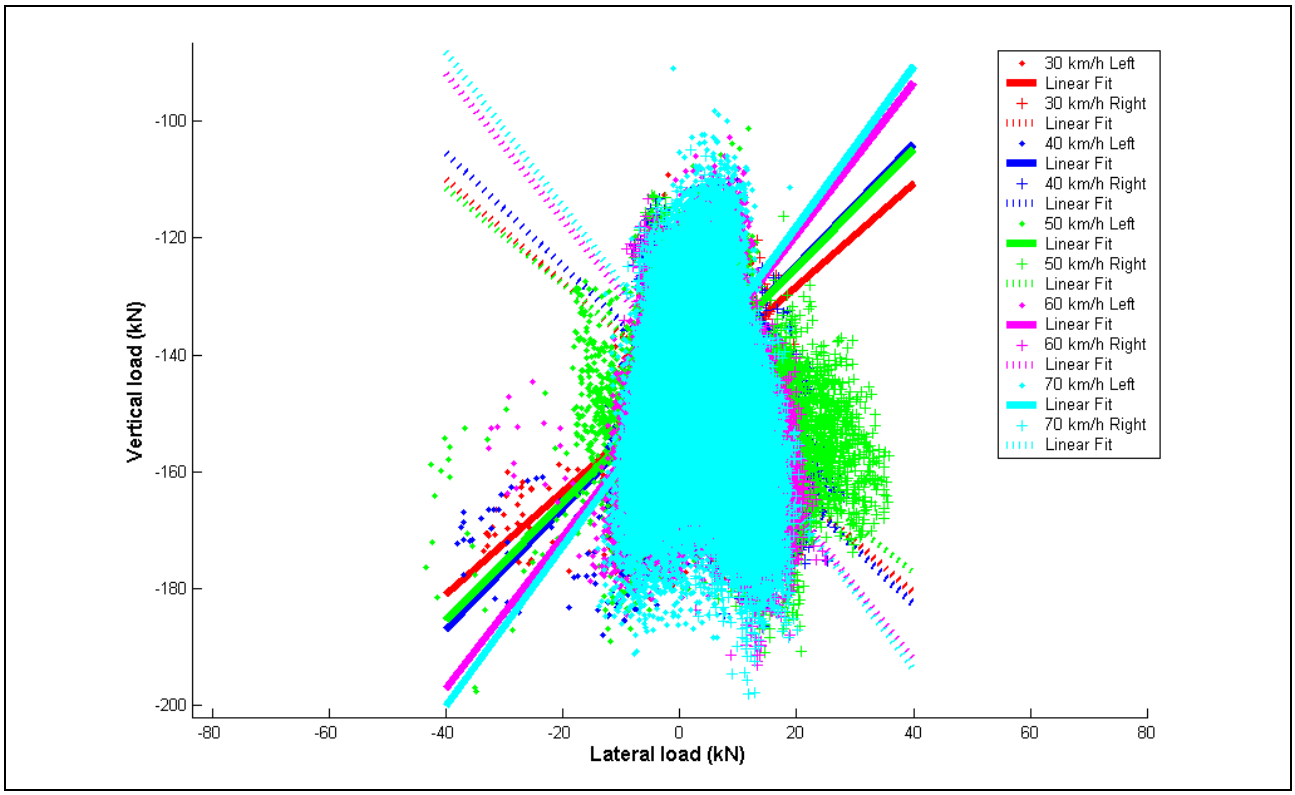

Figure 4-41: Iron Ore Export line vertical rail-wheel forces vs. lateral rail-wheel forces for 30t/axle tests

Table 4-11: Correlation between vertical and lateral force data

	30km/h		40 km/h		50 km/h		60 km/h		70 km/h	
	Left	Right	Left	Right	Left	Right	Left	Right	Left	Right
15t	-0.101	0.156			-0.209	0.299	-0.233	0.344	-0.189	
30t	0.420	-0.475	0.466	-0.496	0.466	-0.479	0.497	-0.538	0.459	-0.461

According to the correlation results there is little confidence in the apparent linear relationship between the vertical and lateral wheel-rail forces. The right leg forces at 60km/h of the 30ton/axle loads have the highest correlation of 54%.

It therefore seems to be the best approach to account for the lateral forces in rail stress calculations by choosing a constant value. Based on the results, the suggested value of 40*kN* seems to be too high. This may be due to the fact that the piece of measured track contained only straight and large radius curves. If this piece of track were representable of the track as a whole, a lateral load of 30*kN* could be used in rail stress calculations. In light of the UIC limits as presented in paragraph 4.1.2.1(i), the total lateral forces in small curves (Radius < R600) may be accepted as high 60*kN*. This is, however, the total lateral force and not the force on each rail. In the above test results, lateral forces with the same sign, on each rail, are actually in opposing directions on the track (refer Figure 4-44).

(iii) Sweden test results

Similar tests to those conducted at Leandra and on the Iron Ore Export line were conducted by Spoornet in Sweden. The Sweden lateral force results were also evaluated statistically and are presented in Table 4-12 and in Figure 4-42.

Table 4-12: Statistical results from lateral left forces of Sweden test data

Axle Load	14.6t			
Speed [km/h]	**40**	**50**	**60**	**70**
Mean	15.72093	15.47391	14.39602	14.50645
Median	16.30859	15.91797	14.55078	14.45313
Range	237.9883	236.3281	231.0547	236.8164
Minimum	-0.87891	0.390625	0.585938	2.832031
Maximum	37.98828	36.32813	31.05469	36.81641
Sample Variance	34.1233	29.96871	29.09316	25.71806
Standard Deviation	21.56245	20.94828	19.78983	19.57774
99.85th Percentile	33.44727	32.24609	28.90625	29.00391
3*Std Dev +mean	33.24548	31.89702	30.57745	29.72034

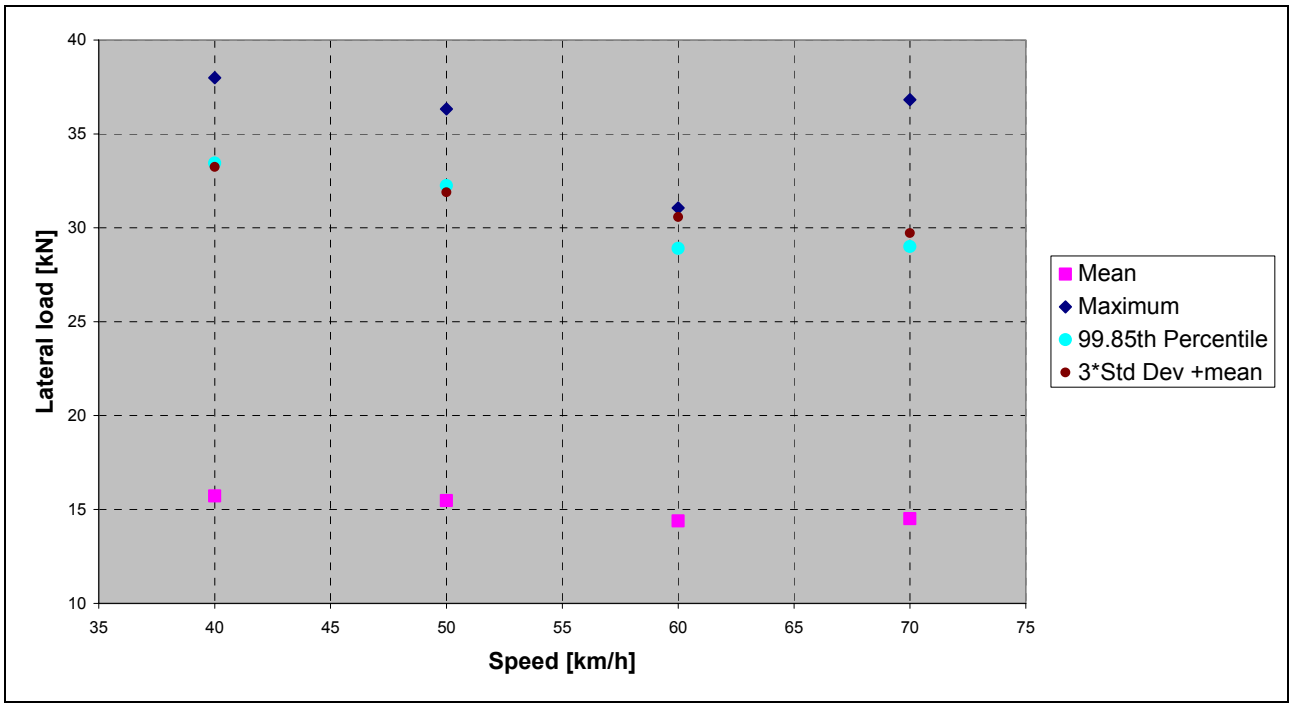

Figure 4-42: Statistical summary of lateral left forces at different speeds

When referring back to the Sweden curve geometry (see Figure 4-23 on page 66) which included a number of representative curves, the lateral load results indicate all values to be below 40*kN*. For this section of line, 40*kN* would therefore be an acceptable value to use for the lateral forces in rail stress calculations.

4.1.2.2. Lateral force analysis

With detailed vehicle and track models, typical lateral forces can also be determined with software packages such as Medyna and MSC.ADAMS. An example of such an analysis will be presented in section 4.1.3.1 under the heading of "Eccentricity analysis". A first order analysis was executed with Medyna. A vehicle was modelled travelling at a speed of 60*km/h* with a new wheel profile through a 500*m* radius curve to the right with a super elevation of 45*mm* on a new rail profile. The results presented are the eccentricity of the vertical wheel forces as well as the lateral track forces.

4.1.3. Eccentricity of vertical wheel load

The eccentricity of the vertical wheel force on the rail is the third factor that the analytical method of determining rail stresses is the most sensitive to and for which no guideline is currently available regarding minimum and maximum values. In the sensitivity study, the eccentricity was varied between –22*mm* and +22*mm*, in conjunction with a lateral force. From Figure 3-2 it can be seen that the position of the vertical force could either contribute to the moment about the rail shear centre due to the lateral force, or oppose it. In the current analytical model, a positive eccentricity opposes the lateral force and vice versa in determining the torsional moment.

Determining nominal values for eccentricity is not an easy task since wheel rail interaction is an engineering science in its own right and a focused study in the field of vehicle design, especially bogie design. Furthermore, it is not only a function of the bogie design and the wheel and rail profile design, but also of the maintenance plans of both the rolling stock and infrastructure departments. The vertical wheel force is a function of especially the wheel and rail profile designs and each railway could have its own design and maintenance philosophy. Maintenance plans are important since they affect the amount of wheel and rail wear that will be allowed before corrective action is taken.

Maintaining the rail profile means the deployment of on-track grinding machines that profile the railhead running surface to a predetermined profile on a predetermined cycle. Maintaining wheel profiles means the removal of vehicles from service, removal of complete wheel-and-axle sets and machining them back to a predetermined profile on a predetermined cycle.

Typical worn wheel profiles become "hollow" and two point contact may occur between wheel and rail. This means that the wheel no longer has only one point of contact with the rail and determining the resultant point of contact of the vertical wheel rail force becomes quite complex. A worn rail profile also changes the behaviour of wheel rail interface, complicating matters further. A method that is used more often these days is to use computer software that is explicitly designed for this

purpose, to determine not only the wheel rail contact points in a centre static position, but also during the dynamic negotiating of a track.

Medyna and ADAMS/Rail are two such packages that can be used to investigate the effect of rail and wheel profiles on the lateral and vertical forces, as well as vertical load eccentricity. The following section will show how typical eccentricity values were determined from an analysis with Medyna.

4.1.3.1. Eccentricity analysis

In order to be able to supply eccentricity values for a user of the analytical rail stress model, a first order analysis was executed with Medyna. A vehicle was modelled travelling at a speed of 60*km/h* with a new wheel profile through a 500*m* radius curve to the right with a super elevation of 45*mm* on a new rail profile. The software analyses the behaviour of the vehicle due to the rail wheel interaction and reports the wheel forces as discrete points with time. These results are presented in Figure 4-45 and the sign conventions are as indicated in Figure 4-44. Positive eccentricity values indicate vertical forces on the outside of the rails and positive lateral forces are also towards the outside of the rails. This means that a positive eccentricity value of the vertical load would contribute to a positive lateral load in increasing the moment about the rail centre, which is contrary to the current analytical model's sign definition where a positive eccentricity value of the vertical load *opposes* a positive lateral load.

It would be recommended that a more detailed study into representative wheel and rail profiles should be performed and that dynamic wheel rail interaction studies should then be performed on such profiles or a variety of profiles to determine nominal eccentricity values. This should then be performed on a variety of track conditions and curve radii to ensure realistic results.

Another reason why extensive research should be performed on this subject is that it is not necessarily true that the extreme eccentricity values would occur simultaneously with the maximum lateral loads. This could be assumed by an inexperienced user of the current analytical model, since the user is simply prompted for these two values and one may intuitively assume that two maximum values might represent the worst-case scenario, which is not the case.

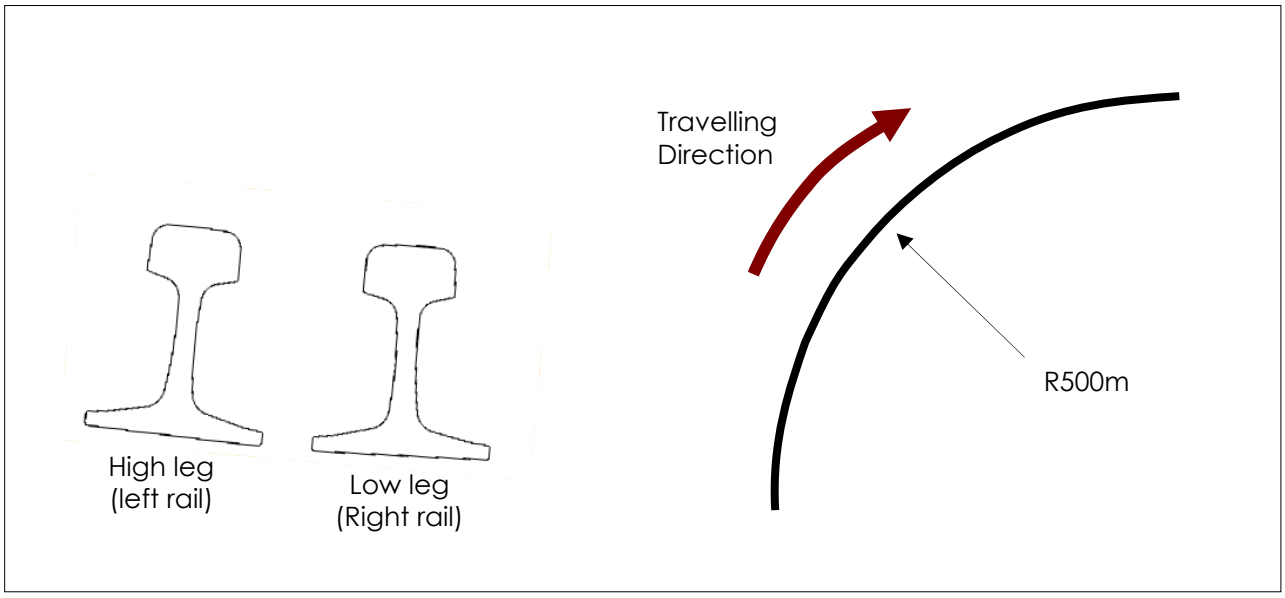

Figure 4-43: Track layout for Medyna analysis

It must be emphasised that this is an analysis on only one specific case. It is not the intention to study all possible cases but rather study trends of eccentricity vs. lateral force magnitude for this nominal case study.

This first order analysis of a new wheel on a new rail profile is not only a good starting point but also represents conditions on a railway line that has a good maintenance schedule with regular re-profiling of wheels and rails back to their design profiles.

The results from Figure 4-45 indicate the complicated pattern of possible combinations of the position of the vertical load and the magnitude of the lateral load (even for a new rail and wheel profile!). It would therefore be incorrect to specify a range of eccentricity values without including a relationship to the magnitude of the lateral load. The high eccentricity values are only occurring with opposing lateral loads while the lower eccentricity values may occur with contributing high lateral loads. Depending on the magnitude of the vertical load, either combination could result in the highest rail stresses.

From the above results it became clear that for the high leg rail a positive eccentricity of 9*mm* could occur with a lateral load of 1.65*kN* in an opposing direction (point A in Figure 4-45) or a 13*kN* load in a contributing direction (B). A maximum eccentricity of 33*mm* can occur together with a 31*kN* opposing lateral load (D) or at 31*mm* with a 58*kN* opposing lateral load (C). It is also important to note that an eccentricity of 32*mm* could occur with a very low opposing lateral load of 3.7*kN* (E), which could also result in the highest rail stresses under a high vertical load.

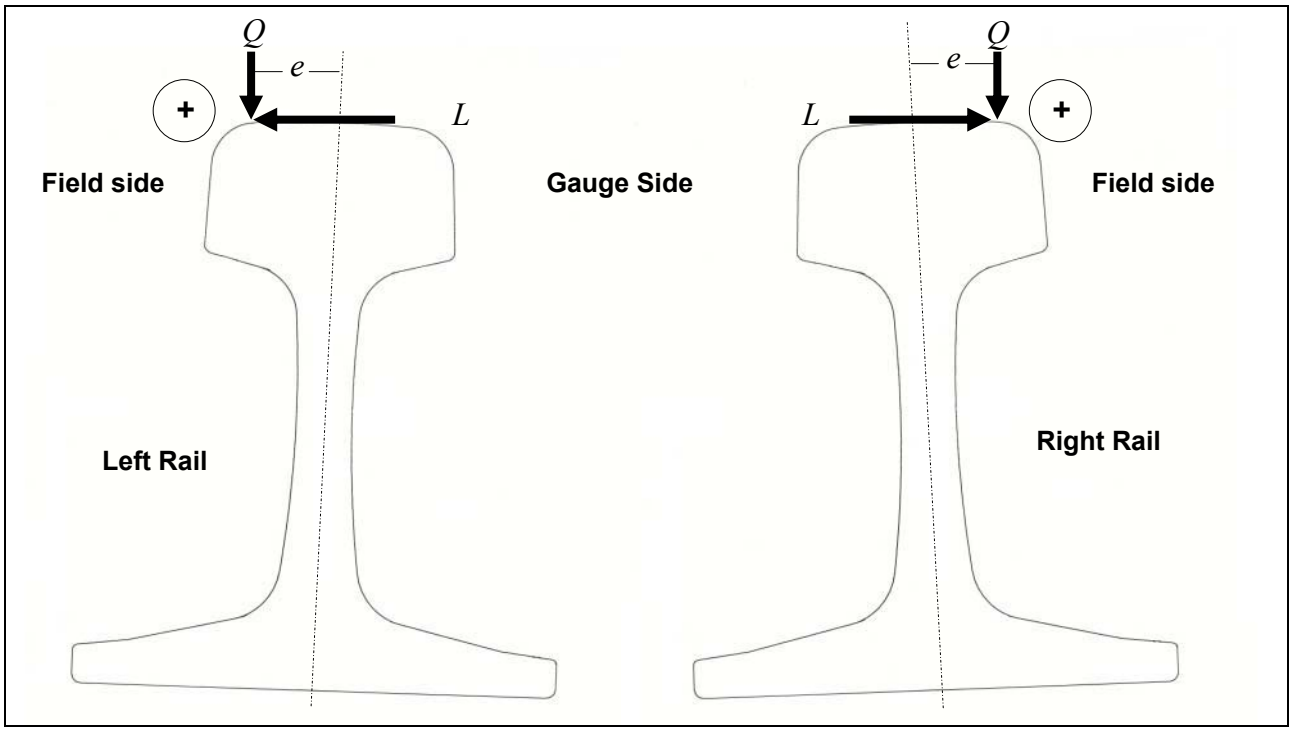

Figure 4-44: Eccentricity and lateral force sign convention of Medyna results

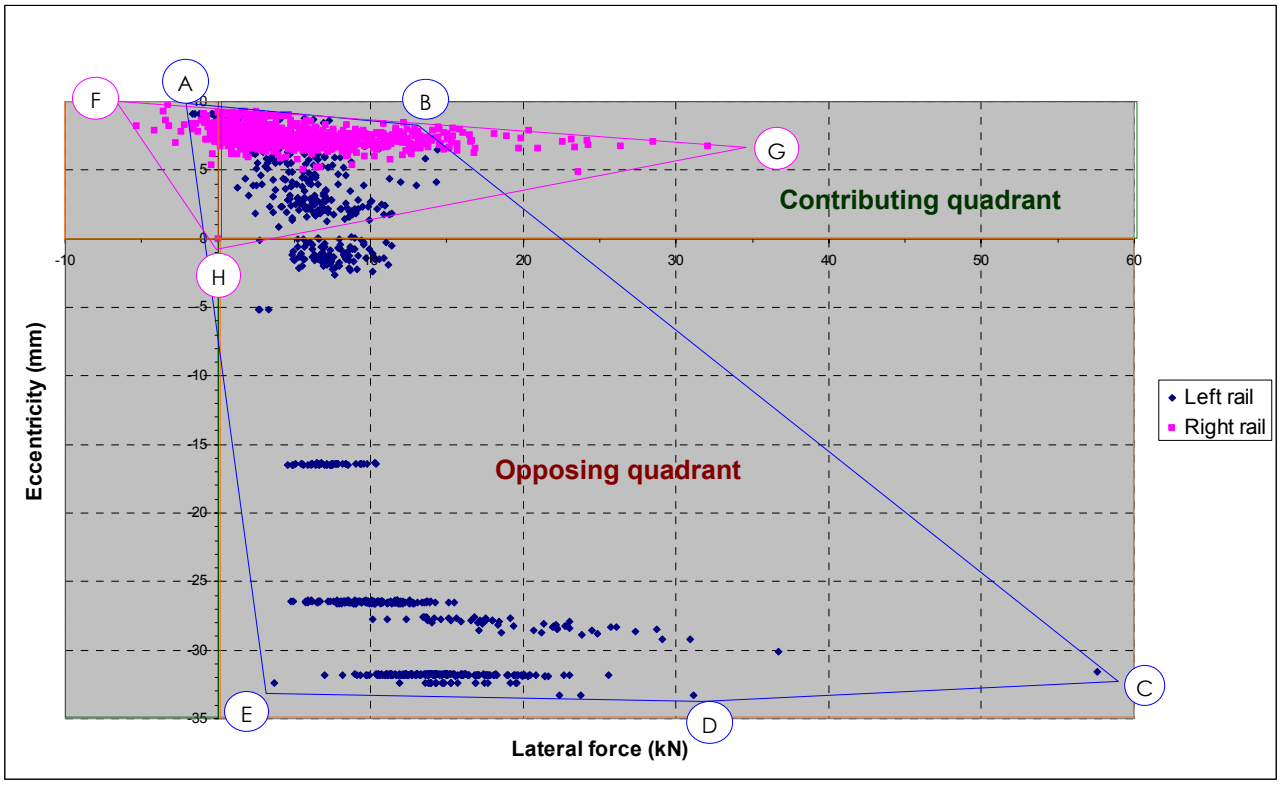

Figure 4-45: Vertical force eccentricity vs. lateral load

For the low leg rail, a maximum eccentricity of 9.2*mm* occurred together with an opposing lateral load of 7.5*kN* (F) and, at an eccentricity of 6.8*mm*, the highest contributing lateral load of 32*kN* (G) was reached.

Table 4-13 indicates the above combinations of eccentricity and lateral load combinations that could result in worst-case scenarios for rail stresses. Each corner of the result envelopes (refer Figure 4-45) was taken as a possible worst-case scenario and is indicated with the letters A to H. The coordinate system from the above results was translated to the rail stress model input coordinate system where the lateral load is always positive with the eccentricity being either positive (opposing the lateral load) or negative (contributing to the lateral load).

Table 4-13: Possible worst-case scenarios for eccentricity and lateral load pairs (rail stress model coordinate system: positive eccentricity *opposing* positive lateral force)

High leg		**A**	**B**	**C**	**D**	**E**
	e (*mm*)	+9	-6.5	+31	+33	+32
	L (*kN*)	1.7	14.3	58	31	3.7
Low leg		**F**	**G**			
	e (*mm*)	9.2	-6.8			
	L (*kN*)	7.5	32			

The highest stresses will occur on either of the extreme points in Figure 4-45 (F,G, C, D or E) since the rail stresses are directly related to the magnitude of the lateral forces and the eccentricity of the vertical forces. Since it was shown that no relationship exists between the lateral and vertical wheel loads, it is important to realise that the magnitude of the vertical forces will determine which combination of lateral loads and eccentricity for a specific scenario would result in the highest rail stresses. For this reason, all the possible worst-case scenarios should be identified and analysed to determine the highest rail stresses.

The above results of this specific case study gave rise to the notion that at least four worst-case scenarios could typically occur namely:

- Maximum lateral force with maximum *opposing* eccentricity (point C and/or D)
- Zero lateral force with maximum eccentricity (~ point E)
- 5% of the maximum lateral force with 30% of the maximum *opposing* eccentricity (point F)
- 50 % of the maximum lateral force with 20% of the maximum *contributing* eccentricity (point G)

4.1.3.2. Summary of the methodology to determine eccentricity vs. lateral load values

Based on these results, it is evident that a rail stress analysis should not only be determined for one maximum eccentricity along with one maximum lateral load. The maximum lateral load does not coincide with the maximum contributing eccentricity of the vertical load and a high eccentricity with a low opposing lateral force could prove to be the worst-case scenario. The reason why the case of a high eccentricity with a high *opposing* lateral force is still regarded as a possible worst-case scenario (Table 4-13), includes the following:

- the vertical force is always significantly larger than the lateral force
- the high eccentricity, together with the high vertical force, could still result in a moment about the centre of the rail that is higher than in the case where the lateral load *contributes* to the moment of the vertical force with a lower eccentricity.

The methodology to follow includes the execution of an eccentricity analysis on either a range of wheel and rail profiles, or on a statistically representative wheel and rail profile pair. From such an analysis the envelope of eccentricity values vs. lateral load values should be determined. A rail stress analysis should then be performed for each possible worst-case scenario as was done in the example of Table 4-13.

4.1.4. Rail stresses calculation improvement

When comparing the rail stresses from the finite element model to the analytical model (3.1.3.1), it was found that there was a slight offset in the rail stresses in the bottom corner of the railhead. After investigation it was found that the definition of the railhead depth (height), as used in the analytical calculations, was causing this phenomenon.

It is generally acceptable to define the railhead as the shaded area in Figure 4-46 where the bottom boundary of the railhead is defined by extending the inclined lines at the bottom of the railhead, until they intersect (Point A in Figure 4-46). The railhead depth was then subsequently defined as the maximum distance between this intersection and the top of the rail. For a 57*kg/m* rail, this distance is 47.5*mm*.

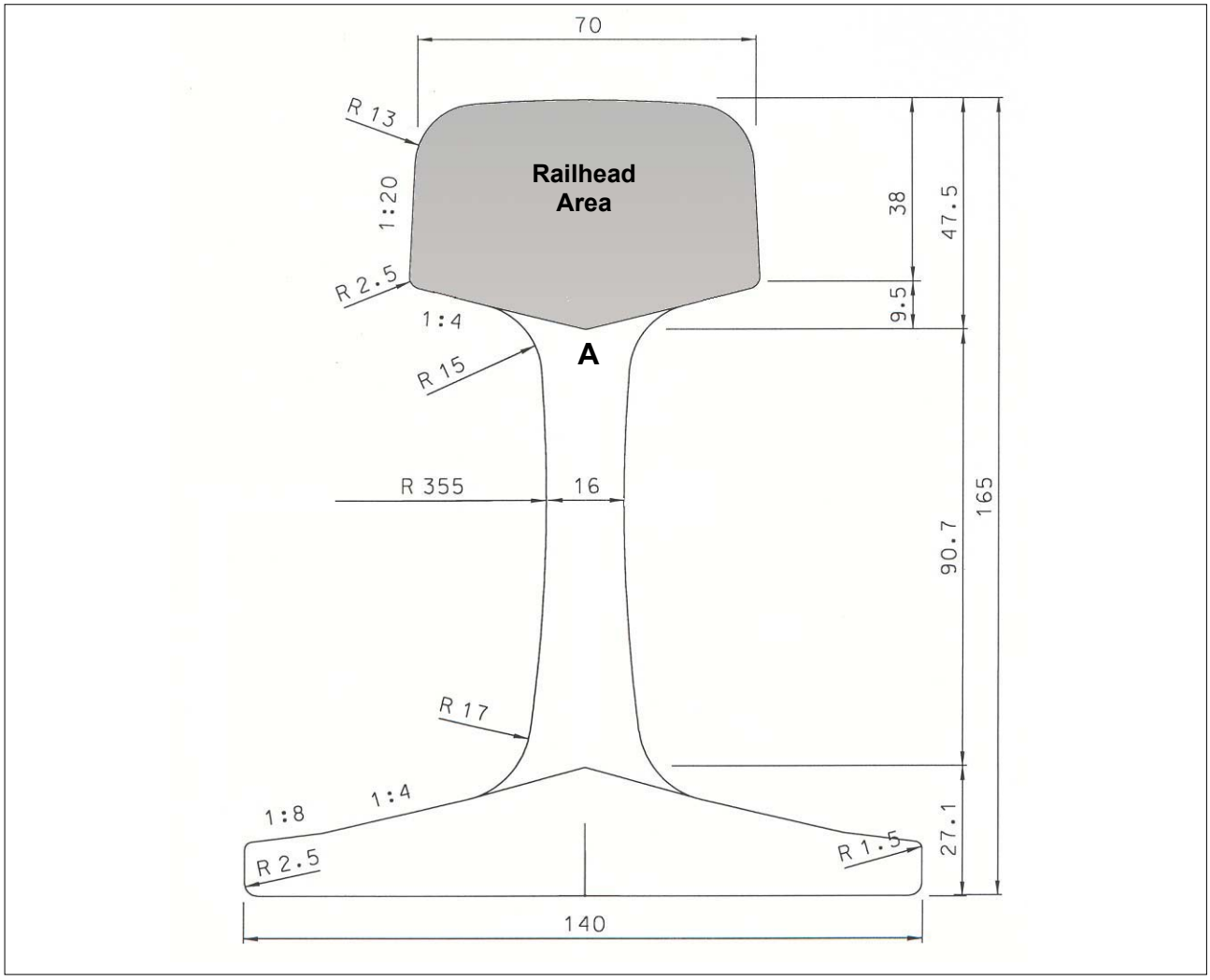

Figure 4-46: Profile properties of a 57*kg/m* rail

In Figure 4-47, the stress results from both the FEA and analytical method are compared, with the railhead depth chosen as 47.5*mm*. The inconsistency of the rail stresses between the two methods can clearly be seen.

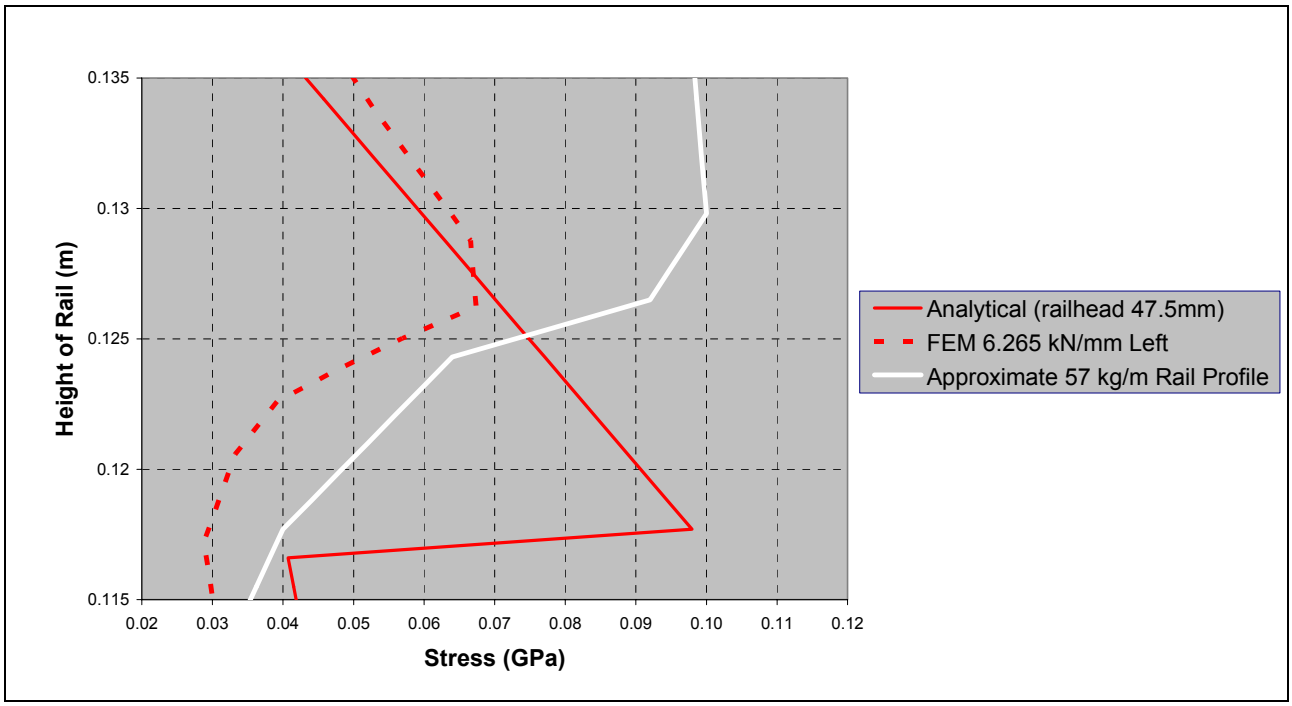

Figure 4-47: Rail stress comparison with railhead depth chosen at 47.5*mm* (100*kN* off-centred vertical load and 50*kN* lateral load)

The stress results in Figure 4-47 indicate that the maximum local tensile stresses of the analytical method with the railhead depth taken as 47.5*mm* are higher than the FEA results (±30*MPa*) and also at a lower position (±10*mm*). The fact that the FEA results indicate the maximum tensile stress to be at a higher location suggests that the definition of the railhead depth, as used in the analytical method, is wrong and should be re-defined. The reason for this is that, although this distance represents the extremities of the railhead, it does not represent the height of a rectangular section of equal area and second moment of area (as is assumed in the calculations).

It could be noted that the analytical calculation gives a rapid change in stress at the bottom corner of the railhead due to the simplification of the rail profile as separate rectangular beams supporting one another as described in 3.1.3. The FEA model on the other hand uses a more accurate profile, thus the smooth transition in stresses at the bottom of the railhead.

Since the railhead area is defined as in Figure 4-46 and is easily calculated with any commercially available CAD package together with the second moment of area, it is proposed to derive the railhead depth and width from the relationships:

$$b = A / h \qquad (4.6)$$

and

$$h = \sqrt{\frac{12 \cdot I}{A}} \qquad (4.7)$$

with A being the railhead area and I being the second moment of area of the railhead about its horizontal axis through its centroid.

This results in dimensions equivalent to that of a rectangular beam section with the same area and second moment of area, which therefore makes a better approximation of the rail stresses.
The railhead depth for a 57*kg/m* rail therefore changes to 43.17*mm* and gives the resultant stress comparison with the FEA results as in Figure 4-48 which differ by approximately 4*MPa* (13% improvement) in magnitude and ±4*mm* in location (50% improvement).

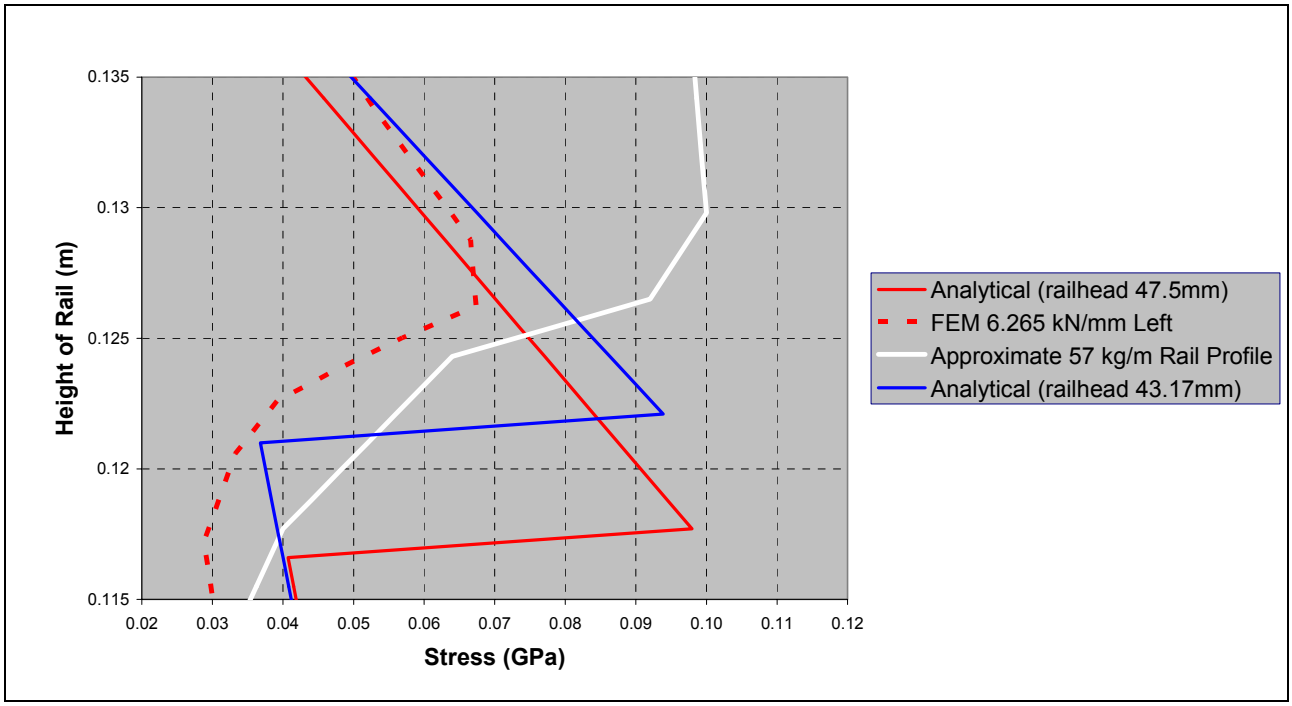

Figure 4-48: Rail stress comparison with railhead depth chosen at 43.17*mm* vs. 47.5*mm* (100*kN* off-centred vertical load and 50*kN* lateral load)

The proposed definition of railhead depth will thus result in new railhead depths for all the different rail profiles as indicated in Table 4-14.

This modified definition of the railhead depth clearly improves the correlation between the results of the FEM and the analytical method.

Table 4-14: New proposed railhead depths for different rail sections

Rail Profile	Current Railhead depth (*mm*)	Proposed Railhead depth (*mm*)
48 *kg/m*	43.0	38.3
57 *kg/m*	47.5	43.2
S60 *kg/m*	47.9	41.1
UIC 60*kg/m*	51.0	43.8

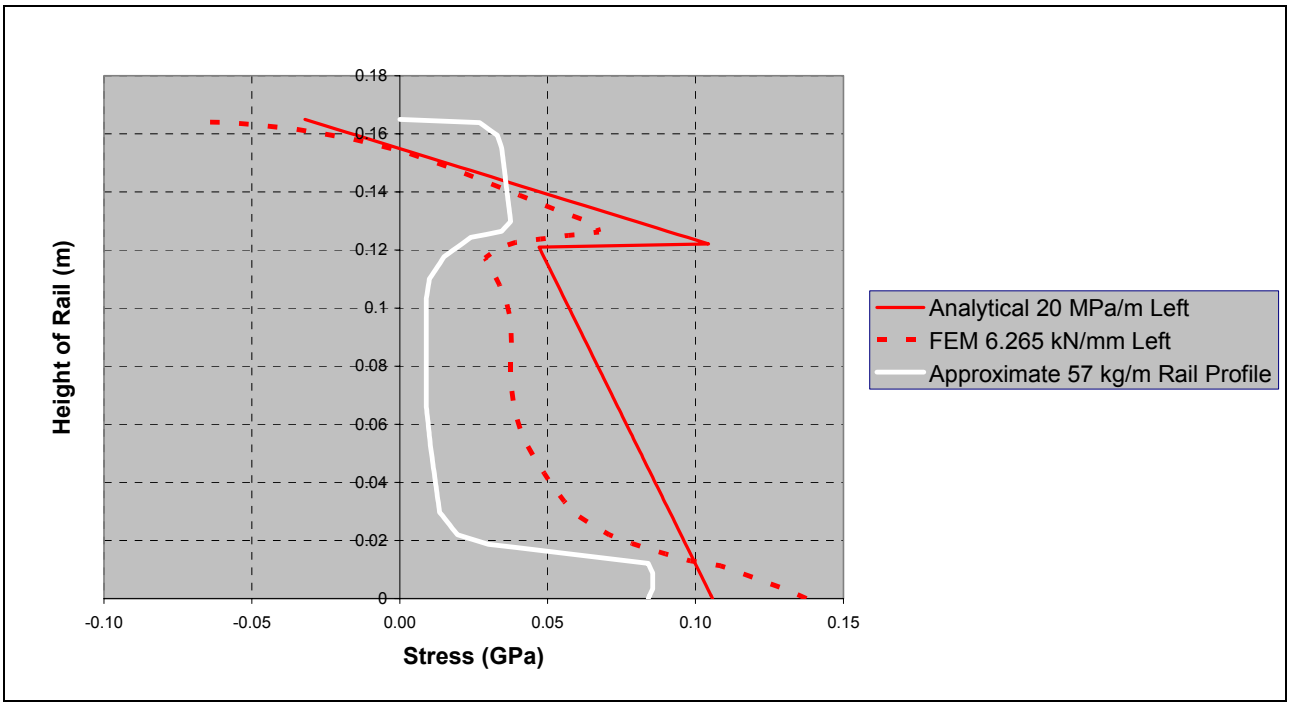

Figure 4-49: Rail stress comparison with railhead depth chosen at 43.17*mm* (full profile scale)

4.2. Sensitivity study on modified analytical method

A sensitivity study was performed on the new model with all the applied modifications in order to identify the parameters to which the modified model was the most sensitive to to enable future users and researchers to focus their efforts on the acquisition of those parameters. Table 4-15 indicates the input parameters and their minimum and maximum values used in the analysis with their individual effect on the rail stresses. Each parameter was held constant at its median (middle) value while varying each one at a time while reporting the effect on the rail stresses. The parameters to which some changes were made in the modified model are indicated in blue: Foundation Modulus (Changed range of values), Eccentricity (Changed range of values and model now automatically use in different combinations with Lateral load), Rail section (change of railhead depth definition) and the Lateral load (Changed factor of static value to force value).

Table 4-15: Input parameter sensitivity analysis

Parameter	Parameter Value			Max Rail Head Tension (MPa) / Max Rail Flange Tension (MPa)			Band Width Max - Min	Sum Head & Flange Band width
	Min	Mid	Max					
	A	B	C	A	B	C		
Dynamic Factor	1.1	1.49	1.73	163.12	185.6	199.75	36.63	86.37
				193.58	224.1	243.32	49.74	
Static Wheel load	67.5	100	150	157.48	185.6	228.89	71.41	168.41
				185.89	224.1	282.89	97	
Foundation Modulus	20	100	200	174.21	185.6	186.72	12.51	35.1
				244.68	224.1	222.09	22.59	
Sleeper Spacing	500	600	700	185.9	185.6	185.3	0.6	12.23
				218.29	224.1	229.92	11.63	
Type of Sleeper	Wood	Concrete	Steel	185.43	185.6	185.47	0.17	0.49
				224.42	224.1	224.34	0.32	
Effective Area of Sleeper	0.4	0.48	0.6	185.24	185.6	185.96	0.72	2.02
				224.76	224.1	223.46	1.3	
E modulus rail	200	205	210	183.23	185.6	187.97	4.74	9.73
				221.61	224.1	226.6	4.99	
Poisson	0.289	0.3	0.33	185.49	185.6	185.91	0.42	0.65
				224.04	224.1	224.27	0.23	
Eccentricity of Vertical force Q	0	0.02	0.03	195.13	185.6	199.19	13.59	71.35
				185.6	224.1	243.36	57.76	
Position of Lateral force below top	0	0.007	0.015	185.6	185.6	185.6	0	3.24
				222.59	224.1	225.83	3.24	
Rail section	48	57	S60	202.64	185.6	195.15	17.04	73.92
				261.24	224.1	204.36	56.88	
Wheel distances	1.56	1.91	10.06	191.34	185.6	166.56	24.78	69.54
				213.74	224.1	258.5	44.76	
Max Temperature change	30	42	55	157.31	185.6	216.25	58.94	117.88
				195.81	224.1	254.75	58.94	
Lateral Load	0	20	40	185.6	185.6	204.65	19.05	34.06
				216.6	224.1	231.61	15.01	

The resultant stress ranges, as a result of changing each parameter, are also graphically displayed in Figure 4-50, with the order of importance indicated by the resultant range in stresses as listed in Table 4-16. The parameters from the Eisenman formula (eq. 3.2) namely the running top condition, confidence level and speed are omitted from the parameter list in Table 4-16 since the Dynamic factor may now be specified without the use of the Eisenmann formula. The rail steel type is also omitted since it influences only the fatigue limit and not the rail stresses.

4.3. Conclusion

By investigating the input parameters to which the analytical model is the most sensitive, the user is now provided with nominal values which he may compare with new input values. The user is also made aware of possible methods that could determine these important parameters and possible problems to avoid. This contribution has improved the available analytical method significantly and enhanced its suitability as a method to calculate track component stresses.

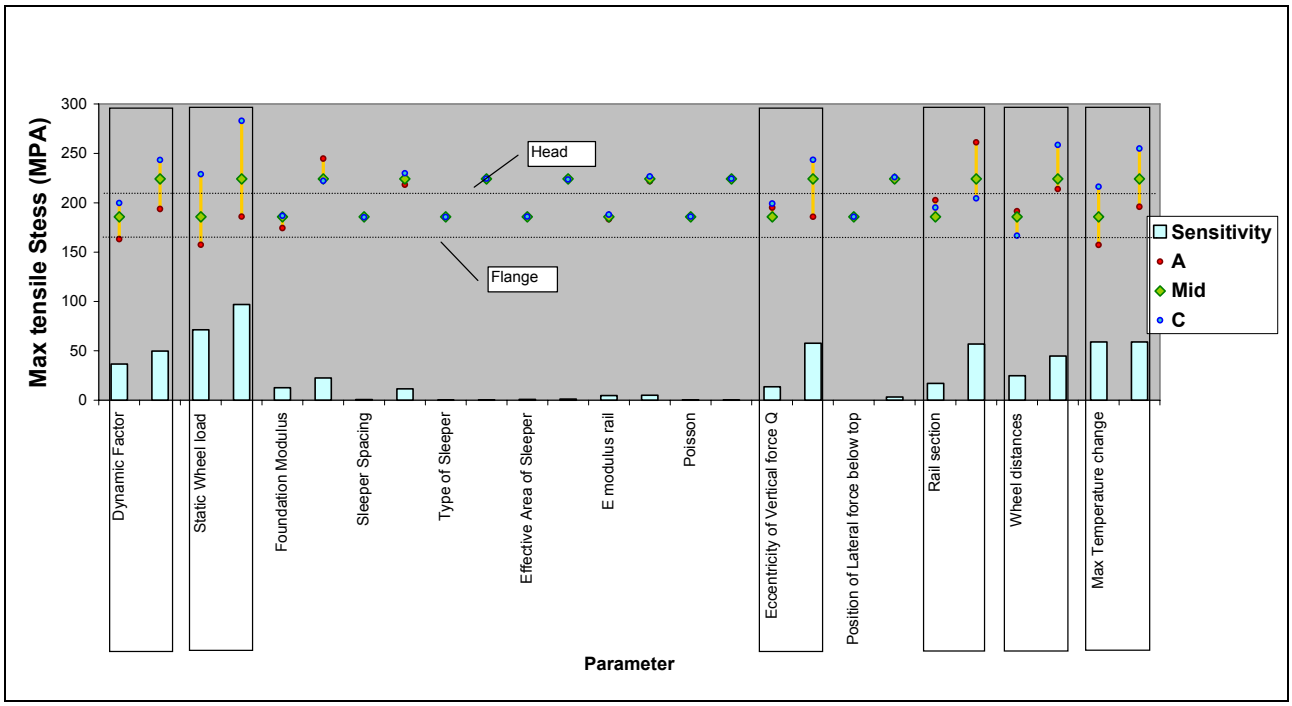

Figure 4-50: Sensitivity analysis of parameters in component stress calculation spreadsheet

Table 4-16: Order of sensitive parameters

Order of Importance	Parameter	Sum of Head & Flange Band widths	Percentage of highest value
1	Static Wheel load	168.41	100%
2	Max Temperature change	117.88	70%
3	Dynamic Factor	86.37	51%
4	Rail section	73.92	44%
5	Eccentricity of Vertical force Q	71.35	42%
6	Wheel distances	69.54	41%
7	Foundation Modulus	35.1	21%
8	Lateral Load	34.06	20%
9	Sleeper Spacing	12.23	7%
10	E modulus rail	9.73	6%
11	Position of Lateral force below top	3.24	2%
12	Effective Area of Sleeper	2.02	1%
13	Poisson	0.65	0%
14	Type of Sleeper	0.49	0%

5 METHODOLOGY FOR CALCULATING TRACK COMPONENT STRESSES

Different investigations were launched regarding the input parameters to which the analytical method was the most sensitive and best practice procedures were identified that could determine input parameter values to ensure acceptable results.

This chapter will summarise the methodology to calculate stresses in track components with reference to the developed spreadsheet that incorporates all the latest modifications to the analytical method.

5.1. Methodology

When the user assesses the process of determining proper input values for the model, it should be emphasised that the available resources should be spent on obtaining proper input for those parameters that the model is the most sensitive to (paragraph 4.2. page 94). From those parameters, the following is the most important (in order of sensitivity): static wheel load, maximum temperature change, dynamic factor, rail section, eccentricity of the vertical wheel load and wheel distances.

Portions from the developed spreadsheet, with which a quasi-static analysis could be performed to calculate track component stresses, are indicated in Figure 5-1 to Figure 5-6. The spreadsheet incorporates the latest modifications to the analytical method. Drop-down boxes indicate where the user has the option to choose input from a list of values and yellow cells indicate where the user may enter a value.

The developed spreadsheet comprises of a multitude of input cells and formulas. These and additional information are grouped under seven headings namely: “Dynamic factor”, “Support condition”, “Material”, “Rail section properties”, “Bogie setup”, “Rail seat stress” and “Railhead and flange stresses”. The methodology to calculate track component stresses will be presented in this order.

5.1.1. Dynamic factor

The dynamic factor is one of the parameters that the analytical model is the most sensitive to (paragraph 4.2. page 94) and which has to be chosen (or calculated) carefully in order to obtain acceptable stress results.
Figure 5-1 indicates the input parameters for calculating a dynamic factor with the Eisenmann formula. This research has shown that the Eisenmann formula is a conservative method to use and

may result in a high dynamic factor (paragraph 4.1.1.5, page 68) depending on the chosen input. The user is encouraged to compare the result of the Eisenmann formula with the results from actual tests (Figure 4-26, page 69).

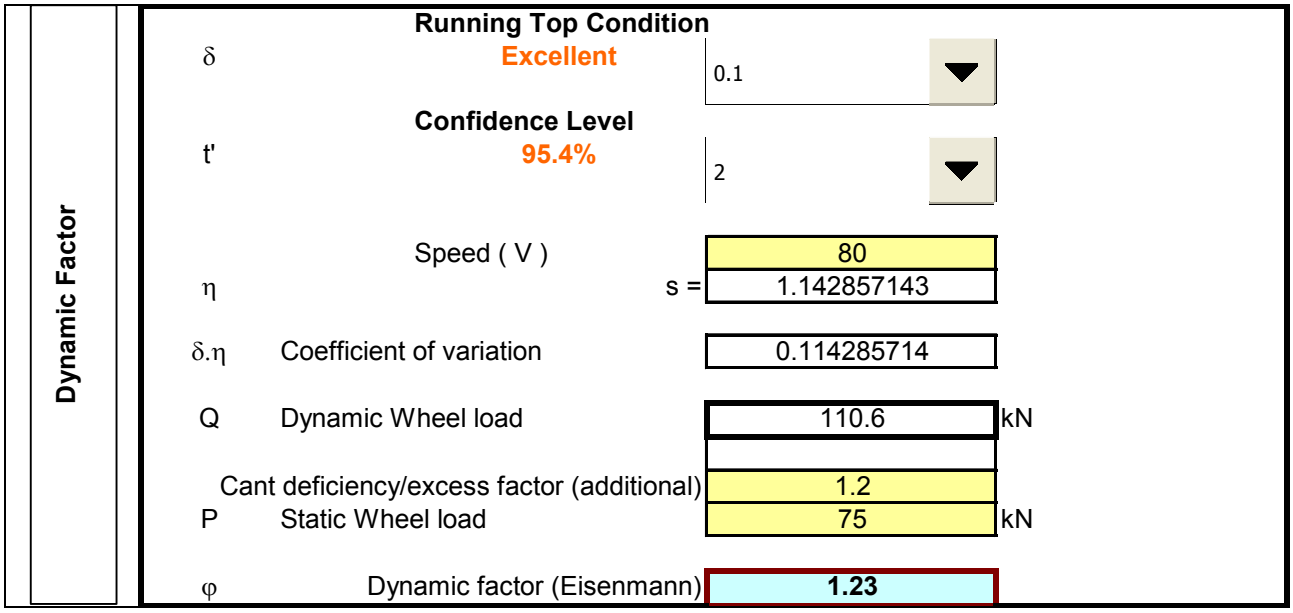

Figure 5-1: Dynamic factor parameters

In order to determine the dynamic factor from the instrumented wheelset results, there are two possible approaches to follow:

- The first approach ignores the existence of a moving average (i.e. there is no distinction made between straight and curved track) and calculates the dynamic factor from the 99.85th percentile (3 times the standard deviation) of the whole track, including irregularities such as turnouts. This method is preferred when the railway line is designed as a whole, without distinguishing between straight and curved track (and even turnouts).
- The second approach is based on the procedure specified in UIC Code 518 (30, p. 28) for testing and accepting railway vehicles based on their dynamic behaviour. The dynamic factor is calculated for short sections of the whole track individually. This method is preferred when evaluating shorter sections of track, where the macrogeometry is taken into account by other means like additional force factors etc.

When determining a dynamic factor that includes macrogeometric deviations (first approach), the dynamic factor should be calculated as follows:

1. A piece of representative track should be measured with the instrumented wheelset at different speeds (up to and including the maximum line speed). It is, however, seldom possible to find a short section of track which is sufficiently representative of the track as a whole and it is thus preferred to measure the whole track under consideration.

2. Calculate the dynamic factor with either of the following equations:

$$\varphi = \frac{3 \cdot \text{Standard Deviation}(\text{Vertical Forces}) + \text{mean}(\text{Vertical Forces})}{\text{mean}(\text{Vertical Forces})} \quad (5.1)$$

or

$$\varphi = \frac{99.85^{th}\ \text{Percentile}(\text{Vertical Forces})}{\text{mean}(\text{Vertical Forces})} \quad (5.2)$$

With currently available calculation tools, both formulas could easily be utilised and the results evaluated to determine which value would be more appropriate to use. Using 3 times the Standard Deviation of the vertical forces could present a less realistic result, when a short piece of track is measured, if the maximum values are a result of localised geometry defects (which would result in a high deviation from the mean). If a sufficiently long piece of track is measured and a Gaussian distribution is present, the results of equations 5.1 and 5.2 should be the same.

When determining a dynamic factor that does not include the effect of macrogeometric deviations (second approach), the dynamic factor should be calculated as follows:

1. The test section should be divided into three zones (30, p. 28), namely:
   - tangent track and large radius curves (R>1200*m*),
   - large radius curves (600*m*<R<1200*m*),
   - small radius curves (R<400*m*).

   The procedure in (30, p. 30) specifies that each zone should have a total of at least 10km, since it is rarely possible to find a short section of track which is sufficiently representative of the track as a whole.
2. Each of these zones should then be divided into sections with a maximum length as indicated in Table 5-1 (for this purpose, the transient curves may be included in the curve sections).

Table 5-1: Test section lengths for statistical analysis

Test Zones		Section Lengths
Tangent track and large radius curves (R>1200*m*)		250*m*
Large radius curves (600<R<1200*m*)		100*m*
Small radius curves	(400<R<600*m*)	100*m*
	(R<400*m*)	70*m*

3. For each of these sections, the following should be calculated: Mean value, Standard Deviation and 99.85th percentile of the measured vertical loads.

4. A dynamic factor is then calculated for each section with the use of equations 5.1 and 5.2 and then calculated for the line as a whole by taking the average of all the values calculated (for either the standard deviation method or the percentile method).

When stress calculations for a new track (non-existing track) are carried out, the user may choose to use the available Eisenmann formula and values for the track condition that match the intended maintenance plans. The alternative is to utilise dynamic factors measured on existing lines which carry the same rolling stock under the same operating conditions as the newly designed track would.

5.1.2. Support condition

Although the support condition does not appear in the "top six" list of parameters to which the analytical model is the most sensitive (paragraph 4.2. page 94) and therefore does not affect the rail stress result as much as the other mentioned input parameters, it does affect the rail deflection significantly (refer Figure 3-5, page 26).

It is important to realise that a stiff support increases the rail stresses while decreasing the rail deflection and vice versa (24, p. 122). However, excessive rail deflection accelerates ballast breakdown, which enhances ballast fouling and eventually stiffens the track again. Unfortunately, this process does not stabilise or lead to an optimally stiff track. Due to this uncontrolled process, portions of the track may foul faster, resulting in irregular support stiffnesses. These irregularities, fuelled by excessive movement of the track, are eventually detrimental to the track geometry.

Choosing the foundation modulus for a piece of track can be done by following the guidelines in Table 5-2 or by extensive testing with the BSSM. The user may then simply choose a value from the drop-down list in the spreadsheet (refer Figure 5-2).

Table 5-2: Foundation modulus values

Foundation Modulus (C) [*MPa/m*]	**Condition description** (1, p. 79) (2, p 36-37)
20	Very bad clay formation and bad ballast condition[††]
50	Bad to average formation and ballast condition
100	Good formation and ballast condition
200	Other: (200=Very good formation and ballast condition)

The next parameter to specify is the sleeper spacing (refer Figure 5-2). The user may simply enter a value for the sleeper centre-to-centre distance. A warning will be displayed if the value does not satisfy the equation:

[††] As mentioned earlier, these unquantified terms do make using these criteria vulnerable to poor user interpretation.

$$a \prec \frac{\pi \cdot \lambda}{4} \qquad (5.3)$$

with λ being the characteristic length as defined by (3.9). Equation 5.3 should be true to ensure that the theory of a continuously supported beam holds for a discretely supported rail.

The type of sleeper may then be chosen from the available list (drop-down box) which then automatically fills in the appropriate effective area for the sleeper and calculates the track modulus.

Support Condition					
	C	**Foundation Modulus**	20		MPa/m
	a	Sleeper Spacing	500		mm
	ν	Type of Sleeper	Concrete		
			PY, FY		
	Ae	Effective Area of whole Sleeper	0.6012		m^2
	κ	Characteristic Value	0.3006		
	k	track stiffness	27.88460038		MN/m
	U	**Track Modulus**	12.024		MPa

Figure 5-2: Support condition parameters

5.1.3. Material

The material properties are specified as indicated in Figure 5-3. The user may select the type of commercial rail steel from the list in the drop-down box which sets the ultimate tensile strength of the material for calculating the fatigue stress limit. The rail fatigue stress limit is calculated as 30% of the UTS.

Material				
	E	E modulus rail	205	GPa
	G	Stiffness modulus	79.51900698	GPa
	υ	Poisson	0.289	
	UTS	Ultimate Tensile Strength	HH (UICA)	

Figure 5-3: Material parameters

5.1.4. Rail section properties

An extensive list of available rail profiles is available in the spreadsheet, which includes standard profiles as well as worn rail profiles. Due to the limitations of the software, only 8 profiles are available from the drop-down box (refer Figure 5-4) at a time but the user may replace any of these with any of the 45 available profiles and their properties.

When the user selects a rail profile, its properties (refer Figure 5-5) are automatically updated in the spreadsheet (refer Figure 5-4).

After selecting the rail profile, the user needs to enter the maximum eccentricity of the vertical force as well as the maximum lateral force.

5.1.5. Vertical load eccentricity

The proposed method to follow when determining eccentricity values is to simulate the wheel-rail interaction (refer 4.1.3, page 85) for the applicable vehicle and track conditions. These simulations can be carried out by using suitable software, such as Medyna or MSC.ADAMS. The maximum eccentricity and maximum lateral forces, as well as the possible worst-case combinations thereof, can then be determined.

Based on these results, it is evident that a rail stress analysis should not be determined only for one maximum eccentricity along with one maximum lateral load. The maximum lateral load does not coincide with the maximum contributing eccentricity of the vertical load and a high eccentricity with a low opposing lateral force could prove to be the worst-case scenario. The reason why the case of a high eccentricity with a high *opposing* lateral force is still regarded as a possible worst-case scenario (Table 4-13), includes the following:

- the vertical force is always significantly larger than the lateral force
- the high eccentricity, together with the high vertical force, could still result in a moment about the centre of the rail that is higher than in the case where the lateral load *contributes* to the moment of the vertical force with a lower eccentricity.

The methodology to follow includes the execution of an eccentricity analysis on either a range of wheel and rail profiles, or on a statistically representative wheel and rail profile pair. From such an analysis the envelope of eccentricity values vs. lateral load values should be determined.

From this point on in the spreadsheet, all calculations are done in fourfold to calculate rail stresses for the four possible worst-case scenarios simultaneously. Although the spreadsheet contains default

values for the lateral loads and vertical load eccentricity, based on this research, the user has the option to change these.

The user needs to specify the maximum eccentricity and the maximum lateral load. The four different scenarios (worst-case scenarios) are then made up with percentages of these maximum values. A positive percentage of eccentricity of the vertical force is in an opposing direction to the lateral force with regards to the resulting moment about the railhead centre.

Rail Section Properties			57			
			42%	42%	57%	55%
			OK, safety envelope:	OK, safety envelope:	OK, safety envelope:	OK, safety envelope:
e	Max Eccentricity of Vertical force Q		0.033	0.033	-0.0099	-0.0066
L or Y	Max Lateral Force (Default = 40kN)		40.0	0	2	20
n'	Position of Lateral force below top		0.005	0.005	0.005	0.005
			Worst-case 1	Worst-case 2	Worst-case 3	Worst-case 4
		% of eccentricity	100%	100%	-30%	-20%
		% of lateral force	100%	0%	5%	50%
			Eccentricity Case 1	Eccentricity Case 2	Eccentricity Case 3	Eccentricity Case 4
A	Section Area		0.007324	0.007324	0.007324	0.007324
Ah	Railhead Area		0.002942	0.002942	0.002942	0.002942
b1	Width of Head		0.068142063	0.068142063	0.068142063	0.068142063
b2	Width of Flange		0.14	0.14	0.14	0.14
t	Web Thickness		0.016	0.016	0.016	0.016
d	Section height		0.165	0.165	0.165	0.165
a1	Head Depth		0.043174507	0.043174507	0.043174507	0.043174507
f	Flange thickness		0.0174	0.0174	0.0174	0.0174
yk	Top to Section NA		0.0864	0.0864	0.0864	0.0864
h	Head NA to flange NA		0.1336	0.1336	0.1336	0.1336
a2	Top to top of flange depth		0.1392	0.1392	0.1392	0.1392
Ixx	Second Moment of Area xx		0.000026508	0.000026508	0.000026508	0.000026508
Izz	Second Moment of Area zz		0.00000442	0.00000442	0.00000442	0.00000442
Ixx Head	Second Moment of Area xx Head		0.000000457	0.000000457	0.000000457	0.000000457
I1 or Izh	Second Moment of Area zz head		0.00000119	0.00000119	0.00000119	0.00000119
I2 or Izf	Second Moment of Area zz flange		0.00000319	0.00000319	0.00000319	0.00000319
J	Polar Inertia moment		0.000030928	0.000030928	0.000030928	0.000030928
Zk	Section modulus Ixx/yk		0.000306806	0.000306806	0.000306806	0.000306806
Zf	Section modulus Ixx/yf		0.000337252	0.000337252	0.000337252	0.000337252
Zxk	Railhead modulus xx		2.11699E-05	2.11699E-05	2.11699E-05	2.11699E-05
Z1 / Zzk	Railhead modulus zz		3.4927E-05	3.4927E-05	3.4927E-05	3.4927E-05
Z2 / Zzf	Rail flange modulus zz		4.55714E-05	4.55714E-05	4.55714E-05	4.55714E-05
h1	Head mmp from rotation point		0.097302283	0.097302283	0.097302283	0.097302283
h2	Flange mmp from rotation point		0.036297717	0.036297717	0.036297717	0.036297717

Figure 5-4: Rail section properties and load position input

		Different Rail Sections								
		48	57	S60	UIC60	s60cw_7.5sw_15	S60	s60cw 10sw_10	60	60
Section Area	A	6.1250E-03	7.3240E-03	7.6760E-03	7.6710E-03	6.8130E-03	7.6760E-03	6.7850E-03	7.6130E-03	7.6130E-03
Railhead Area	Ah	2.5140E-03	2.9420E-03	2.8960E-03	3.0850E-03					
Width of Head	b1	6.5566E-02	6.8142E-02	7.0433E-02	7.0448E-02	6.0700E-02	7.28E-02	6.4600E-02	7.00E-02	7.00E-02
Width of Flange	b2	1.2700E-01	1.4000E-01	1.5000E-01	1.5000E-01	1.5000E-01	1.50E-01	1.5000E-01	1.40E-01	1.40E-01
Web Thickness	t	1.4100E-02	1.6000E-02	1.6000E-02	1.6500E-02	1.6000E-02	1.600E-02	1.6000E-02	1.900E-02	1.900E-02
Section height	d	1.5000E-01	1.6500E-01	1.7200E-01	1.7200E-01	1.6450E-01	1.720E-01	1.6210E-01	1.710E-01	1.710E-01
Head Depth	a1	3.8343E-02	4.3175E-02	4.1117E-02	4.3791E-02	4.0000E-02	4.790E-02	3.7600E-02	4.750E-02	4.750E-02
Flange thickness	f	1.7300E-02	1.7400E-02	1.8000E-02	1.7900E-02	1.8000E-02	1.800E-02	1.8000E-02	1.940E-02	1.940E-02
Top to Section NA	yk	7.8900E-02	8.6400E-02	9.3500E-02	9.1500E-02	9.6700E-02	9.350E-02	9.4500E-02	7.900E-02	7.900E-02
Head NA to flange NA	h	1.2100E-01	1.3360E-01	1.4010E-01	1.3840E-01	1.3560E-01	0.1401	1.3490E-01	1.333E-01	1.333E-01
Top to top of flange depth	a2	1.2480E-01	1.3920E-01	1.4320E-01	1.4050E-01	1.3580E-01	1.432E-01	1.3330E-01	1.288E-01	1.288E-01
Second Moment of Area xx	Ixx	1.8506E-05	2.6508E-05	3.0815E-05	3.0350E-05	2.4290E-05	3.0815E-05	2.3802E-05	2.703E-05	2.703E-05
Second Moment of Area zz	Izz	3.2160E-06	4.4200E-06	5.4160E-06	5.1130E-06	4.8910E-06	5.4160E-06	4.9380E-06	4.454E-06	4.454E-06
Second Moment of Area xx Head	Ixx Head	3.0800E-07	4.5700E-07	4.0800E-07	4.9300E-07	1.8700E-07	4.0800E-07	1.6600E-07	4.570E-07	4.570E-07
Second Moment of Area zz head	I1 or Izh	8.6800E-07	1.1900E-06	1.1080E-06	1.1820E-06	5.8900E-07	1.1080E-06	6.2600E-07	1.190E-06	1.190E-06
Second Moment of Area zz flange	I2 or Izf	2.3140E-06	3.1900E-06	4.2410E-06	3.8800E-06	4.2410E-06	4.2410E-06	4.2410E-06	3.190E-06	3.190E-06

Figure 5-5: Rail section property list

5.1.6. Bogie setup

Regarding the bogie setup, the user has to enter the distances between four wheels (or axles). Figure 5-7 indicates how four wheels would each cause the rail to deflect. Since the deflections caused by the four wheels overlap, these are added to present the total deflection as indicated in Figure 5-7. From this example it is clear that, although the fourth wheel is relatively far away from the second, it still influences the total displacement of the rail below the second wheel. It should be noted that the total deflection caused by two or more wheels is higher than by one wheel alone but that the bending moment is lower than under a single wheel. Therefore, multiple wheels reduce rail stresses, while increasing the maximum deflection (24, p. 123).

Bogie set-up	x1	Distance from wheel in front	1.83	1.83	1.83	1.83	m
	x2	Distance from wheel behind	3.66	3.66	3.66	3.66	m
	x3	Distance from 4th wheel	5.49	5.49	5.49	5.49	m
	η1	Influence factor (wheel in front)	-0.207868198	-0.207868198	-0.207868198	-0.207868198	
	η2	Influence factor (wheel behind)	-0.041941405	-0.041941405	-0.041941405	-0.041941405	
	η3	Influence factor (4th wheel)	0.008978909	0.008978909	0.008978909	0.008978909	

Figure 5-6: Bogie setup

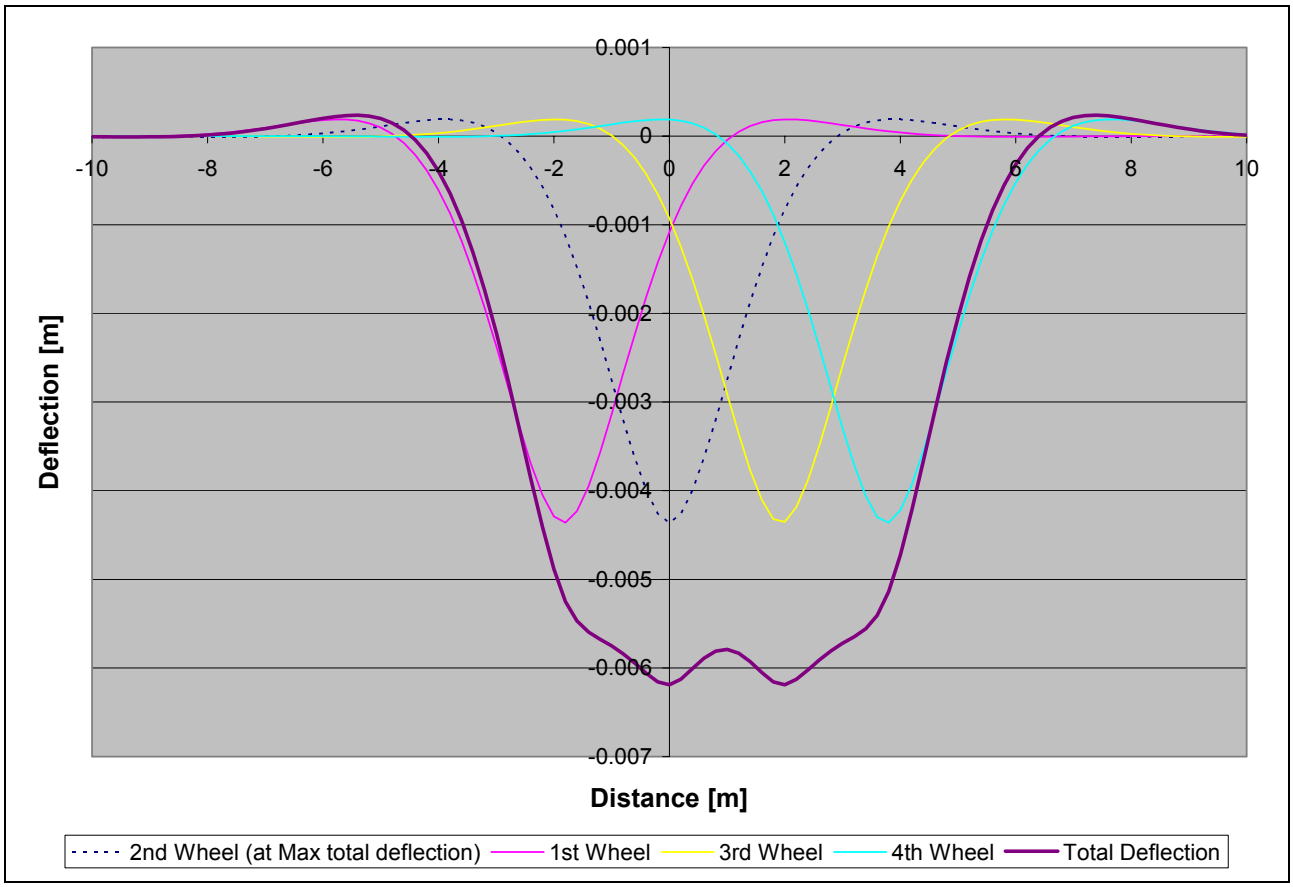

Figure 5-7: Rail deflection due to wheel spacing

5.1.7. Rail seat stress

The user needs to enter the pre-tension force of the rail clips as well as the baseplate area (contact area between rail and sleeper). From these values and the calculated rail seat force, the rail seat stress (pad stress) is calculated. This stress is then compared to guidelines from Esveld (1, p. 91) depending on the type of sleeper chosen. The sleeper-ballast stress is also calculated and compared to acceptable values as specified by (1, p. 92).

Rail Seat Stress							
	M	Rail Bending Moment	24.334	24.33363739	24.33363739	24.33363739	kNm
	R	Rail Seat Force	18.098	18.09823023	18.09823023	18.09823023	kN
	Ro	Design reaction force	36.19646047	36.19646047	36.19646047	36.19646047	kN
	Mmax	Sleeper bending moment	108.81	108.8065602	108.8065602	108.8065602	kNm
	Fo	Pretension Force (due to clips)	10	10	10	10	kN
		Baseplate area	0.036	0.036	0.036	0.036	m^2
		Rail Seat Stress (Pad stress)	0.78	0.780506395	0.780506395	0.780506395	MPa
			OK for Concrete	OK for Concrete	OK for Concrete	OK for Concrete	
		Sleeper Ballast stresses	0.015	0.015	0.015	0.015	MPa
			Ok	Ok	Ok	Ok	

Figure 5-8: Track setup

5.1.8. Railhead and flange stresses

From the available theory (see 3.1.3, page 18), the rail stresses are calculated along the rail profile for the four different loading scenarios (see 4.1.3.1, page 89). Figure 5-9 indicates the stress results as calculated for the four different loading scenarios (E1 to E4) and presents the axial stresses of the rail on both the left and right side of the profile.

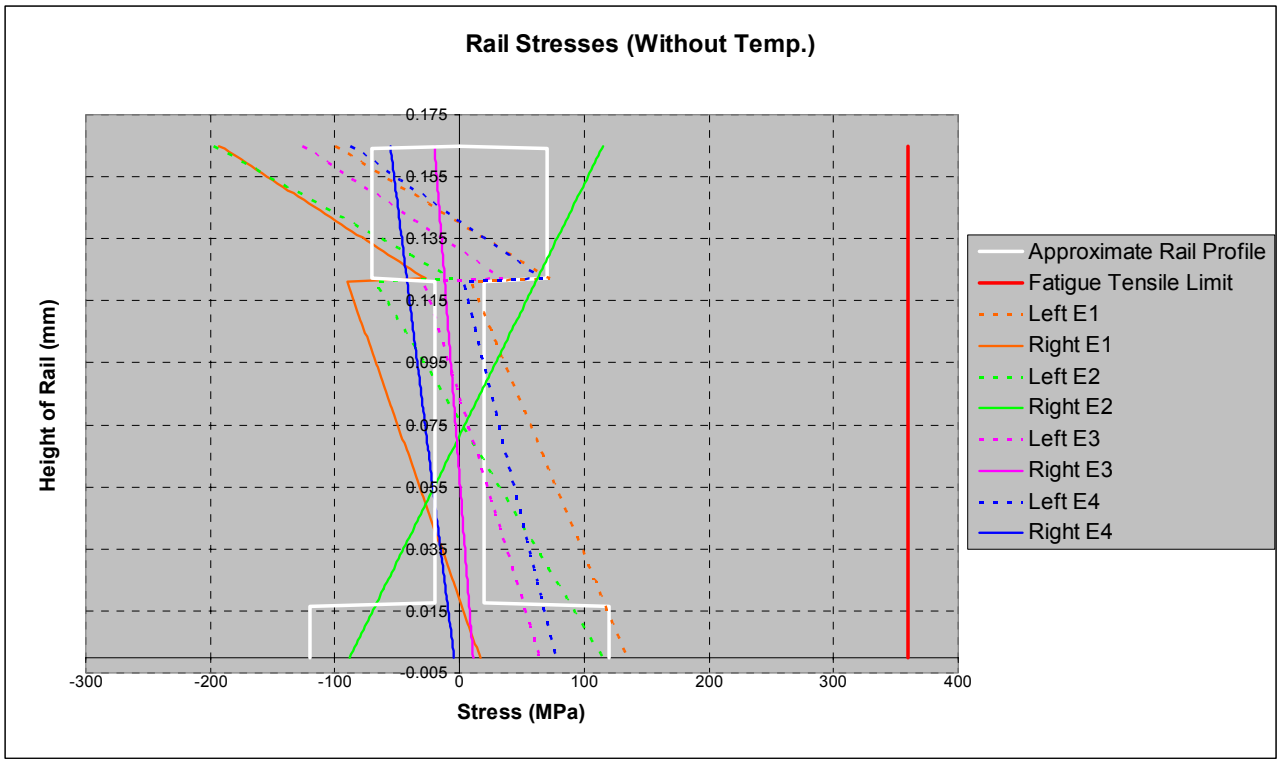

Figure 5-9: Rail axial stresses (without temperature stresses)

The last input parameter for the user to specify is the maximum temperature change the rail may experience. This value is dependent on the geographic position of the rail and the rail stress relief strategy followed by the maintenance personnel. After the static wheel load, this parameter has the single most influence on the resultant rail stresses and should be chosen carefully.

Rail temperature ranges were not investigated as part of this study but are easily obtainable from the various maintenance depots throughout the country which are managing rail stress relief programmes. Typical temperature ranges are also obtainable from the rich archive of local research on the subject.

Figure 5-10 indicates the resultant rail stresses with the added tensile stress due to a maximum decrease in rail temperature.

It should be noted that the stress-free temperature as maintained by the maintenance depot, minus the minimum rail temperature due to ambient temperature drop, determines the value to be used in these calculations. Using the maximum temperature range is representative of a rail which is stress-free at the maximum rail temperature (due to ambient conditions). This case is, however, unlikely to occur due to rail de-stressing strategies which do not allow rails to be de-stressed at maximum ambient temperatures.

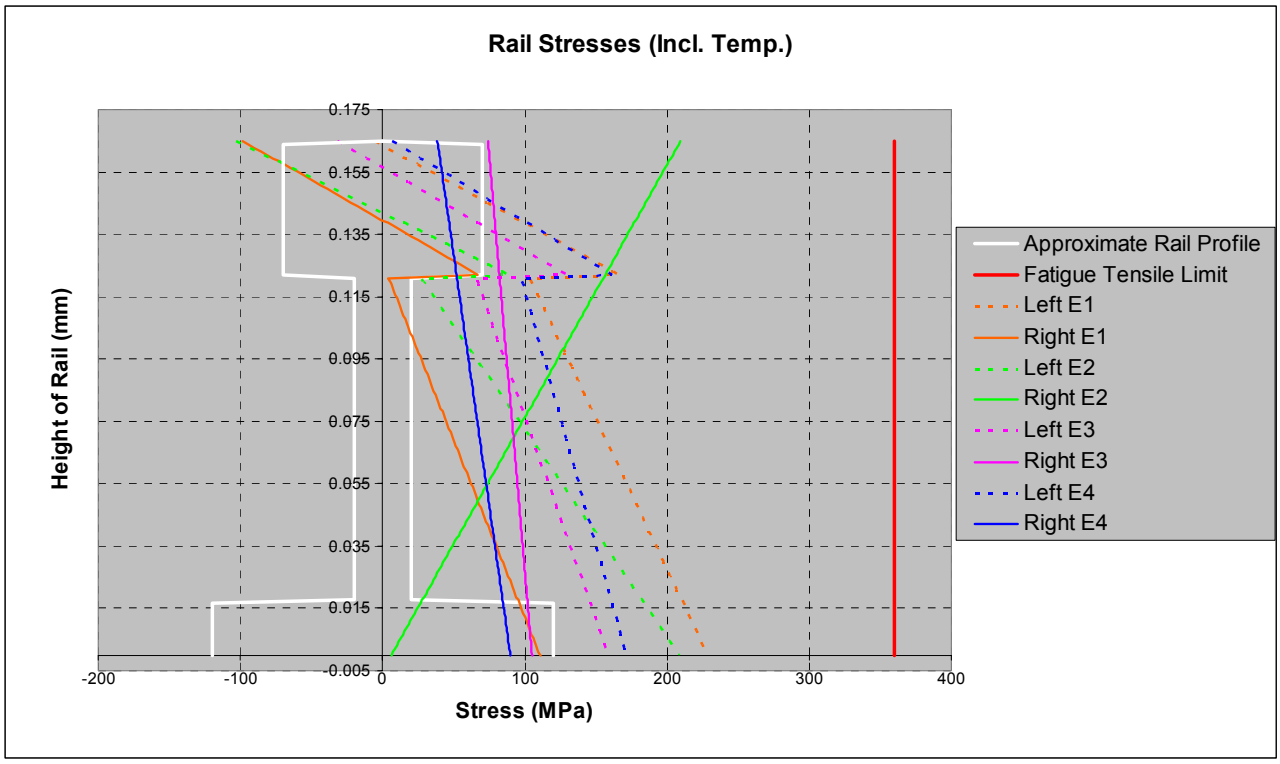

Figure 5-10: Rail axial stresses (with temperature stresses)

The stress results in Figure 5-10 can be compared to those of Figure 5-9 to indicate the effect of temperature on rail stresses.

5.2. Conclusion

This chapter summarised the methodology for calculating stresses in track components in reference to the developed spreadsheet. From the different investigations into the input parameters to which the analytical method is the most sensitive, best practice procedures were identified that could determine input parameter values to ensure acceptable results.

6 CONCLUSION

Railway track deteriorates over time due to the dynamic loading of passing rolling stock over its elastic structure. To ensure the safe passing of trains, the track has to be properly designed and maintained. This study focused on the development of a methodology for calculating stresses in track components and emphasis has been placed on ways to determine representative input parameter values, with the focus on identifying the parameters of highest importance. An existing analytical method has been utilised and improved that could calculate track component stresses in a fast and reliable manner.

The primary objective of the study was:

- To present a methodology for reliably calculating track component stresses under current and future operating conditions.

The secondary objectives were:

- to identify parameters not included in the current analytical method that may have a significant effect on track component stresses.
- to identify the parameters to which the analytical method is the most sensitive
- to provide nominal values to be used for the sensitive parameters where uncertainty exists regarding appropriate values to use when calculating track component stresses
- to validate the analytical method with results from finite element models and field test results.

6.1. Summary of contributions

The following contributions have been made through this study:

- The analytical method proved to be a valuable tool in the calculation of track component stresses.
- The assumption of a continuously supported beam of infinite length holds for a discretely supported beam of finite length under certain conditions.
- The user's attention has been focused on the input parameters that the analytical method is the most sensitive to. This will help to eliminate unnecessary allocation of resources to obtain input to unimportant parameters and places the focus on the parameters which proved to be the most important.

A number of enhancements have been made to the analytical method itself and the final model was validated against empirical results and other well-established methods. The following enhancements have been made:

- The upper limit of C (Foundation modulus) will be changed from 100^{+} for a very good foundation and track condition, to $200 MPa/m$ in accordance with (1, p. 79).
- The definition of the railhead depth (height) was changed to improve the analytical approximation of stresses.
- A methodology was developed to determine dynamic factors from measured wheel-rail forces.
- Running top condition is only an important parameter when using Eisenmann's dynamic factor formula
- A guideline has been presented to indicate when to use the relevant statistical confidence levels together with the Eisenmann formula
- For low speed operations, the dynamic factor does not exceed 1.2.
- Eccentricity should not be regarded only as a maximum together with an opposing lateral load, but should be used in different combinations to cover all possible worst-case scenarios.
- A methodology was developed on how to study wheel rail eccentricity and to determine possible worst-case scenarios in conjunction with a maximum lateral load
- The spreadsheet version of the analytical model was enhanced by including 4 worst-case scenarios of eccentricity vs. lateral load.
- The lateral load is not a function of the vertical load and should be used as a design maximum for track component calculations.
- An additional vertical load factor has been introduced to account for higher loads in curves.
- It was shown that a fixed lateral load limit is sufficient to account for loads in all curves since a proper track design should limit the lateral forces.
- Rail – sleeper stress limits have been introduced into the spreadsheet version of the analytical model
- The fastening system's pretension force has been taken into account in the rail seat stress calculations.

The analytical method is thus a very useful method that could calculate track component stresses.

6.2. Recommendations for future work

Valuable contributions to work done in this study could be made if future field test results (instrumented wheelset, weighbridge or wayside tests) were to be analysed according to the presented methodology in order to broaden the empirical base of input data.

Finite element methods are used extensively throughout the railway industry and additional comparisons of track model results with the analytical model would surely enrich both methods and strengthen the applicability of the analytical method or indicate areas for improvement.

The possibility of integrating available calculation tools for managing rail stress relief programmes could be investigated as an enhancement to the presented spreadsheet to be able to have zone specific temperature change data available for calculating track component stresses.

6.3. Conclusion

It may be concluded that the results of this study proved the usefulness of the analytical method as a trustworthy method with which to design and maintain railway track to ensure the safe passing of trains.

REFERENCES

1. Esveld C., Modern Railway Track, 2nd ed., MRT Productions, Zaltbommel, ISBN: 90-800324-3-3, 2001.
2. Lombard P. C., Spannings in die Spoorbaan struktuur, Spoornet (handwritten internal document), 1972.
3. Naudé F.P., Track & Rail Stress Calculations - A Step By Step Guide, Spoornet, submitted to Spoornet Engineering, report no. BBB2540ver1, 2001.
4. RAILROAD HISTORY, National Railroad Museum, http://inventors.about.com/gi/dynamic/offsite.htm?site=http://www.nationalrrmuseum.org/EdPacket/html/Tguide1.htm, 1999, Date downloaded 30/4/2002.
5. Bellis M., The History of Railroad Inventions, http://inventors.about.com/library/inventors/blrailroad.htm, 1996, downloaded 30/4/2002.
6. Gross E., This Day in American History, Neal-Schuman Publishers, Inc., New York, 1990.
7. International Union of Railways , Loading Diagram to be taken into consideration for the calculation of rail carrying structures on lines used by international services, UIC CODE, UIC, 2nd, 702-O, 1974.
8. International Union of Railways, Factors affecting track maintenance costs and their relative importance, UIC CODE, UIC, 3rd, 715-R, 1992.
9. Ebersohn W, Selig E.T., Track design and maintenance, Railway Geotechnology course notes, University of Pretoria, 1992.
10. International Heavy Haul Association, Guidelines to best practices for heavy haul railway operations: Wheel and rail interface issues, 1st ed., IHHA, Virginia Beach, 2001
11. International Union of Railwails, Loading Diagram to be taken into consideration for the calculation of rail carrying structures on lines used by international services, UIC CODE, UIC, 2nd ed., 702-O, 1974.
12. Marczyk J., Beyond Optimization in CAE, International Center for Numerical Methods in Engineering (CIMNE), Barcelona, ISBN: 84-95999-11-0, 2002.
13. Fastenrath F., Railroad track, 1st ed., Frederick Ungar Publishing Co., New York, ISBN: 0-8044-4231-2, 1977.
14. Popp K., Kruse H., Kaiser I., Vehicle-Track Dynamics in the Mid-Frequency Range, Vehicle System Dynamics - International Journal of Vehicle Mechanics and Mobility, vol. 31, no. 5-6, p. 423, 1999.
15. European Rail Research Institute, Rail rolling contact fatigue - Stress analysis of rail rolling contact fatigue cracks – Interim Report, ERRI D 173/RP11, 1995
16. Maree J. S., Dynamic behaviour of track with resilient rail pads, thesis for Masters in Engineering, lead by Prof. Vernon Marshall, Civil Engineering, University of Pretoria, Pretoria, 1993.

17. Wang J., The influence of track and vehicle properties on dynamic impact forces, Spoornet, submitted to Spoornet Engineering, 2002.
18. Bezin Y, Iwnicki S, Stow J, Development of a method to predict stresses in rails using ADAMS/Rail and ABAQUS, Manchester Metropolitan University, Manchester, 1998
19. Eisenmann, J., Germans gain a better understanding of track structure, Railway Gazette International, 1972.
20. Ebersohn W., Selig E. T., Introduction to Multi Disciplinary Concepts in Railway Engineering, Chair in Railway Engineering, University of Pretoria, 1994.
21. Timishenko, S., Method of analysis of statical and dynamical stresses in rail, Proceedings of the Second International Congress of Applied Mechanics, Zurich, 1927.
22. Esveld C, Modern Railway Track, 1st ed., MRT-Productions, Duisburg, ISBN: 90-800324-1-7, 1965.
23. Tomas M. D., Ogies - Saaiwater project. Stresses in 48, 57, and 60 *kg/m* rails from traffic-1st interim report, submitted to Spoornet Engineering, Spoornet, Report no. BBB2501, 2001.
24. Wilson B.W., On strength of railway track, Proceedings of the South African Society of Civil Engineers, 1941
25. Brinkman, Stresses in the rail as a result of dynamic forces, Klöckner-Werke AG Werk Osnabrück, Osnabrück, 1972
26. Igwemezie, J.O., Morgan, C.A., Stress analysis of transposed 102.4, 115, 136 LB/YD and jointed 100 LB/YD rails, Applied Rail Research Technologies Inc., submitted to Canadian Pacific Rail Systems, ARRT Report No. 1093, 1993.
27. Labuschagne, T.J., The calculation of bending stresses in rails on curved track, The Civil Engineer in South Africa, 1960.
28. Frohling R. D., Maartens S. J., Pretorius G. J., Dip Joint Analysis On The Orex Line, Spoornet, submitted to Spoornet Engineering, 2002.
29. Fröhling, R.D., Summer commissioning and verification tests on the MTAB iron ore prototype wagon, submitted to Spoornet Engineering, Report E/MT/TMO/040, 1999.
30. International Union of Railways, Test and acceptance of railway vehicles form the point of view of dynamic behaviour, safety, track fatigue and quality of ride, UIC CODE 518 OR, 2nd edition, International Union of railways, 1999.
31. Lombard, P.J., Track structure – optimization of design, Heavy Haul Railway Conference, Institute of Engineers - Australia, Perth, 1978.
32. Eisenmann J.,The rail as travelling way, Technishe Universität München, München , 1970

APPENDIX A
Stochastic rail stress distributions (Different iterations with the same model)

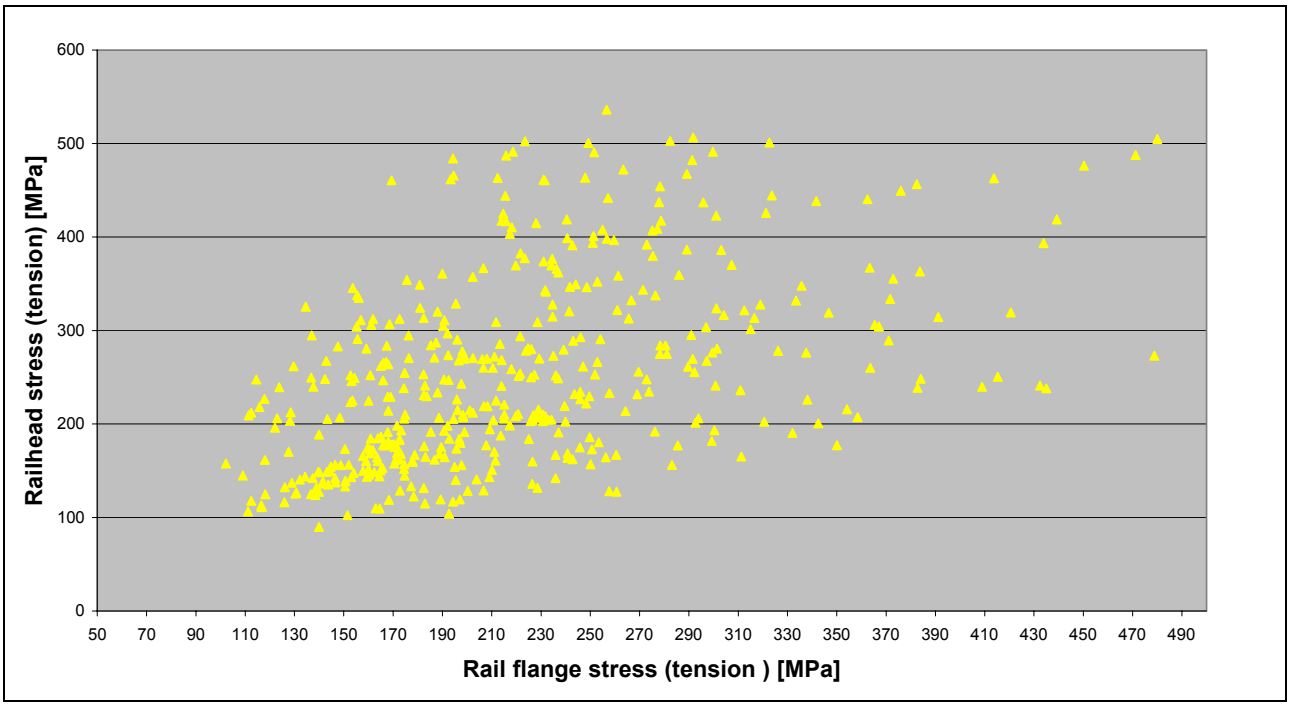

Figure A-1: Stochastic rail stress distributions

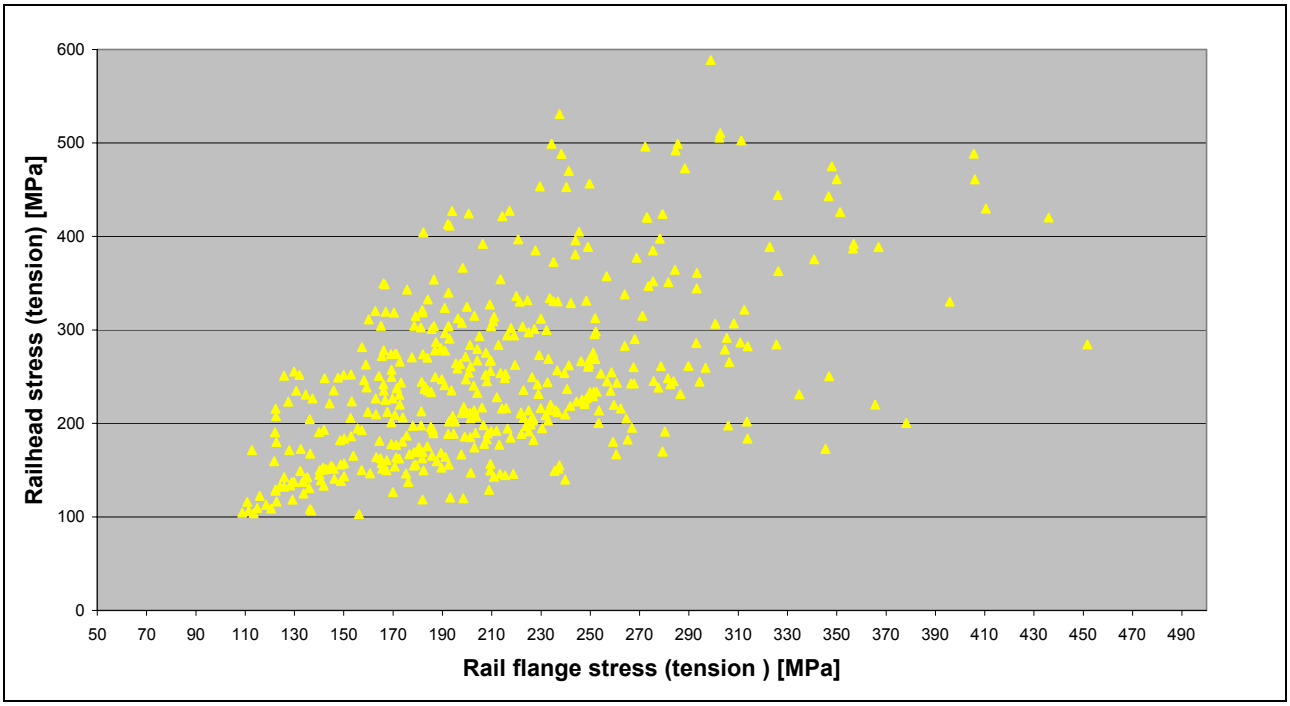

Figure A-2: Stochastic rail stress distributions

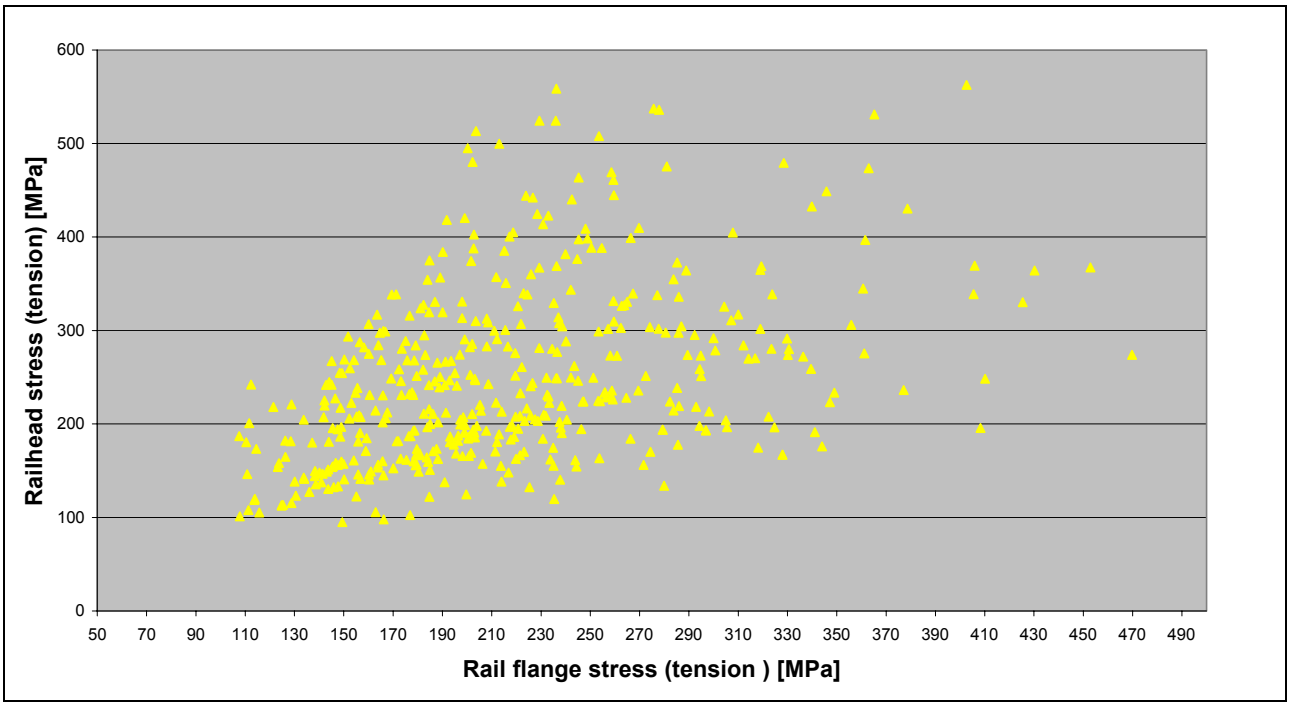

Figure A-3: Stochastic rail stress distributions

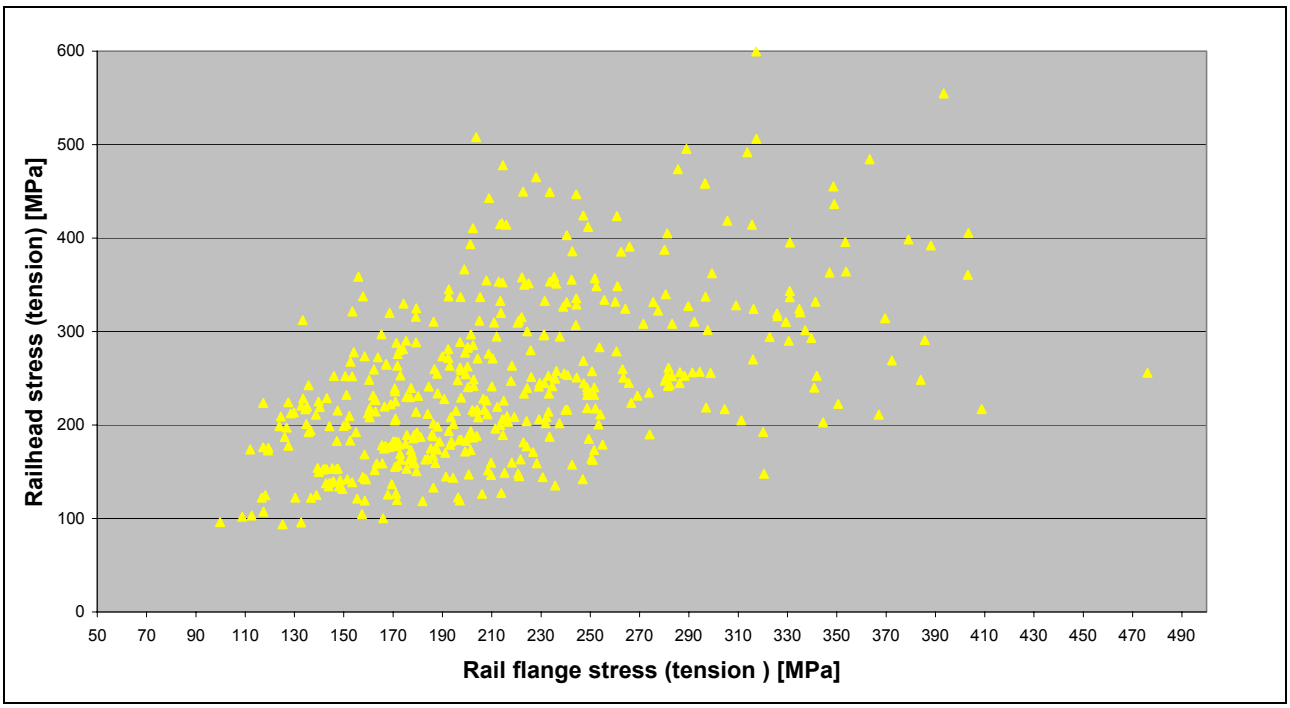

Figure A-4: Stochastic rail stress distributions

APPENDIX B
Histograms of Leandra test data

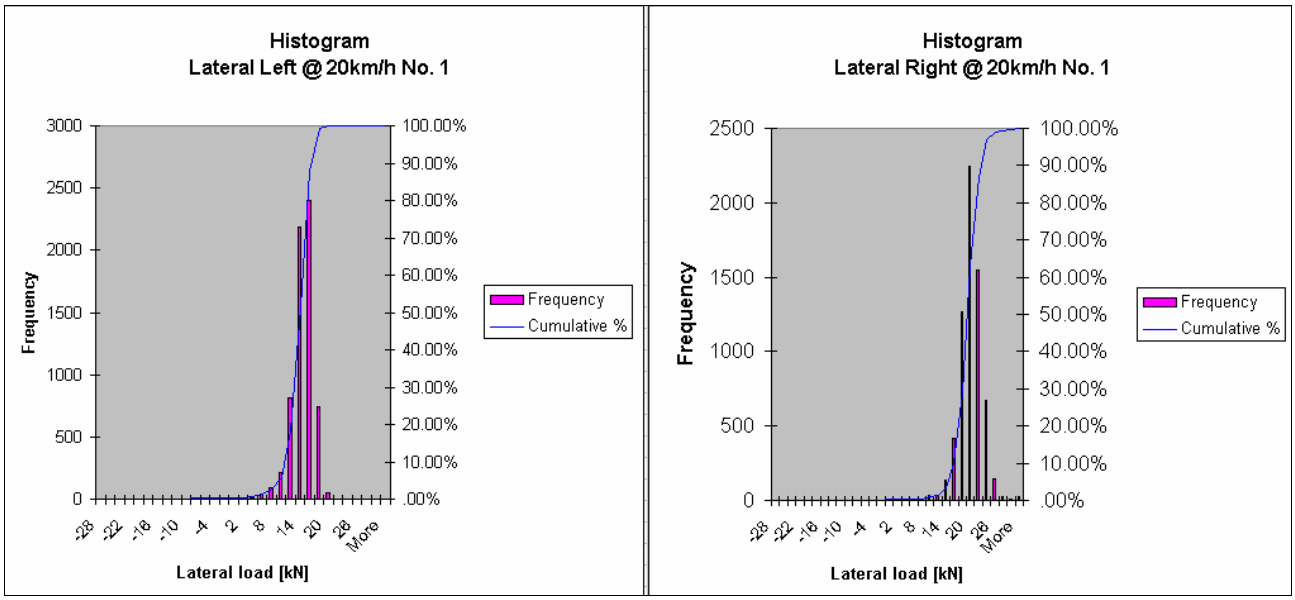

Figure B-1: Histograms of lateral forces at 20km/h

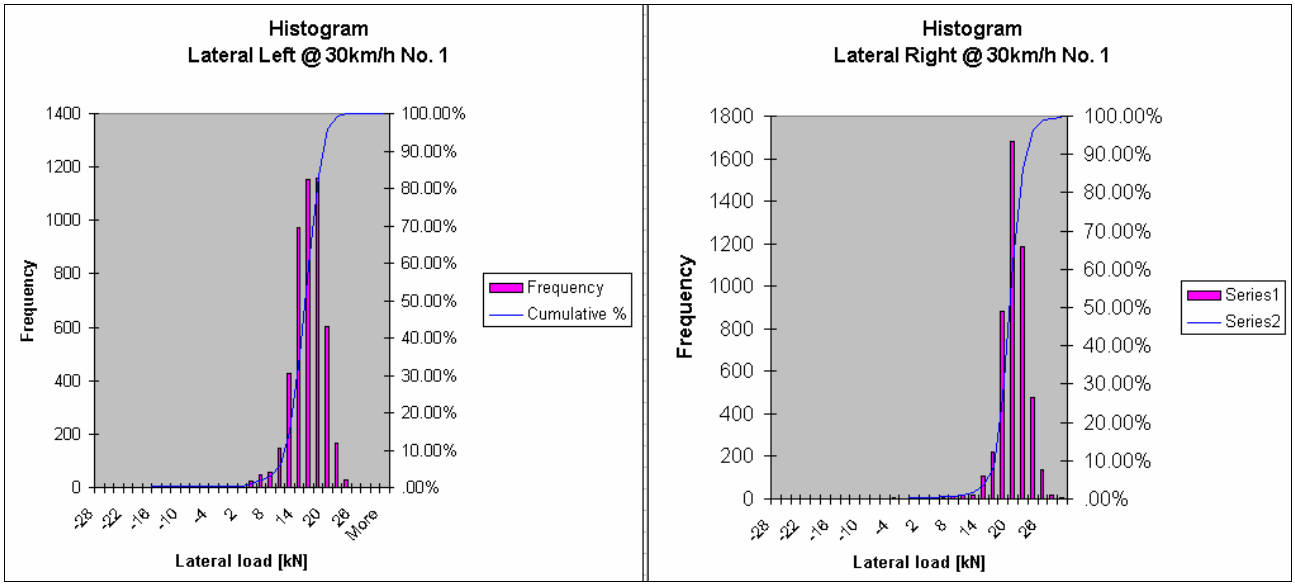

Figure B-2: Histograms of lateral forces at 30km/h

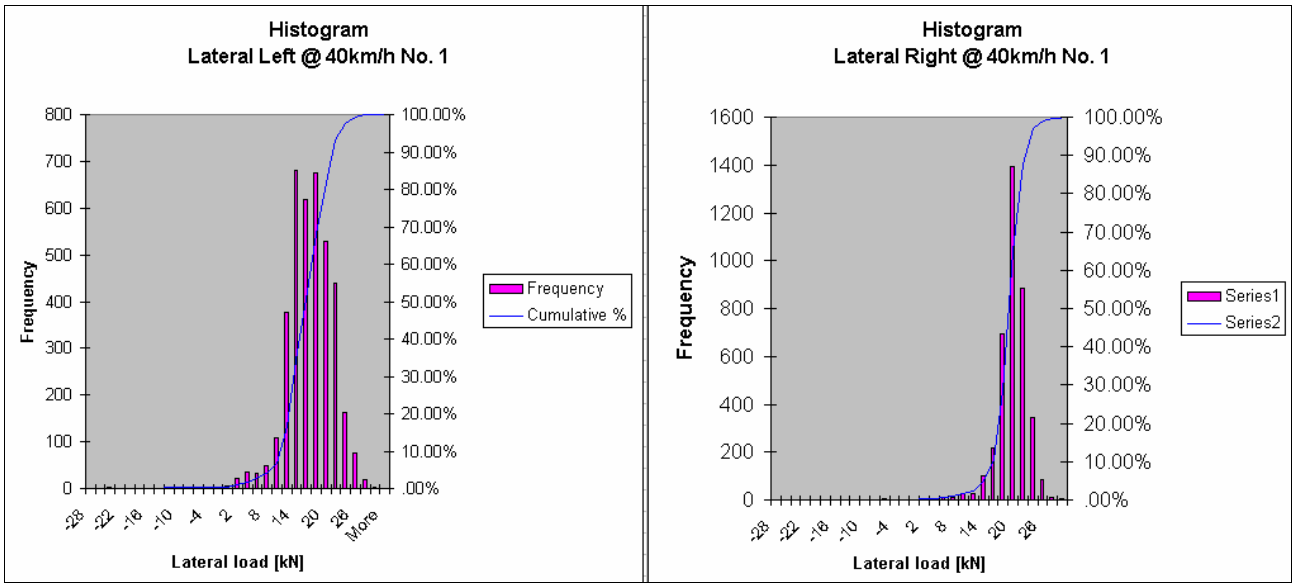

Figure B-3: Histograms of lateral forces at 40km/h

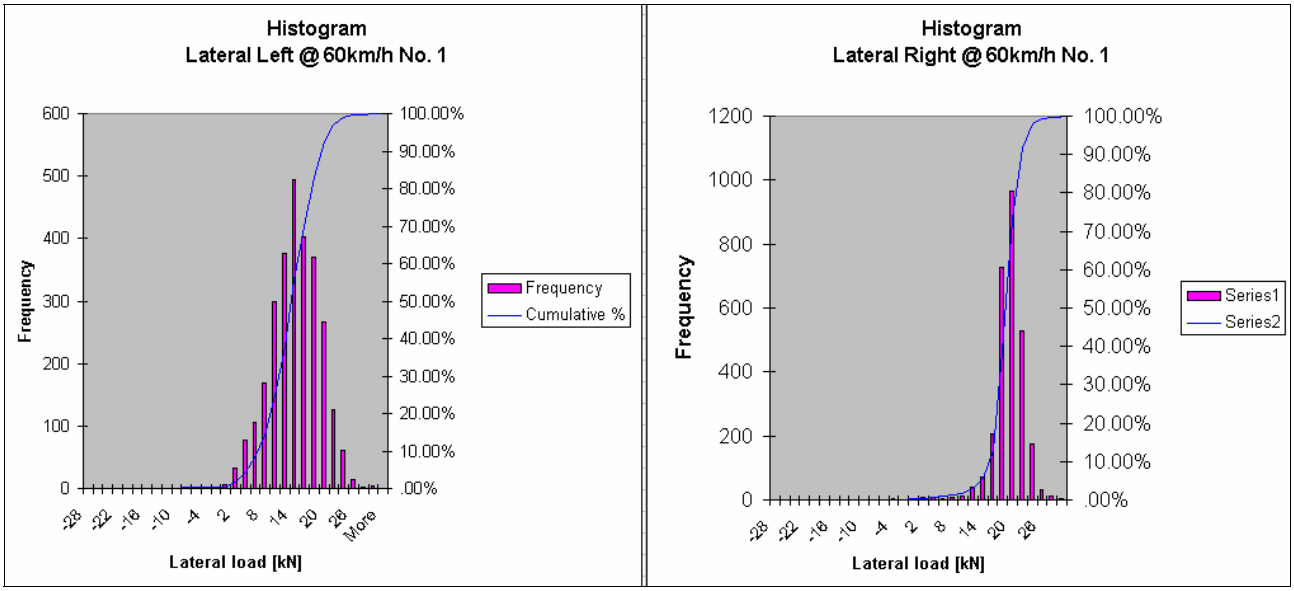

Figure B-4: Histograms of lateral forces at 60km/h

APPENDIX C
Lateral force graphs of Iron Ore Export line data

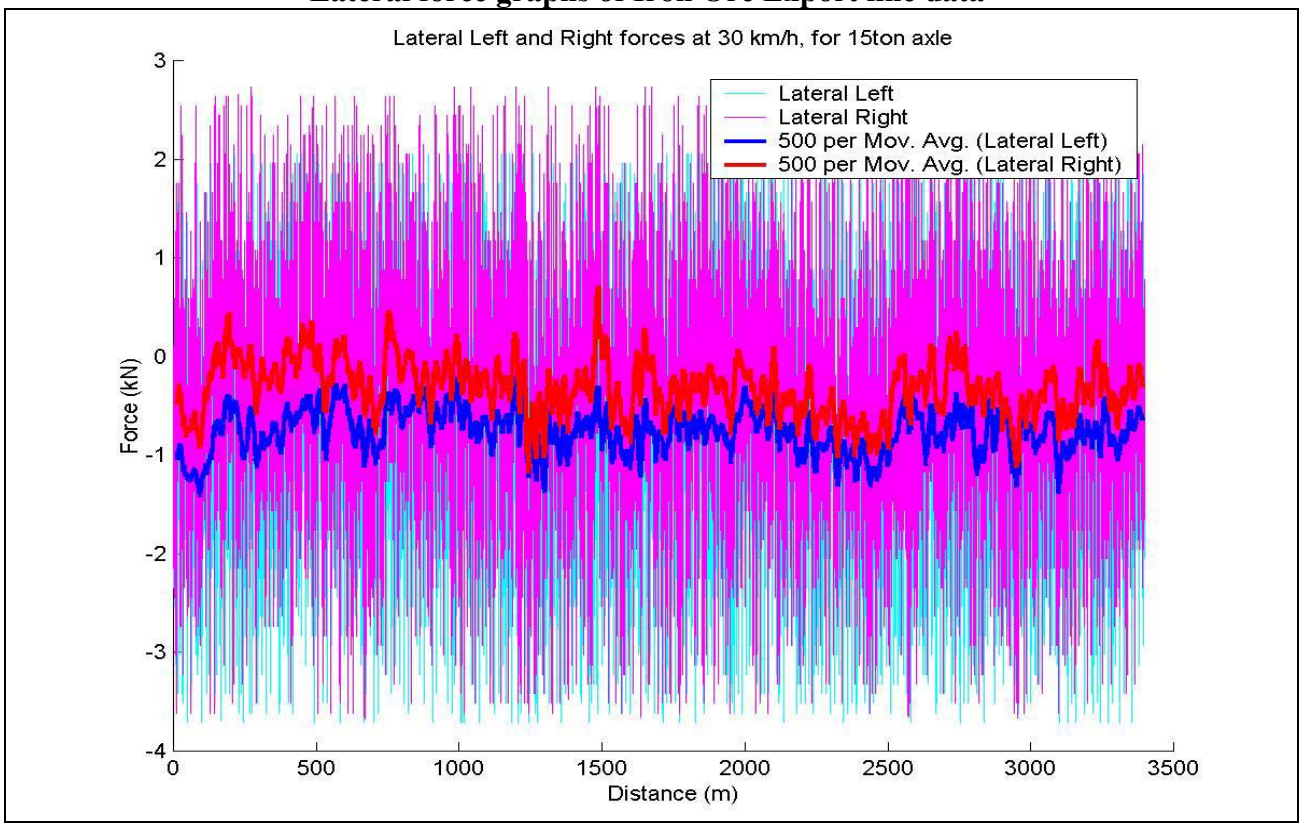

Figure C-1: Lateral left and right forces at 30 km/h, for 15 ton axle

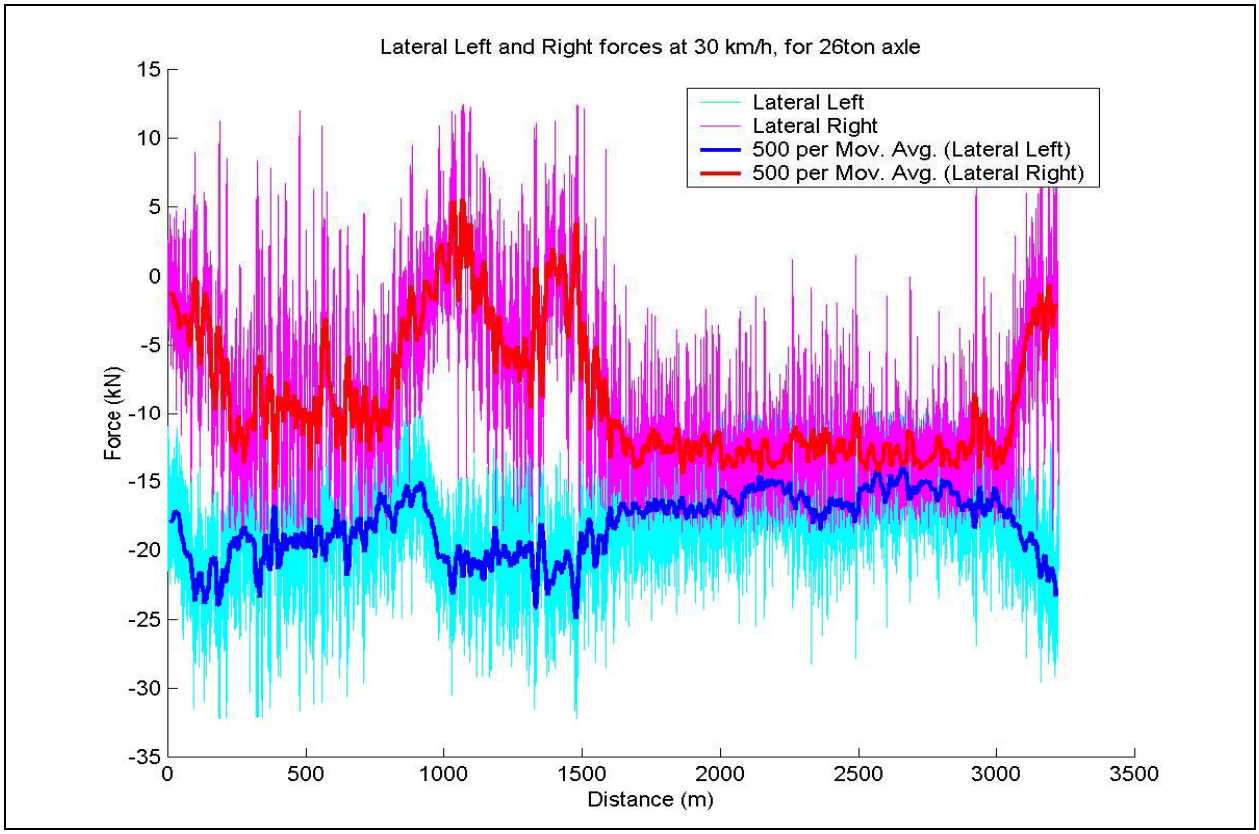

Figure C-2: Lateral left and right forces at 30 km/h, for 26 ton axle

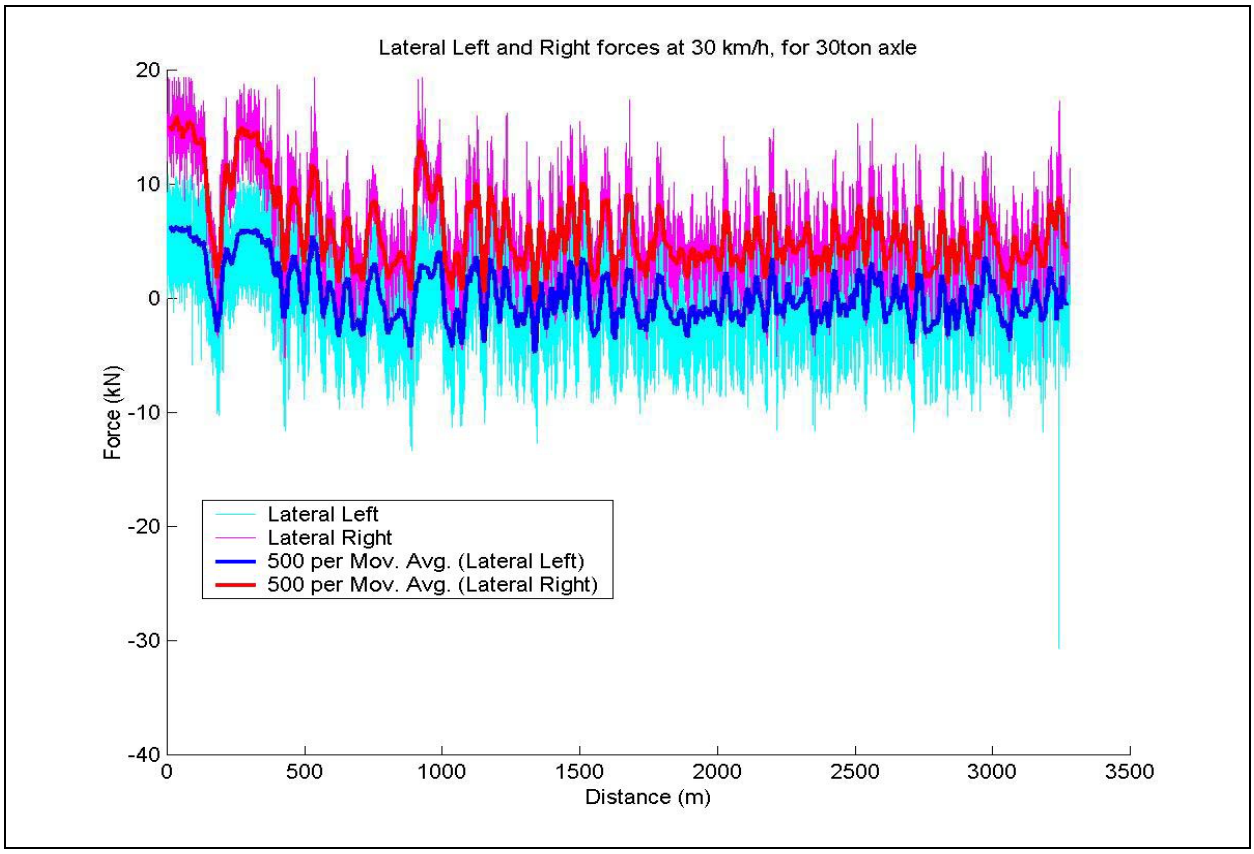

Figure C-3: Lateral left and right forces at 30 km/h, for 30 ton axle

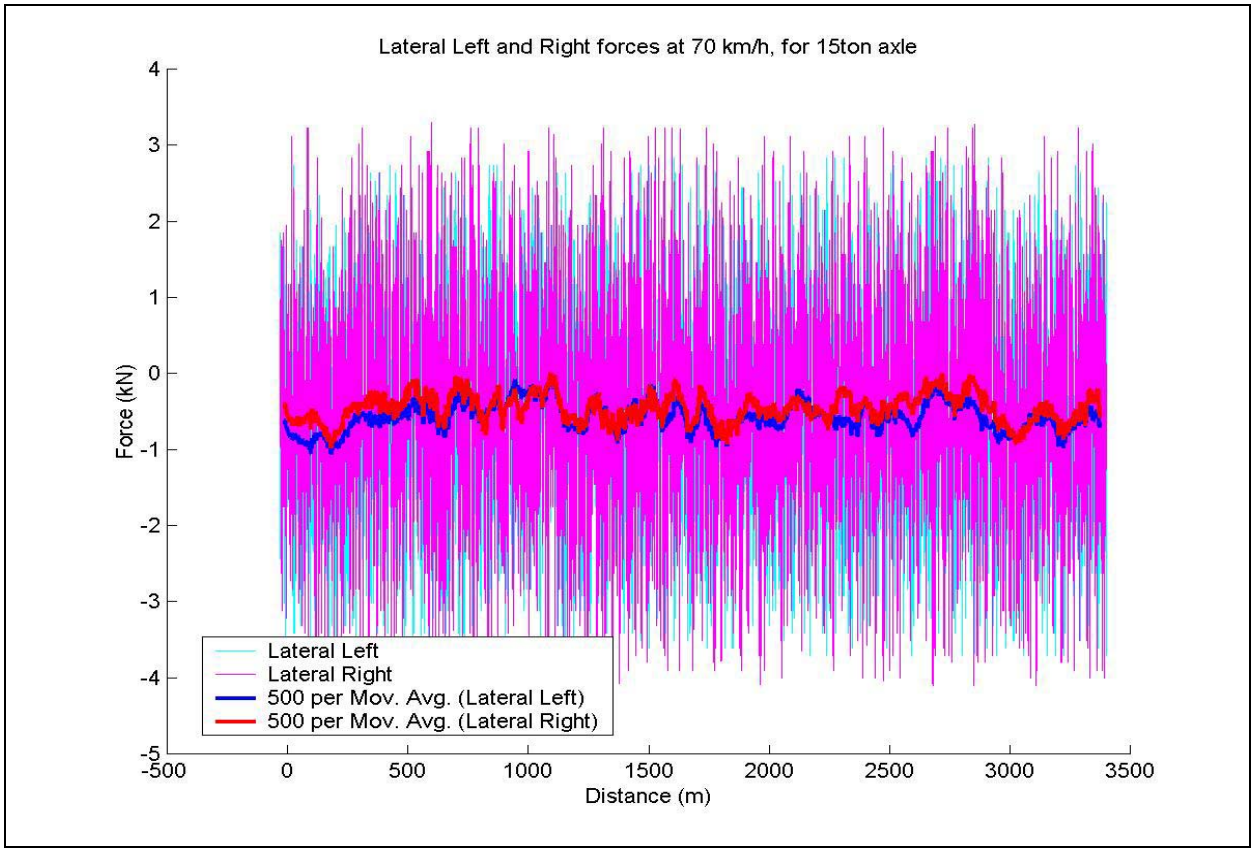

Figure C-4: Lateral left and right forces at 70 km/h, for 15 ton axle

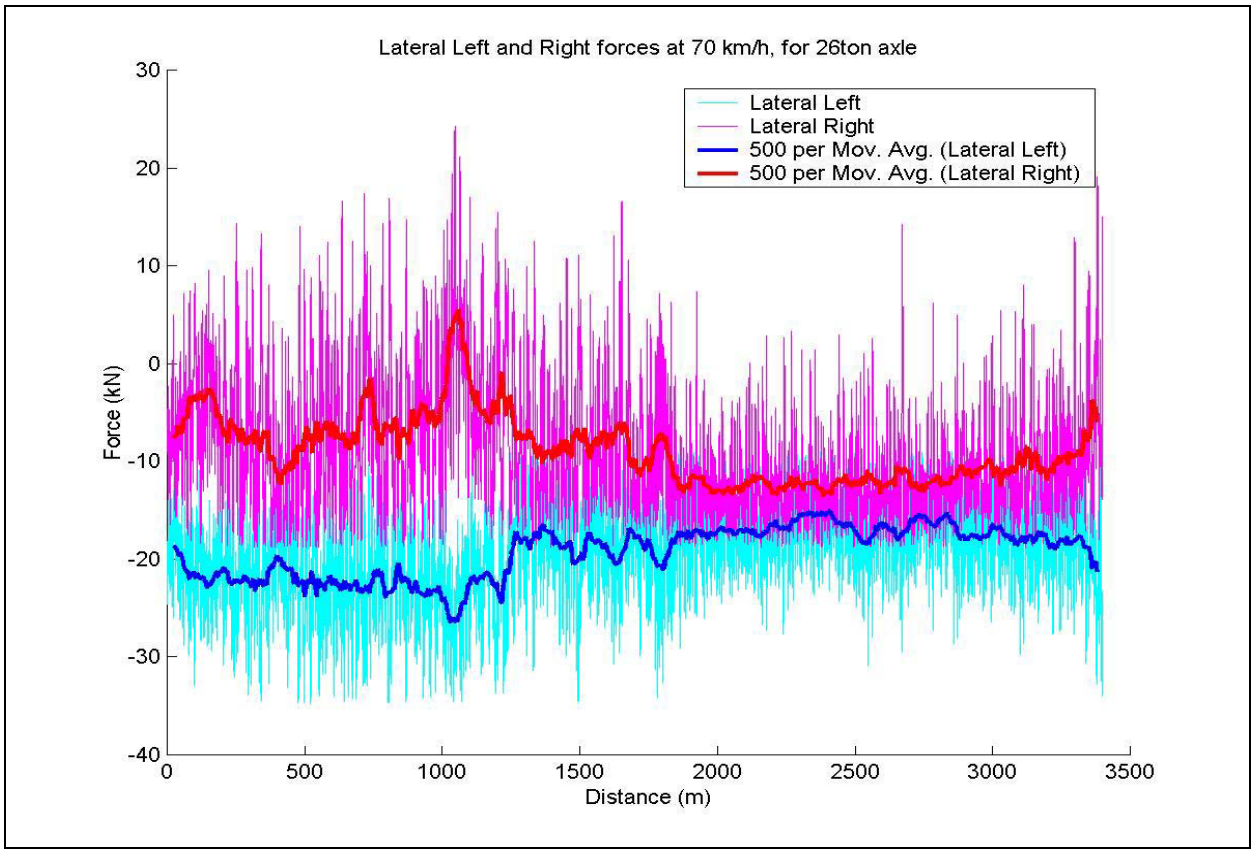

Figure C-5: Lateral left and right forces at 70 km/h, for 26 ton axle

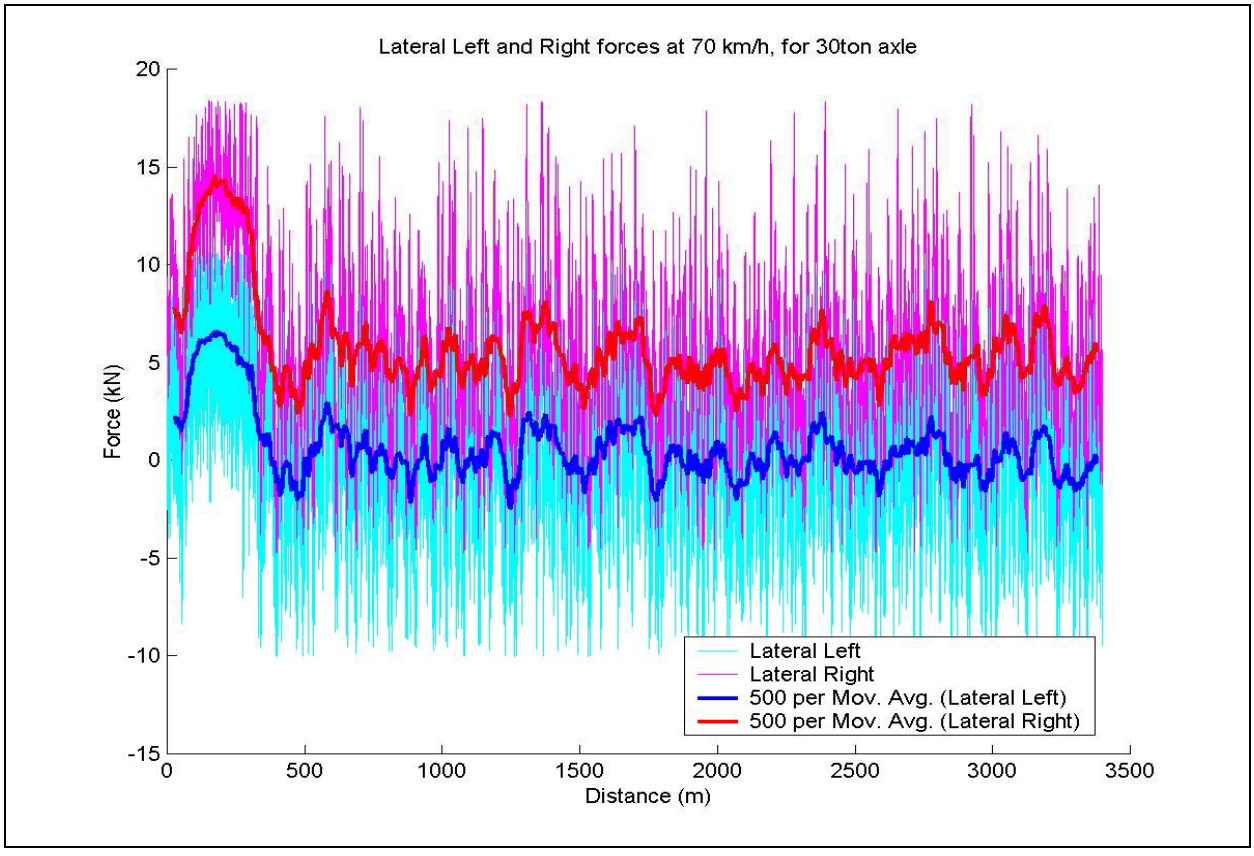

Figure C-6: Lateral left and right forces at 70 km/h, for 30 ton axle

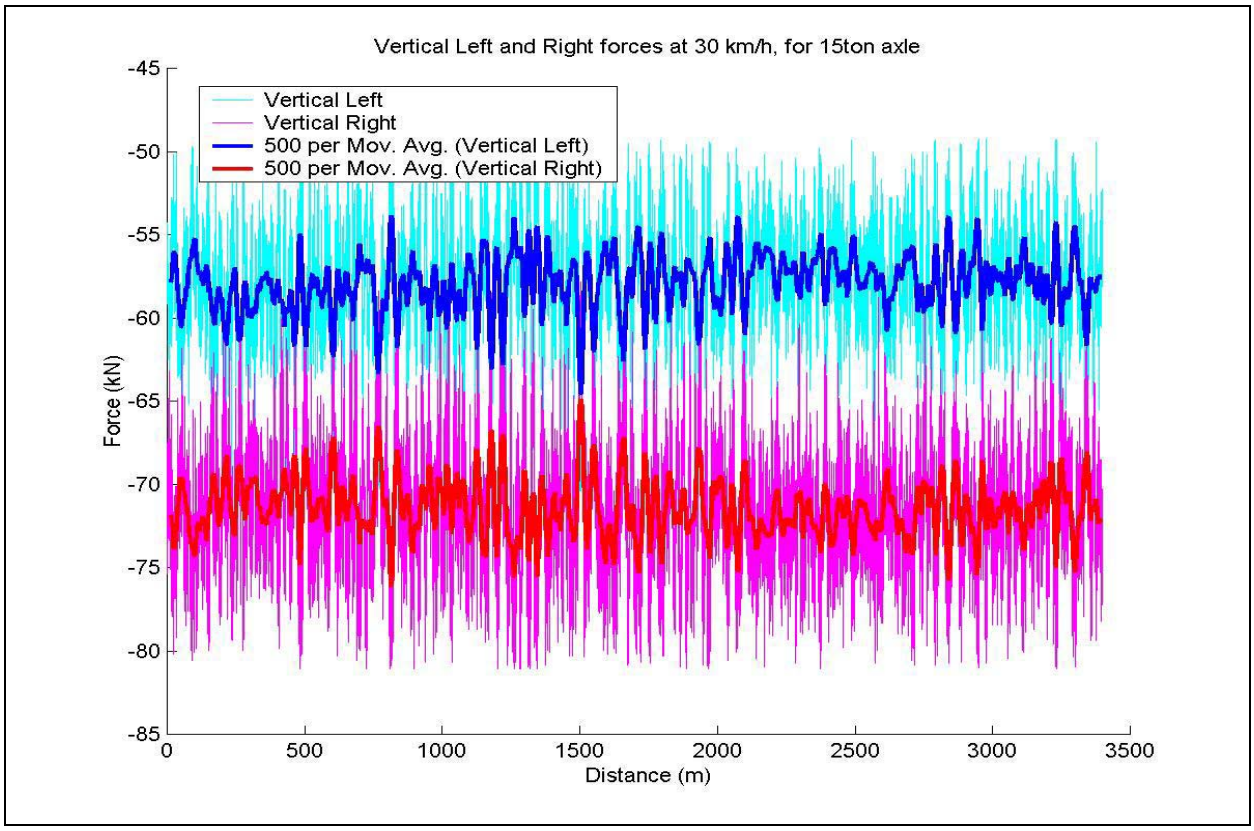

Figure C-7: Vertical left and right forces at 30 km/h, for 15 ton axle

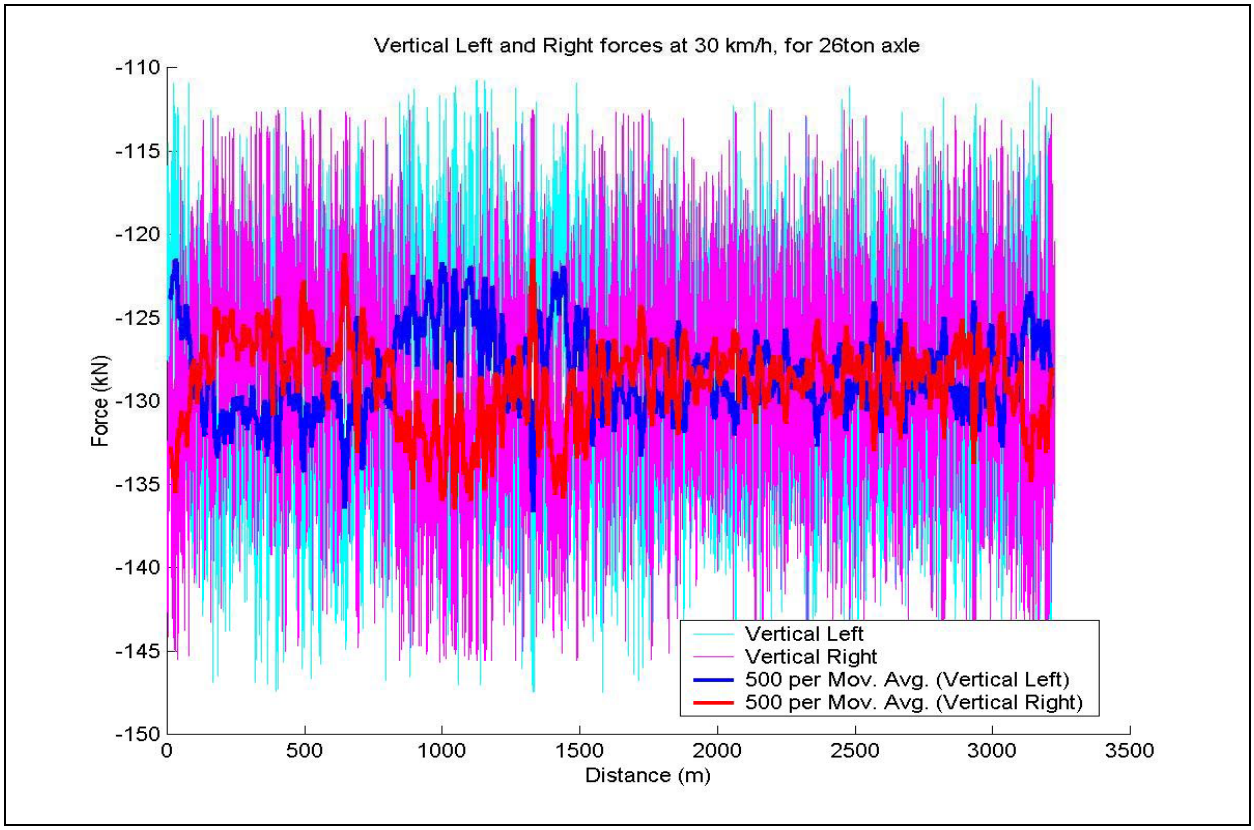

Figure C-8: Vertical left and right forces at 30 km/h, for 26 ton axle

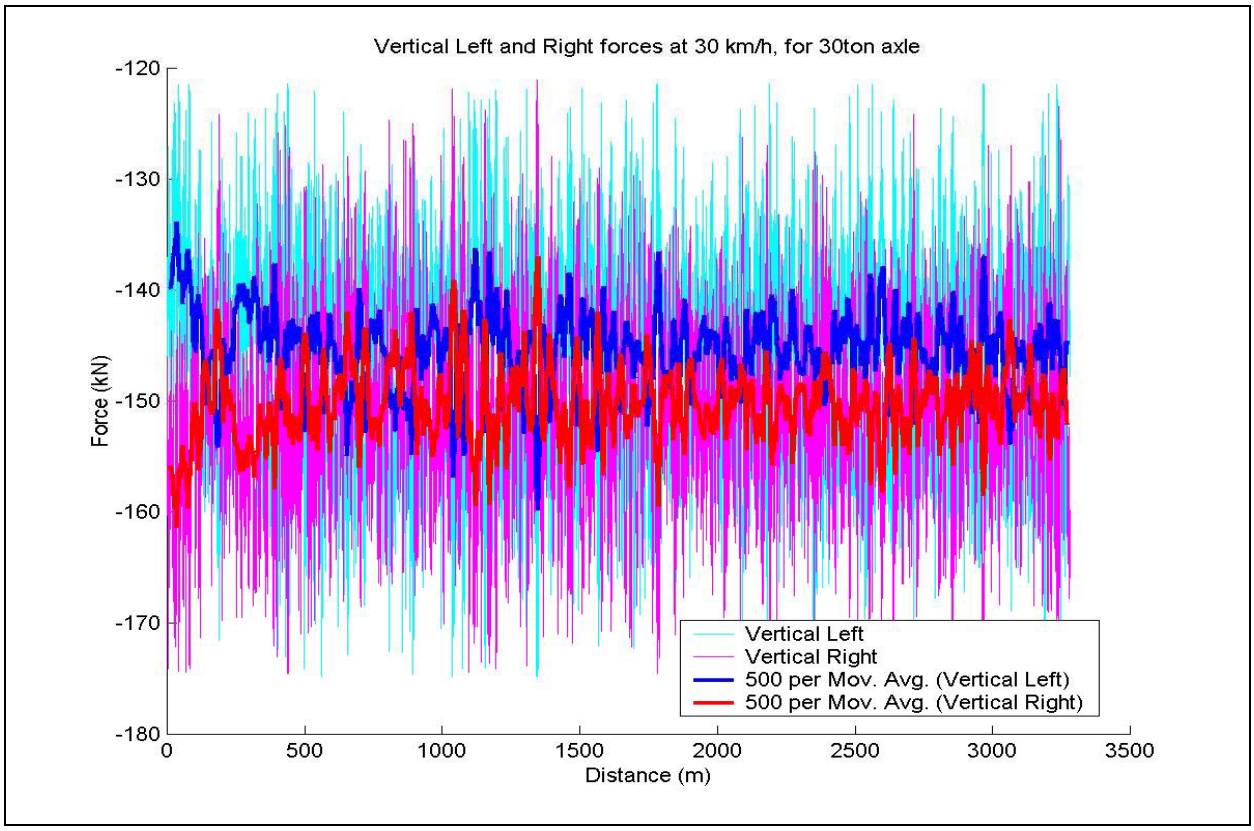

Figure C-9: Vertical left and right forces at 30 km/h, for 30 ton axle

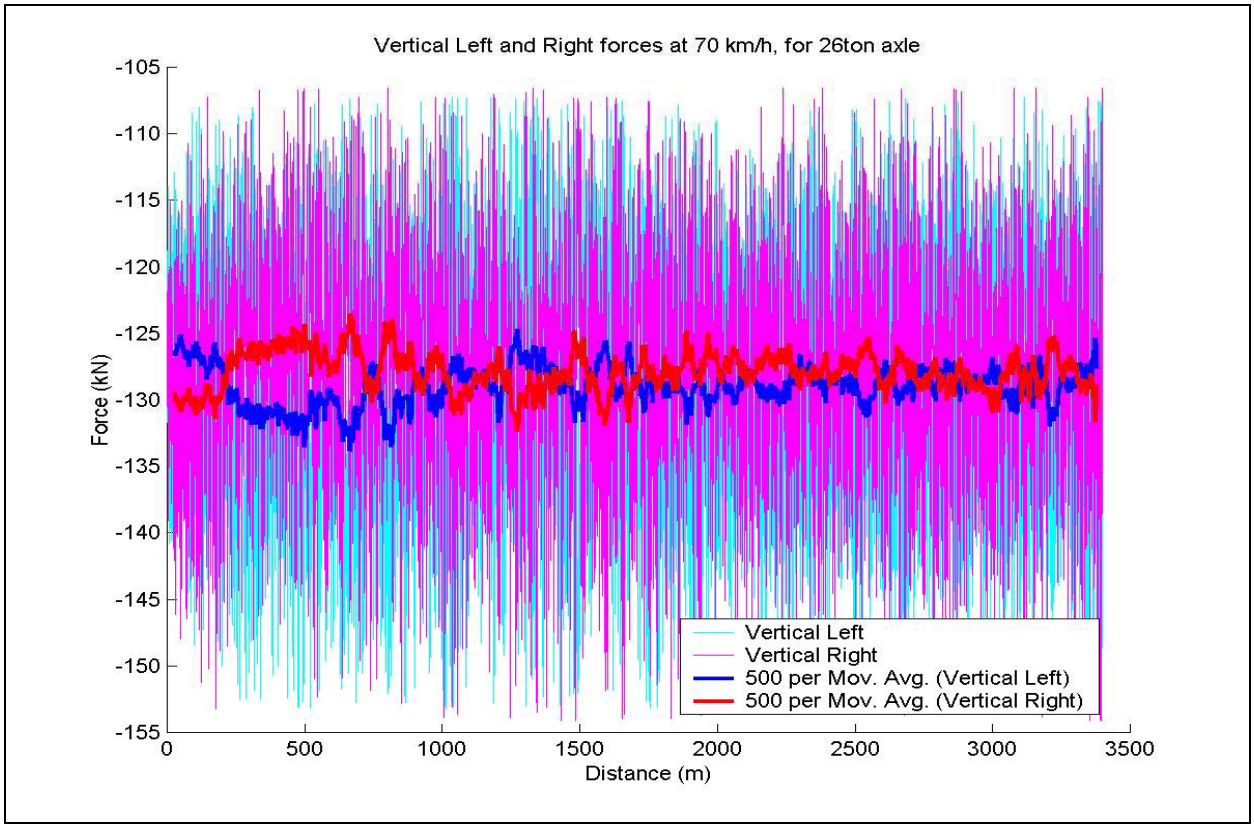

Figure C-10: Vertical left and right forces at 70 km/h, for 26 ton axle

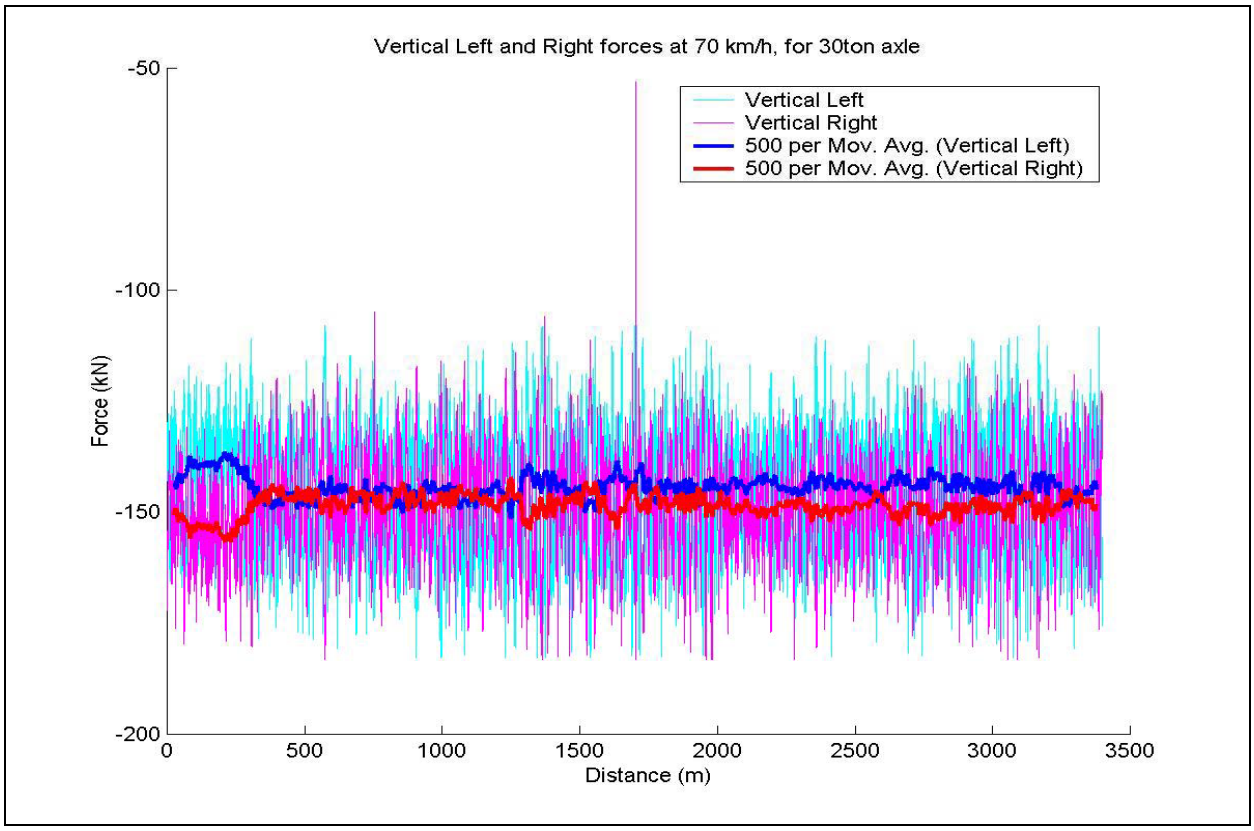

Figure C-11: Vertical left and right forces at 70 km/h, for 30 ton axle

APPENDIX D
Summary of dynamic factors

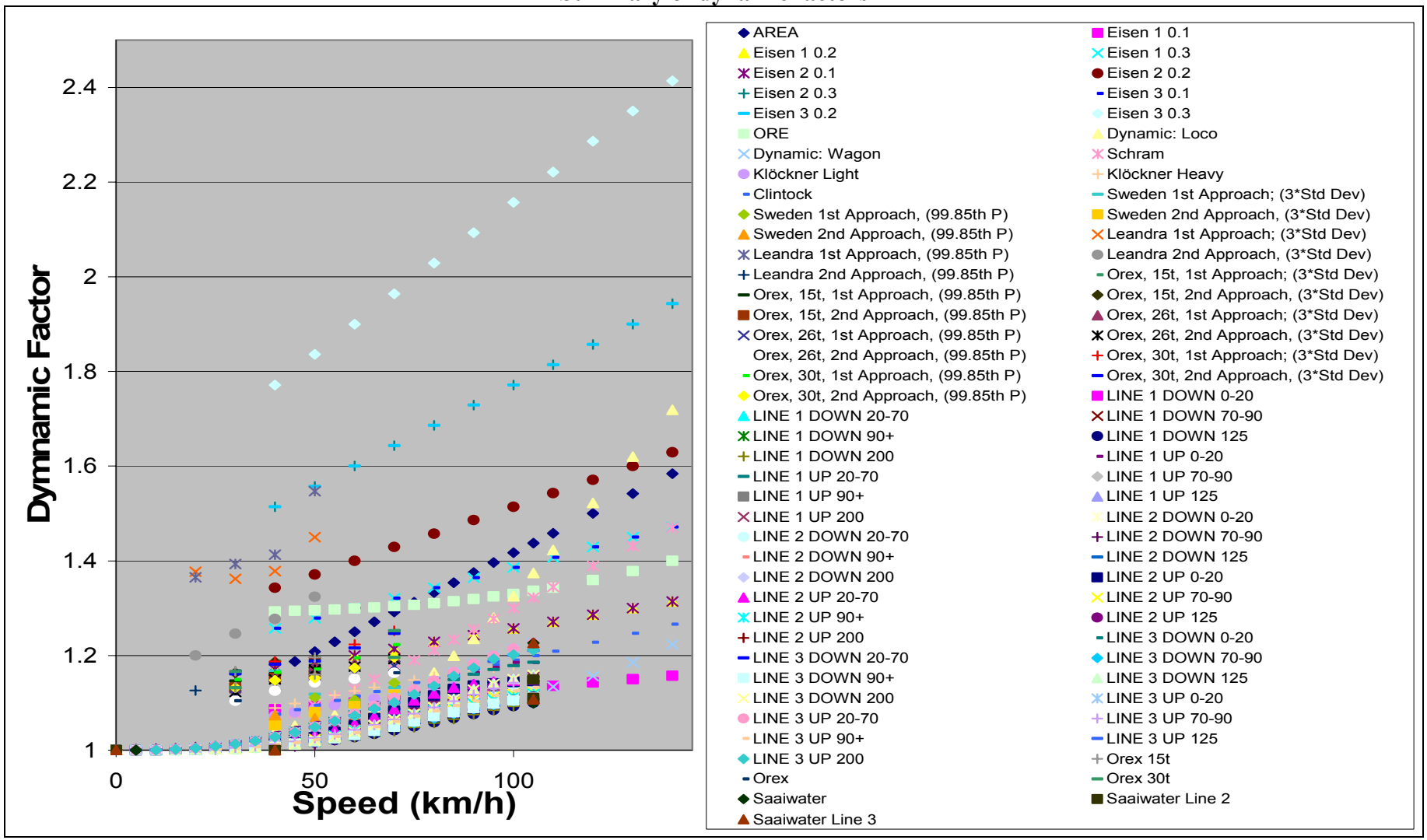

Figure D-1: Summary of all dynamic factors